Resum

Aquest projecte, té com a objectiu determinar la validesa de les dades proporcionades pel simulador FDS en funció de la seva similitud amb dades experimentals obtingudes en el marc de diverses tesis doctorals.

En primer lloc, es descriu, en un apartat d'antecedents, què s'entén com a foc i com a flames, quins són els principals tipus d'incendis que poden produir-se a la indústria i, finalment, quines són les característiques principals que defineixen els incendis de bassal, objecte d'estudi d'aquest projecte. En aquest apartat introductori també s'ha fet una breu introducció a la dinàmica de fluids computacional (CFD), a les principals estratègies de simulació (RANS, LES i DNS) i les eines que s'han fet servir en l'obtenció de les simulacions.

S'ha dedicat un capítol sencer a la descripció dels principals models matemàtics que el simulador *Fire Dynamics Simulator* (FDS) fa servir per realitzar els seus càlculs pel que fa a la pròpia hidrodinàmica de fluids, a la combustió i al transport de la radiació tèrmica. També s'ha realitzat un breu resum dels estudis de validació realitzats prèviament amb FDS i que guarden alguna relació amb els incendis de bassal o amb algun dels aspectes estudiats en el present projecte.

Posteriorment, s'ha dedicat un capítol a descriure la instal·lació experimental on es van realitzar les proves que es compararan amb els resultats de les simulacions. A més de descriure físicament l'escenari experimental, també s'han descrit els mètodes de mesura de les diferents variables i s'han indicat quins foren els resultats obtinguts.

A continuació s'ha explicat com s'ha implementat l'escenari experimental a FDS (originalment s'ha volgut reproduir l'escenari més similar possible a la instal·lació real) i quins han estat els mètodes de registre de variables utilitzats.

Descrit l'escenari simulat, s'ha procedit a realitzar els estudis d'emplaçament adients, (domini, mallat, simetria) de forma que els resultats fossin el més propers possibles a les dades experimentals sense que això suposés un gran cost computacional. A més d'estudiar l'efecte de les pròpies característiques de l'emplaçament simulat en els resultats, s'ha analitzat l'efecte que comporta canviar la forma de la bassa de circular a quadrada i quin és el comportament de cadascuna de les formes vers un increment de la velocitat del vent.

A continuació, s'ha realitzat un breu estudi de sensibilitat per comprovar com varien els resultats quan es modifiquen lleugerament algunes variables d'entrada.

Finalment, s'han elaborat estudis de sostenibilitat i de costos del projecte, s'ha descrit la planificació de les tasques realitzades i s'han exposat les conclusions del projecte.

Summary

This project has as a main target to determine the validity of data provided by FDS simulator in function of its similitude with experimental data obtained through different PhD thesis.

To start with, in a background section, is explained what is understand for fire and flames, which are the main types of fires that can occur in industry and, finally, which are the main features that define pool fires, which are object of study of this project. In this section, a brief introduction of computational fluids dynamic (CFD) has also been described, as the main simulation strategies in CFD (RANS, LES and DNS). Finally, the used simulation tools have been described.

A whole chapter has been dedicated to the description of the different mathematical models FDS uses in order to perform its calculations, regarding to fluids hydrodynamics, combustion and thermal radiation transport. A brief summary of found validation results performed previously with FDS and which are related to the matter of this project have been summarized.

After FDS introduction, a chapter has been dedicated to the description of the installation where the experiments were performed, the results of which will be compared with simulation data provided by FDS. Besides the description of the experimental scenario, the different measurement methods used experimentally to catch the registered variables are also described, and experimental results obtained have been compiled.

Described the experimental installation and the measurement methods, it has been explained how experimental scenario has been implemented into FDS (originally, the reproduced scenario has been set as similar as possible to the real installation), and which have been the measurement methods for the output variables.

Later, emplacement studies have been carried out, in order to find which domain and grid size (symmetry has also been studied) can provide the data which is most nearby to experimental results and, at the meantime, does not require an excessive computational time to be calculated. In addition to the study of the effect of the emplacement on the simulation results, the effect of setting a square pool shape instead of circular on the simulation results has also been studied, and which is the behaviour of both pool shapes when wind speed is increased.

Following the pool shape study, a brief sensitivity study in order to check how simulation results vary when some input variables are slightly modified.

Finally, sustainability and costs studies have been performed, the tasks planning during the entire stance at CERTEC has been presented and the project conclusions have been exposed.

Table of contents

Nomenclature

Symbol	Units	Description
Cp	kJ·kg^{-1}·K^{-1}	Specific heat
C_v	-	Deardorff constant, 0.1
D	m	Pool diameter; depth
D^*	m	Characteristic fire diameter
D_e	m^2·s^{-1}	Diffusivity of an e species
E	kW·m^{-2}	Emissive power
F	-	Mean output value of base case simulation of sensitivity study
f	s^{-1}	Flame shedding frequency
f_i	N·m^{-3}	Drag force due to lagrangian particles
g	m·s^{-2}	Gravitational acceleration, 9.81 m·s^{-2}
H	m	Characteristic dimension of square burners; height
h_e	kJ·kg^{-1}	Enthalpy of an e species
I	kW·m^{-2}	Radiation intensity per unit of solid angle
k	W·m^{-1}·K^{-1}	Thermal conductivity
k_{sgs}	m^2·s^{-2}	Subgrid scale kinetic energy per unit mass
L	m	Flame length
M_e	kmol·kg^{-1}	Molecular weight of an e species
$\dot{m}$	kg·s^{-1}	Mass flux
$\dot{m}''$	kg·m^{-2}·s^{-1}	Mass loss rate per unit area
$\dot{m}_e'''$	kg·m^{-3}·s^{-1}	Mass production rate of species e
p	Pa	Pressure
$\dot{Q}$	kW	Total heat release rate (HRR)
Q^*	-	Fire Froude Number
$\dot{q}''$	kW·m^{-2}	Heat release rate unit area
$\dot{q}'''$	kW·m^{-3}	Heat release rate per unit volume
R	J·K^{-1}·mol^{-1}	Ideal gas constant, 8.31 J·K^{-1}·mol^{-1}
SF	-	Sensitivity coefficient
$\vec{s}$	-	Unit vector in direction of radiation intensity
T	K	Temperature
t	s	Time
$\vec{u} = (u, v, w)$	m·s^{-1}	Velocity vector
u^*	-	Non-dimensional wind speed
u_c	m·s^{-1}	Characteristic wind speed
W	m	Width
$\vec{x} = (x, y, z)$	m	Position vector
Y_e	kg·kg^{-1}	Mass fraction of an e species
α	-	Arbitrary coefficient, statistical significance value
β	-	Arbitrary coefficient
γ	-	Arbitrary coefficient
Δ	m	Cell *weighed* width
ΔH_c	kJ· kg^{-1}	Heat of combustion
Δh_f	kJ· kg^{-1}	Enthalpy of formation
δx	m	Grid cell size length in x direction
ε	-	Emissivity
ζ	kg·kg^{-1}	Unmixed fraction
η	-	Combustion efficiency
θ	°	Flame inclination angle
κ	m^{-1}	Absorption coefficient
μ	kg· m^{-1}·s^{-1}	Dynamic viscosity
ν_e	mole	Stoichiometric coefficient of an e species
ρ	kg·m^{-3}	Density
σ	W· m^{-2}· K^{-4}	Stefan-Boltzmann constant, 5.67·10^{-8} W· m^{-2}· K^{-4}
τ	N·m^{-2}	Viscous stress
ϕ	-	Arbitrary scalar quantity
χ	-	Radiative fraction

Subscripts

b	Blackbody
c	Convective
$chem$	Chemical reaction
d	Diffusive
e	Arbitrary chemical species
F	Fuel
f	Feedback
$flame$	Flame surface
g	Buoyant
i	Spatial coordinate in x direction
j	Spatial coordinate in y direction
k	Spatial coordinate in z direction
lum	Fire light emitting region
max	Maximum
min	Minimum
$mean$	Mean value
mix	Mixing, mixture
r	Radiative
sgs	Sub-grid scale
$soot$	Fire soot region
t	Turbulent
u	Advection
λ	Wavelength
0	Initial
∞	Ambient, environmental air

Emphasis

$\bar{u}$	Average value of u velocity component at the grid centre
$\hat{u}$	Velocity weighed value over adjacent cells
$\widetilde{Y_e}(t)$	Cell mean mas fraction of species e (function of time)
$\hat{Y}_e$	Mass fraction of species e in the mixed reactor zone
$\bar{\phi}$	Low pass-filtered parameter
$\tilde{\phi}$	Favre-filtered parameter
$\dot{\phi}$	Flux
$\vec{\phi}$	Vector

Preface

Fire has been the most important discovery in prehistory; it has meant the beginning of the evolution of our ancestors to the current human being. Control of fire brought initially the possibility to cook meals, give heat in cold seasons, illuminate dark areas and protect from predators. Later, it also allowed making new materials like ceramics or glass and melting metals, and therefore, creating items like tools, weapons and buildings that contributed to difference the human being from the rest of species, and gave the possibility to shrive to the first civilizations.

However, accidents or the misled usage of fire has also brought negative consequences to humans since beginning of time, as wild fires. With the recent development of industry (especially chemical companies) and its requirement to use heating systems, electricity or operating with different substances at drastic conditions, the number of fires has increased (and with them, some collateral effects, like explosions), provoking several material damages, and often also deaths.

Due to the danger that fire supposes, science and engineering have tried to know its nature and predict its behaviour in order to prevent possible accidents. Given the complexity of all the phenomena involved in fires and the new possibilities that computers provide, simulation of fire phenomena has won a very important role in risk analysis. Simulation has even beaten experimentation, as these simulations perform the calculations very fast, do not require any economical expense, do not provoke environmental impact or suppose any risk. That is the main reason why it is necessary to know how well, data obtained from simulation, agrees with experimental results.

Precisely, validation is the concept that fits in the idea of checking how well calculated data explains a reality. The word validation is defined by Rubini (Björklund, 2009) in the lecture notes *Credible CFD-Verification and Validation* (Rubini, 2008) as:

"The process of determining the degree to which a model is an accurate representation of the real world from the perspective of the intended uses of the model".

Very often, validation and verification concepts seem difficult to be distinguished. Rubini (Rubini, 2008) defines verification as:

"The process of determining that a model implementation accurately represents the developer's conceptual description of the model and the solution to the model".

In other words, validation checks that the right equations are solved and verification checks that the equations are solved in the right way (Björklund, 2009).

This work will reproduce with the Fire Dynamics Simulator (FDS) experiments carried out by CERTEC some years ago with pool fires of gasoline and diesel, in order to validate the reliability of this so useful tool.

1 Introduction

1.1 Objectives

The main objective of this project is the validation of Fire Dynamics Simulator for well-ventilated, medium scale pool fires.

This project has as objective to find the most appropriate domain, grid size and geometry in order to get the results, which are more nearby to experimental data found in the same conditions as indicated in simulations. This project will also provide a sensitivity study that will indicate which parameters variations may affect most the simulation results.

1.2 Scope

Due to lack of time and computational resources, the scope of this project has been reduced to only gasoline and diesel pool fires of 1.5 m in diameter. As specific composition of gasoline and diesel was unknown, a model for the simulation of the thermal pyrolysis reaction could not be set, and therefore, equivalent formulas for the fuels had to be chosen for the combustion and mass loss rate per unit area had to be specified as a constant value.

All the experimental data used for the simulation results checking has been extracted from the PhD thesis of Josep Maria Chatris Riu (Chatris, 2001), Miguel Ángel Muñoz (Muñoz, 2005) and Fabio Ferrero (Ferrero, 2006).

As chosen domain, due to lack of computational resources, was considerably narrow, radiometers could not be set, as these could not be placed at the same positions as Muñoz and Ferrero did. Therefore, only temperature and flame height results are considered in this project, as radiation measured several meters away from the fire cannot be obtained from the simulations.

Specific evaporation and reaction models are not specified, and therefore, parameters involved in the evaporation phenomena, such as fuel boiling temperature, could not be considered in the sensitivity study. Due to lack of time, only fuel properties involved directly in FDS hydrodynamic models or related to empirical estimations of flame lengths were studied.

1.3 Finality

The finality of this project is to serve as guide for future users of FDS for the simulation of well-ventilated large or medium scale pool fires. In order to provide solid arguments for the usage of certain domains, grid sizes, pool shapes and fuel properties and reach then, the most appropriate simulation scenario, which could provide the simulation results most approximated to reality.

The sensitivity study has as finality give a tool for future FDS users in order to identify which parameters could be incorrectly specified if simulation results seem to be wrong, as this indicates how simulation temperature results at different positions vary when some fuel properties do.

2 Background

2.1 Fire types

Oxford Dictionary for advanced learners defines *fire* as:

"Set of flames, light, heat and often smoke that are produced when something burns, that is, when a combustion reaction takes place".

A flame could be defined as a chemical reaction producing temperatures of the order of at least 1500 K, and a fire, as a turbulent ensemble of flames (Quintiere, 2006). This chemical reaction, called combustion, is a drastic oxidation. This combustion requires a substance to be ignited (combustible), a heavy oxidizing substance (oxygen) and a source of energy that permits to beat the barrier of activation energy and so, start the reaction, which can be external (for example, a spark) in the case of piloted ignition or thanks to temperature in the case of auto ignition.

However, the word *fire* also refers to the spread of flames that go out of control and become destructive, and, in this denotation of fire, is it possible to distinguish between wild fires and industrial fires. Industrial fires are normally provoked by the leak of a flammable substance that takes place under conditions that provide the energy needed to start a combustion (a spark, a high temperature...) and of course, inside an oxidizer atmosphere, within which oxygen is able to oxidize the leaked flammable substance.

Depending on the physical state and the motion of the fuel, fires product of a leak can be classified into different groups:

<u>Product of a Liquid Fuel Leak</u>

- Pool fires, which will be described with more detail in the next section.
- Moving fires, which happen after a liquid in movement (for example going a slope down) is ignited.
- Fireballs, which happen after a BLEVE (Boling Liquid Expanding Vapour Explosion), when an external fire provokes the heating of a recipient containing a liquid fuel, it explodes after the evaporation of the combustible and sudden increase of pressure and finally the leaked fuel vapours are ignited.

<u>Product of a Gas Fuel Leak</u>

- Flares or flash fires, product of the ignition of gas fuel clouds.
- Jet fires, product of the ignition of a high-velocity flux of gas.

2.2 Pool Fires

According to Health and Safety Executive, a pool fire is a turbulent diffusion fire burning above a horizontal pool of vaporising hydrocarbon fuel where the fuel has zero or low initial momentum. In a first stage, liquid fuel is evaporated when the energetic barrier defined by the vaporization enthalpy is beaten; in a second stage, fuel vapour reacts with oxygen, in presence of a source of ignition or temperature enough to begin the auto ignition.

In this kind of fires, once the fuel has been ignited and the flame appears, the liquid receives heat by convection and radiation from the flame and exchanges heat to the surface below the layer of burning fuel. Convective heat transfer driven by induced flow movement is of particular importance in the early stage of fire growth, when the radiative contribution is small (Yao et al., 2013).

The phenomenon of exchange between flame and surface becomes especially important when the surface under the fire is water or metallic structures, which are sensitive to temperature changes and could lose their mechanical properties. In the first case, heat exchange may become very important due to the high capacity of heat absorption of water at ambient temperature, which will help to weaken the fire unless the ignited fuel is cryogenic. If the fire lasts several hours under a relatively thin layer of water, *boilover* or evaporation of water layer may happen.

The pools may have any form of geometry, but, as simplifying hypothesis, in experimental studies most authors consider, an equivalent circular shape with just one dimension, a characteristic diameter D, as Hamins and Kashiwagi proposed (Hamins et al., 1995).

The main features of this kind of fires are:

- In pool fires, once fire is established, flames transfer the heat required by the liquid to burn in a feedback mechanism. This supposes an equilibrium state, which is reached few seconds after the ignition begins. The soot production, turbulence fluctuation and fire size are parameters which play an important role in the determination of the heat feedback from the flames to the pool surface (Yao et al., 2013). However, the feedback ratio does not vary with the fuel layer thickness (Ferrero, 2006).

- Turbulence is significantly increased with the diameter of the pools. Pools of less than 0.1 m in diameter present laminar flux flames. When the diameter is increased, combustion speed increases too, and slowly the flux is no longer conditioned by buoyancy and is conditioned by inertial forces (Muñoz, 2005).

- In pools of more than 1 m of diameter, large amounts of soot are produced because fuel is not completely burnt in all regions of the flames. This makes these fires well ventilated in open areas, but under-ventilated in most of cases within enclosures.

- Flame height (L) is about the double of the fire diameter (D), as different empirical relationships, as equations (*2.7*) and (*2.8*) reflect.

- Because of vortex formation, flame height oscillates between a maximum and a minimum value (authors that performed former studies considered as flame length the mean value between maximum and minimum). The vortex formation and extinction frequency (vortex shedding) depends on the pool diameter, according to equation (*2.13*), (Pagni, 1989).

2.3 Characteristic parameters of pool fires

2.3.1 Radiation and surface emissive power

Heat transfer is the phenomena that consist in the release of thermal energy from a given system to another one, which is colder, until a thermal equilibrium between both systems is reached. Heat can be transferred through conduction (if energy is transported through a solid), convection (if energy is transported through a fluid media) and radiation (if heat transport is performed by electromagnetic waves between an emissive body and a receptor).

In fires, heat is released through radiation emission (Q_r) and convection between flames and hot smoke to environmental air (Q_c). In pool fires, as was explained before, a feedback mechanism is established, in which flames give energy to the liquid fuel (Q_f) cyclically once fire is established and until its burnout. Heat balance of a pool fire flame can be expressed as:

$$\dot{Q} = \dot{Q}_r + \dot{Q}_c + \dot{Q}_f \tag{2.1}$$

Flames release heat in all three dimensions. However, three dimensional analysis of energy spread can be tedious as radiometers cannot measure radiation contribution of fire products (water steam, CO_2 and carbon particles), therefore, in order to measure in a simple form how strong radiation-emitter a flame is, surface emissive power was introduced (Cowley & Johnson, 1991). This parameter is defined as the heat emitted by radiation per unit area of flame surface and it given by equation (*2.2*) and expressed commonly in kW/m^2.

$$E = \varepsilon\sigma\left({T_{flame}}^4 - {T_\infty}^4\right) \tag{2.2}$$

In hydrocarbon pool fires, radiation phenomena is very important, as hot soot (carbon particles product of the combustion reaction of hydrocarbon fuels) behaves as a black body in terms of radiation emission (Muñoz, 2005), producing very bright flames.

Emissivity (ε) is a factor compressed between 0 (white body) and 1 (black body), it is different for different materials. Average emissivity of a flame can be expressed as the difference of the sum of all constituents' partial emissivity and a corrector factor for the overlapping of CO_2 and H_2O bands. Chatris, after several experiments measuring thermal radiation in gasoline and diesel pool fires through temperatures caught by thermographic cameras, saw that emissivity increased with the pool diameter, until arriving to a constant value of 0.94, finding a correlation, equation (*2.3*), where pool diameter (D) must be expressed in meters (Chatris, 2001).

$$\varepsilon = 0.94 - \frac{0.035}{D} \tag{2.3}$$

A flame is constituted by different species, its radiation has a continuous component in the case of smoke (soot), which behaves as a grey body and shows a continuous spectrum that goes from visible light zone to infrared, while gaseous components (mainly water vapour and carbon dioxide) emit radiation in discrete spectral bands.

In (Muñoz, 2005) two models are proposed in order to estimate surface emissive power of a flame, for gasoline (*2.4*) and diesel (*2.5*) respectively, based on the flame fraction that is

occupied by a luminous zone and a non-luminous zone and their contributions to the radiation emission (E_{soot}=40 kW/m^2 and 40 kW/m^2<E_{lum} <120 kW/m^2):

$$E = 0.45E_{lum} + 0.55E_{soot} \quad (2.4)$$

$$E = 0.30E_{lum} + 0.70E_{soot} \quad (2.5)$$

Turbulence assumes an important role in the development of a fire, flow motion does not follow a constant tendency, combustion reaction speed may vary and heat transfer is not constant. This is the reason why it is necessary to difference between punctual emissive power at a given instant of time and average emissive power (Muñoz, 2005).

Muñoz also found that radiative fraction of a pool fire, (the fraction between the total heat emitted as radiation and the theoretical combustion heat), only depends on the pool size. It increases with the diameter until $D = 4\,m$ and from this to larger sizes, radiative fraction decreases, as equation (*2.6*) illustrates.

$$\chi = \begin{cases} 0.158D^{0.15}, & D \leq 4\,m \\ 0.436D^{-0.58}, & D > 4\,m \end{cases} \quad (2.6)$$

2.3.2 Flame length

Since the decade of 1950, different authors have studied flame lengths in fires. One of the first studies was performed by Blinov and Khudiakov (Blinov et al., 1957), who realized that in laminar and transitory regimes, the fraction between the mean length of the flame (L) and the pool diameter (D), L/D decreases when pool diameter rises, reaching an approximate constant value of $L/D = 2$ in turbulent regime.

However, was in 1963 when Thomas developed one of the most used empirical relationships between maximum flame height and diameter, involving more parameters, such as mass loss rate per unit area and air properties (Thomas, 1963):

$$\mathrm{L} = 42\ \mathrm{D}\left(\frac{\dot{\mathrm{m}}''}{\rho_\infty\sqrt{\mathrm{g\ D}}}\right)^{0.61} \quad (2.7)$$

Probably, the most used empirical correlation nowadays is the Heskestad equation (Heskestad, 1998). This expression was developed under the hypothesis that chemical reaction is instantaneous, and grovelled air under the flame is just the necessary to allow the reaction and the moved air amount is proportional to the stoichiometric requirements of the reaction:

$$L = D(-1.02 + 3.7Q^*) \quad (2.8)$$

Where Q^* is a parameter introduced in 1985 by Zukoski et al. (1985) defined by the equation (*2.9*).

$$Q^* = \frac{\dot{\mathrm{m}}'' \cdot \Delta \mathrm{H}_c}{\rho_\infty \cdot Cp_\infty \cdot T_\infty \cdot D^2 \cdot \sqrt{g\ D}} \quad (2.9)$$

In addition of proposing equation (*2.7*), Thomas also studied the effect of wind on flame length and found a relation with the structure of equation (*2.10*):

$$L = \alpha\, D \left(\frac{\dot{m}''}{\rho_\infty \sqrt{g\, D}} \right)^{\beta} u^{*\gamma} \qquad (2.10)$$

Where α, β and γ are different constants and u^* is the non-dimensional wind speed, which can vary according to wind speed (u) and characteristic wind speed (u_c):

$$u^* = \begin{cases} 1, & if\ u < u_c \\ \dfrac{u}{u_c}, & if\ u \geq u_c \end{cases} \qquad (2.11)$$

Characteristic wind speed can be defined as:

$$u_c = \left(\frac{g \cdot \dot{m}'' \cdot D}{\rho_\infty} \right)^{1/3} \qquad (2.12)$$

Different authors have proposed several different values of α, β and γ according to their results (Muñoz, 2005). This data is summarized in Table 2.1.

Table 2.1. Summary of the diverse empirical coefficients for flame length determination.

Reference	Year	α	β	γ
Thomas (without wind speed infl.)	1963	42	0.61	0
Thomas (wind speed influenced)	1963	55	0.67	-0.21
Moorhouse - Cylindrical	1982	6.2	0.254	-0.044
Moorhouse- Conical	1982	4.7	0.21	0.114
Mangialavori and Rubino	1992	31.6	0.58	0
Pritchard and Binding	1992	10.615	0.305	-0.03
M.A. Muñoz et al.	2004	11.5	0.375	-0.1

2.3.3 Vortex shedding

After several experiments with different fuels and pool sizes, Pagni (1989) established a correlation that relates frequency of vortex-formation that an observer can appreciate as the fluctuation of the flame length, as equation (*2.13*) indicates. This phenomena must not be confused with the flame flickering in laminar diffusion flames, for example of a candle, which is independent of the diameter (Pagni, 1989).

$$f = 1.5\, D^{-1/2} \qquad (2.13)$$

2.4 Computational simulation of fire phenomena

Fires can be modelled through two types of widely used fire models: zone models and field models (Muñoz, 2005).

- Zone models divide the study domain into two regions: a hot region and a cold region. These models are based on empirical relationships between different fire parameters and are much simpler than field models. Their results are not as realistic as results given by field models, because many more simplifications are used.

- Field models are based on Computational Fluid Dynamics (CFD), a branch of fluid mechanics that, due to the calculation complexity of the differential equations involved in the problems related to the flux of fluids, uses algorithms and numerical methods with the aid of a computer, which performs these operations considerably faster. These models divide a control volume into different cells, where Navier Stokes equations of mass, species, momentum and energy conservation are solved. The large calculation capacity of modern computers to solve these operations make these models a suitable option for fire modelling nowadays.

CFD models can be divided into three types, according to the strategy of resolution of the equations (Björklund, 2009):

- **Direct Numerical Simulation** is a CFD method that implies to solve the Navier Stokes transport equations directly, what requires a huge computational capacity and makes this method unpractical for most engineering applications, including fire simulations.

- **Reynolds Averaged Navier Stokes (RANS)** is a numerical method that uses as approach the decomposition of instantaneous values to a mean value with fluctuations. Softwares based on RANS method (for example, SOFIE) are recommended to be used for steady state simulations because this method executes Taylor expansion series with convergence for every time step (Björklund, 2009). This makes it independent of what has happened earlier (in time) in the simulation, which is appropriate for steady state fires. However, this strategy is not recommended to perform simulations with many time steps, due to lack of time efficiency.

- **Large-eddy simulation (LES)** is a numerical technique for integrating spatially filtered equations of motion that describe high-Reynolds number time-evolving, three-dimensional turbulence. Given this limitation, only a portion of the scale range can be explicitly resolved. LES solves just the most important scales of the flow of interest and approximates the other scales. As the grid resolution of LES becomes finer, a wider range of turbulent eddies is resolved, less are parameterized, so an excessive fine mesh would imply a Direct Numerical Simulation. LES is, then, a compromise between Direct Numerical Simulation (DNS, in which all turbulent fluctuations are resolved) and traditional RANS approach (in which all turbulent fluctuations are parameterized and only ensemble averaged statistics are calculated). In LES, every calculation is based on the calculation performed in the previous time step.

2.5 Simulation tools description

This work has been performed at CERTEC premises, located at 2nd floor of G building of ETSEIB (*Escola Tècnica Superior d'Enginyeria Industrial de Barcelona*) which belongs to UPC University (*Universitat Politècnica de Catalunya*). CERTEC (*Centre d'Estudis del Risc Tecnològic*) is an organization, founded in 1992, which has as objectives the research and formation of specialists in the field of industrial risk, dividing its activity into four main sections:

- Risk analysis in process industries
- Environmental impact evaluation
- Research on wild fires
- Research on indoor fires

CERTEC disposes of 5 computers reliable to do simulations, with Intel core i7 processors, which have 4 physical cores. 4 of these have 64 bits version of Windows 8, which is needed for using more than 4 GB of RAM memory. These computers can solve at the mean time four different meshes.

Table 2.2. Summary of CERTEC computer used for simulations and their features[1]

CERTEC ID	Processor	Velocity	Cores	Threads	RAM	OS
41	Intel® Core i7-3770	3.4 GHz	4	8	16 GB	WIN 8
42	Intel® Core i7-3770	3.4 GHz	4	4	16 GB	WIN 8
44	Intel® Core i7-3770	3.4 GHz	4	4	16 GB	WIN 8
45	Intel® Core i7-3770	3.4 GHz	4	8	16 GB	WIN 8

Simulations have been carried out with CERTEC 41. This computer, as 42, 44 and 45 have installed FDS v. 6.2.0 (SVN 22343). From FDS 6 forth, computational time is significantly higher, so *OpenMP* (Multi Processing that allows paralleling internal tasks of FDS if the computer has multiple cores) and *MPI* (Multiple mesh running for a same simulation) strategies must be followed.

Offices also dispose of personal computers with Intel Core2 vPro™ processors, which have 2 physical cores and can solve two meshes at the same time.

[1] A computer performs the calculations with the help of its *CPU* or *processor*. These processors may have multiple *cores*, which at the same time contain different execution *threads*, which are the process basic units capable to work in parallel.

3 Fire Dynamics Simulator

3.1 FDS mathematical models

3.1.1 Hydrodynamic model

Fire Dynamics Simulator (FDS) is a CFD (Computational Fluid Dynamics) software, developed by the National Institute of Standards of Technology, which applies large eddy simulation (LES) numerical method to solve low speed (low Mach numbers), heat-driven-flow Navier-Stokes equations for a single or multiple species fluid. These low-speed equations are obtained by filtering out pressure waves from Navier-Stokes equations (Floyd et al., 2003), so they allow for large variations in density but not in pressure, fact that conditions its applications to simulation of stages with no significant sudden pressure changes. As FDS is developed to low-speed flows (Ma≤0.3), it cannot be used to model flow, which involves speed approaching the speed of sound, for example, explosions (Nielsen, 2013).

FDS uses sub-grid models to calculate that which cannot be resolved in the largest eddy (grid). In the model used in FDS for turbulence modelling, small eddies (cells which are not completely filled with the same obstacle) are filtered off and solved by the Smagorinsky turbulence model (Björklund, 2009) in former versions and by the Deardorff turbulence model from the version 6 forth. However, if cell size is too small (under 1 mm width), calculations are performed through DNS strategy (McGrattan et al., 2014).

LES equations used by FDS are derived by applying a low-pass filter parameterized by a width δ to the transport equations for mass (*3.3*), momentum (*3.4*), species (*3.5*) and energy (*3.6*). For example, the 1-Dimensional filtered density[2] field for a cubical[3] cell of width $\Delta = \delta x$ is (Mcdermott et al., 2011):

$$\bar{\rho}(x,t) = \frac{1}{\Delta}\int_{x-\frac{\Delta}{2}}^{x+\frac{\Delta}{2}} \rho\,(x,t)\;\, d\rho \tag{3.1}$$

Filtering of pressure shows the same structure. However, velocity, species fractions, temperature and enthalpy, and any ϕ scalar quantity must be filtered through Favre-filters (Wen et al., 2006). Favre-filtered quantities are denoted by a tilde and are defined as:

$$\tilde{\phi} = \frac{\overline{\rho\phi}}{\bar{\rho}} \tag{3.2}$$

The Navier Stokes filtered equations, which are governing flow motion in FDS are, for the i[th] component of velocity are (Wen et al., 2007):

$$\frac{\partial \bar{\rho}}{\partial t} + \frac{\partial \bar{\rho}\tilde{u}_j}{\partial x_j} = 0 \tag{3.3}$$

[2] Material properties, such as density, which are not denoted with a subscript, correspond to the fluid, which is a mixture of different species.

[3] $\Delta = \sqrt[3]{\delta x \delta y \delta z}$, what supposes $\Delta = \delta x$ when cubical cells are used.

$$\bar{\rho}\left(\frac{\partial \tilde{u}_i}{\partial t}+\frac{\partial \tilde{u}_i\tilde{u}_j}{\partial x_j}\right)=-\frac{\partial \bar{p}}{\partial x_i}+\bar{\rho}g+f_i+\frac{\partial \tau_{ij}}{\partial x_j} \tag{3.4}$$

$$\frac{\partial(\bar{\rho}\tilde{Y}_e)}{\partial t}+\frac{\partial(\bar{\rho}\tilde{u}_j\tilde{Y}_e)}{\partial x_j}=-\frac{\partial}{\partial x}\left(\overline{\rho u Y_e}-\bar{\rho}\tilde{u}\tilde{Y}_e\right)+\frac{\partial}{\partial x}\left(\overline{\rho D_e\frac{\partial \tilde{Y}_e}{\partial x_j}}\right)+\bar{\dot{m}}_e'''' \tag{3.5}$$

$$\frac{\partial(\bar{\rho}\tilde{h})}{\partial t}+\frac{\partial(\bar{\rho}\tilde{u}_j\tilde{h})}{\partial x}=\frac{D\bar{p}}{Dt}-\frac{\partial \dot{q}''_{r,j}}{\partial x_j}+\frac{\partial}{\partial x_j}\left(k\frac{\partial \tilde{T}}{\partial x_j}\right)+\sum_e\frac{\partial}{\partial x_j}\left(\bar{\rho}D_e\tilde{h}_e\frac{\partial \tilde{Y}_e}{\partial x_j}\right)+\dot{q}''' \tag{3.6}$$

Where g is the gravity, $\bar{p}$ is the total (fluid average) pressure, k is the mixture thermal conductivity[3], t is the time and ρ is the mixture density. u, x and $\dot{q}''_r$ refer to velocity, position and radiation heat release vectors respectively (in the i,j and k directions); D_e, h_e and Y_e are respectively the diffusivity[4], the enthalpy and the fraction of an e species. f_i is the drag force due to unresolved lagrangian particles, which will not affect in the cases studied in this project, as there is not any lagrangian particle. τ_{ij} is the stress due to viscous forces, which can be found according to equation (*3.7*). Finally, $\dot{m}'''_e$ and $\dot{q}'''$ are the source terms of their respective equations, determined through FDS combustion model (McGrattan et al., 2014).

$$\tau_{ij}=2(\mu+\mu_t)\left(\frac{1}{2}\left(\widetilde{\frac{\partial u_\iota}{\partial x_j}}+\frac{\partial u_\jmath}{\partial x_\iota}\right)-\frac{1}{3}(\nabla\cdot\tilde{u})\delta_{ij}\right) \tag{3.7}$$

Mass and species transport is governed by equations (*3.3*) and (*3.5*) respectively, while momentum and thermal energy are governed by equations (*3.4*) and (*3.6*) respectively. In addition to these main governing equations, FDS uses an ideal gases equation (*3.8*), which includes density and fluid average molar mass, in order to compute temperature at each time step (McGrattan et al., 2014).

$$\rho=\frac{\bar{p}M}{RT} \tag{3.8}$$

As can be seen in equation (*3.7*), viscous stress depends directly on velocity components, on fluid viscosity (computed by FDS from density, velocity and grid size) and on turbulent (or eddy) viscosity, which is modelled from FDS version 6 forth through a slight modification of Deardorff turbulence model (equation (*3.9*)), which also depends on velocity components, density and grid size. δ_{ij} is Kronecker delta, which is 1 if $i=j$ or 0 if $i\neq j$ (McGrattan et al., 2014).

$$\mu_t=\rho C_v\Delta\sqrt{k_{sgs}} \tag{3.9}$$

$$k_{sgs}=\frac{1}{2}(\bar{u}-\hat{u})^2+(\bar{v}-\hat{v})^2+(\bar{w}-\hat{w})^2 \tag{3.10}$$

k_{sgs} is the *subgrid scale kinetic energy* per unit mass, $\bar{u}$ is the average value of the u velocity component at the grid centre, while $\hat{u}$ is the weighed value of u over the adjacent cells (the respective values for v and w components are determined exactly). C_v is a constant value

[4] Both diffusivity and thermal conductivity are estimated from turbulent viscosity and turbulent Schmidt and Prandtl numbers respectively, which are constant values set to 0.5 by default. These numbers can be modified by FDS users, although its modification is not recommended. See FDS user's guide (Mcgrattan, 2015b) for further information.

(Smagorinsky constant), which is 0.1 by default and can be changed, although bibliography recommends this value (Deardorff, 1980).

Calculation of turbulent viscosity can be performed also through other models if the user indicates which model will be used. Vreman and Smagorinsky turbulent viscosities, however, also depend on velocity components, density and grid size. This is the reason why the most affective input variables seem to be fluid density (which depends on user-defined liquid fuel density), grid size and velocity (which can be modified as the environmental wind speed).

3.1.2 Combustion model

A source common of confusion in FDS and, generally, in fire science, is the distinction between gas phase *combustion* and *pyrolysis* (in case of solid phase) or liquid phase vaporization. While, pyrolysis refers to the reaction of formation of flammable fuel vapour and oxygen from a source fuel in solid phase, combustion refers to the chemical reaction between flammable fuel vapour and oxygen. In this project, flammable fuel vapours formation rate is given by a constant mass loss rate per unit area (see section 5.2). However, parameters such as formation of combustion products and heat produced due to the chemical reaction are modelled through a combustion model.

In order to model combustion, last FDS version uses a single-step, mixing controlled fast chemistry combustion model (Mcgrattan et al., 2015b), which is based on the mixture fraction model used in FDS previous versions. This former model considers that the reaction is infinitely fast, as by default, FDS considers a non-premixed combustion (Kwon et al., 2007) (this can be modified through changing the option INITIAL_UNMIXED_FRACTION (ζ_0), set to 1 by default in LES and to 0 in DNS (Mcgrattan et al., 2015b)). Diffusive and convective time needed is much higher than the time for combustion reactions to occur, which is supposed to be zero (Kwon et al., 2007). Although FDS considers by default infinitely fast reactions, users are allowed to define Arrhenius-law parameters in order to model non-infinitely fast reactions.

Only a fuel is possible to be used in FDS v.6, although from version 5 forth is it possible to set lumped-species fuels (mixtures of different pure chemical substances that constitute a single fuel); unfortunately, this feature could not be used, as exact chemical composition of fuels was not known. For an infinitely-fast combustion, the reaction of fuel and oxygen is not necessarily complete, and reactant species in a given grid cell are converted to product species at a rate determined by a characteristic mixing time, t_{mix} (McGrattan et al., 2014).

FDS models the combustion as a partially stirred batch reactor, and the used combustion turbulence model is based on the eddy dissipation concept model for initially unmixed reactants, that considers that “all mixed is burnt"; it implies that fuel vapour disappearance is controlled by the limiting reactant at a rate set by mixture time (McGrattan et al., 2014). The basic idea behind the model used by FDS in order to determine characteristic mixing time is to consider the three physical processes of diffusion (t_d), subgrid scale advection (t_u), and buoyant acceleration (t_g), and to take the fastest of these processes (locally) as the controlling flow time scale. However, the mixing time must be larger (or at least equal) than time required for the chemical combustion reaction to take place t_{chem}, which is zero by default. Then, mixing time is given by equation (*3.11*).

$$t_{mix} = \mathrm{Max}(t_{chem}, \min(t_d, t_u, t_g) \tag{3.11}$$

$$t_d = \frac{\Delta^2}{D_{mix}} \tag{3.12}$$

$$t_u = \frac{0.4\,\Delta}{\sqrt{{}^2/_3\ k_{sgs}}} \tag{3.13}$$

$$t_g = \sqrt{\frac{2\Delta}{g}} \tag{3.14}$$

The unmixed fraction decreases with time, according to equation (*3.15*) (McGrattan et al., 2014).

$$\zeta(t) = \zeta_0 e^{-{}^t/_{t_{mix}}} \tag{3.15}$$

Once the unmixed fraction at a given computational cell is known, the composition of this point at any time step ($\widetilde{Y_e}(t)$) may be determined according to equation (*3.16*). The product of the time differential of the *e* species composition and the mixture density gives the species source term used in equation (*3.5*). Known the composition of an *e* species in a given point, the variation of mean fuel mass concentration can be also determined according to equation (*3.20*) in the fast chemistry model that FDS uses by default (McGrattan et al., 2014).

$$\widetilde{Y_e}(t) = \zeta(t)\widetilde{Y_e^0} + (1 - \zeta(t))\widehat{Y_e}(t) \tag{3.16}$$

$$\dot{m}_e''' = \rho \frac{d\widetilde{Y_e}(t)}{dt} \tag{3.17}$$

$$\Delta\hat{Y}_F = -min\left(\hat{Y}_F\,, \hat{Y}_e\ \frac{\nu_F M_F}{\nu_e M_e}\right) \tag{3.18}$$

Heat release rate per unit volume obtained from the gas phase chemical reaction (source term of equation (3.6)) can be found as the sum of products between species formation rate and enthalpy of formation for all species (McGrattan et al., 2014).

$$\dot{q}''' = -\sum_e \dot{m}_e''' \Delta h_{f,e} \tag{3.19}$$

Enthalpies of formation of combustion products and common fuels are by default stored in FDS library. However, in the case of non-common fuels or mixtures like gasoline, the user is obliged to specify either the enthalpy of formation of the fuel or its heat of combustion, from which this former parameter is calculated. In addition, FDS could calculate heat release rate as the product of depleted oxygen mass flux and heat release per mass of oxygen consumed. See section 12.1.2 of FDS User's Guide (McGrattan et al., 2015b) for further information.

According to Nielsen (2013), FDS combustion model makes a good approximation for large-scale, well ventilated fires, but in under-ventilated fires, in FDS Technical Reference Guide Vol.1 (McGrattan et al., 2014) is it proposed to introduce a burn no burn criterion to make possible the mixing of fuel and oxygen without combustion. However, in the simulation of pool

fires at the open air, default FDS model is noticed to work properly and therefore, no changes have been made for this study.

As seen through these equations, critical parameters in FDS for combustion modelling are computational cells width, fluid density, velocity, heat of combustion, stoichiometry and molar mass, which, in order to be computed, the fuel chemical formula is specification is necessary.

3.1.3 Thermal radiation transport model

While heat transfer by convection is estimated by solving the filtered Navier-Stokes equations, FDS calculates the net contribution from thermal radiation to heat release as (McGrattan et al., 2014):

$$\dot{q}_r''' = \kappa(x)\left[\int_{4\pi} I(x,\vec{s})d\vec{s} - 4\pi I_b(x)\right] \quad (3.20)$$

For a non-scattering gas, radiation intensity I emitted in $\vec{s}$ direction is obtained by solving the radiative transport equation:

$$\vec{s}\cdot\nabla I_\lambda\,(x,s) = \kappa(x,\lambda)[I_b(x) - I_\lambda\,(x,\vec{s})] \quad (3.21)$$

However, an exact solution of this equation may result very computationally expensive given the dependence on electromagnetic wavelength λ. This problem may be solved by considering the global radiation intensity as the sum of N different partial intensities corresponding to the N different bands in which the electromagnetic spectrum is divided. As each band has its own absorption coefficient $\kappa(x)$ (which depends on the cross sectional area of the radiation emitting particles and on optical parameters, and due to their complexity, further study of absorption coefficients is out of the scope of this project), radiation intensity of an n band is given by the expression *(3.22)* for n=1, 2, 3...N.

$$\vec{s}\cdot\nabla I_n\,(x,\vec{s}) = \kappa(x)[I_b(x) - I_n\,(x,\vec{s})] \quad (3.22)$$

Despite dividing the total spectrum into different single bands, calculation is computationally expensive and some simplifications must be done:

- In large scale pool fires, soot production is much higher than CO_2 and water steam production, and as radiation spectrum of soot is continuous, gas released by a fire can be considered as a grey medium (McGrattan et al., 2014) with a single band. This is the default mode of FDS.

- In optically thin fires, soot production is smaller and then, contributions of CO_2 and water steam are most relevant, and considering all gas as a grey medium would imply an over-prediction of the emitted radiation (McGrattan et al., 2014). In most cases, dividing the spectrum into 6 bands provides good enough results. However, as fires simulated in this work are considered of large scale, no further investigation in this aspect will be performed.

In FDS, radiation intensity of the black body (source term) at a given x position is calculated from the temperature raised to the forth power in this position. However, temperatures inside the flame zone can be under estimated if grid size is not fine enough, what provokes a high error in the source term, as this depends on the temperature raised to the forth power.

This is the reason why FDS provides two options in order to determine the radiation source term, as equation *(3.23)* reflects, allowing to determine radiation inside flame through a product between total heat release rate and a radiative fraction that users can specify (0.35 by default) (McGrattan et al., 2014). For regions outside flame, as temperatures are not under estimated, this source term is estimated through the expression at right of equation *(3.23)*.

$$\kappa(x) \cdot I_b(x) = Max\left(\frac{\chi \cdot \dot{q}'''}{4\pi}, \frac{\sigma T(x)^4}{\pi}\right) \tag{3.23}$$

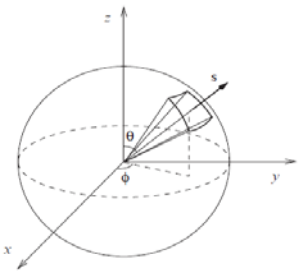

Figure 3.1 Circumference of all possible directions to which radiation is emitted. Image taken from FDS Technical reference guide vol. 1 (McGrattan et al., 2014).

For an emissive particle, radiation is emitted in all the directions (describing a circumference, as Figure 3.1 shows). However, as is dividing this circumference into infinite angles would require an infinite number of $\vec{s}$ vectors for equation *(3.22)*, FDS solves the radiations transport equations on a spherical mesh with a finite number of discrete angles, which can be modified by the user and are 100 by default (Nielsen, 2013).

3.2 Previous validation work performed in FDS

Different validation efforts have been performed to confirm that FDS gives simulation results, which represent the reality, even before the first public release in February of 2000. Since FDS version 5 was released, its developers also publish a FDS Validation Guide (McGrattan et al., 2015a) that recompiles validation work performed by different authors previously to the release of the publication. This compilation includes validation of different FDS features, such as fire plumes modelling, pool fires, air and gas movement, wind engineering, atmospheric dispersion, growing fires, flame spread, compartment fires, suppression by water, airflows, tunnel fires, smoke detection, combustion model and soot deposition.

Validation tests were performed through the comparison of experimental data, empirical correlations or theoretical expressions. However, validation work with FDS done so far is very wide and, therefore, all the available information cannot be written here. The validation results published by different authors related to the theme of this project (found in the FDS Validation Guide or in other projects, reports, thesis and articles) are summarized below in chronological order.

3.2.1 Validation studies mentioned in FDS Validation Guide

One of the first validation works for FDS was performed by Ma et al., (2003) in FDS v.2. They compared predicted flame lengths to empirical correlation of Heskestad (equation (*2.8*)), finding a good agreement in the plume region, but a high grid-size dependence for the region near the flame, especially for low Q^* fires. These authors and a researcher's team from NIST, at the meantime, arrived to the conclusion that $D^*/\delta x$ is a critical parameter. The authors found that if this parameter can be considered well-resolved, agreement with empirical correlations was good; however, if $D^*/\delta x$ is not large enough model is not well resolved and results obtained from simulations did not have a good agreement with empirical correlations, which seemed logical, given the high grid-dependence of the resolution of filtered Navier Stokes equations.

Hostikka et al., (2003) reproduced small and low sooting pool fires of methane and natural gas in FDS in order to explore the application of Large Eddy Simulation to model pool flames. The pool diameters tested were 1, 10, 30 and 100 cm in a computational grid of 50x50x100 cells, whose size varied among 0.525, 2.1 and 5.0 cm. They focused in testing the radiation solver, finding that the predicted radiative fluxes are higher than measured values in both radial and vertical positions, especially when the heat release rate was low. The results, obviously, showed that, turbulence increased significantly with the pool diameter, showing different flame shapes for the four different pool dimensions, but measured values of burning rates were significantly different to predicted values. However, this work proved that there is a qualitative dependence between pool size and burning rate in the results provided by the simulator.

In 2004, Hietaniemi, Hostikka and Vaari (Hietaniemi et al., 2004) simulated different heptane pool fires of various diameters in FDS v.4, in order to compare how experimental data, taken from the recompilation of 1999 by Hamins and McGrattan (Hamins et al., 1999) and simulation results agreed. They found that the curve that relates the burning rate per unit area and the pool diameter obtained from simulation results drew the same tendency as the experimental curve, but this first was scarcely displaced to the right (to larger pool diameter values).

Xin (Xin, 2005) simulated a one-meter diameter methane fire, where FDS v.4 was used in order to model a 1 m diameter methane pool fire in a computational domain of 2×2×4 m using a cell width of 2.5 cm. This author realized that there was a good agreement between the data calculated by FDS and the experimental results of Tieszen and co-workers (Tieszen et al., 2004) obtained at Sandia National Laboratory, despite some discrepancy in the vertical velocity of the fires when radiation heat loss is not considered (15 % higher approx.). However, this work confirmed the viability of FDS in simulating relatively large pool fires.

3.2.2 Wen, Kang, Donchev and Karwatzki (2006)

In 2006, Wen, Kang, Donchev and Karwatzki carried out a validation work for FDS when it is used for predicting medium-scale pool fires (Wen et al., 2007). They simulated a medium-scale methanol fire placed in a rectangular computational domain of 1.6 m width, 1.6 m depth and 3.2 m height with all boundaries set as open, excepting the ground. They found that a narrow width and depth (less than 4 times of burner diameter) gave incomplete description of air entrainment, but that the usage of a large domain (more than 8 times the diameter width and depth) would imply using a coarser grid size due to the limit of the computational capacity of their computers. They used three different grid sizes: 64×64×96 cells (coarse), 108×108×108

cells (medium) and 128×128×128 cells (fine) and the pools were modelled as circular surfaces, which were combination of different rectangular obstacles. Temperature distributions for these three grid sizes and experimental data by Weckman and Sobiesiak (Weckman et al., 1988) were compared, finding that larger discrepancy was given by the simulation carried out with coarser cells. Finally, fine grid size was selected in order to perform a study of comparison of default FDS combustion mixture fraction model and an additional sub-grid-scale combustion model based on the laminar flamelet approach in temperature and axial velocity distributions.

The results showed that FDS version 4 could provide accurate predictions for most important parameters of pool fires that are of significance in the fire safety context, such as mean values of temperature, axial velocity distributions, and the air entrainment ratios. Flame heights also showed reasonable values, as simulations showed that flame zone reached a height comprised between one and two pool diameters. The overall agreement demonstrated the robustness of the FDS mixture fraction combustion model for medium-scale pool fire predictions.

3.2.3 Trouvé - Second International Energy 2030 Conference (2008)

Trouvé presented in November of 2008 an article (Trouvé, 2008) which focused on studying the change observed in flame structure when its size is increased from laboratory to large scales. Predictions of combustion efficiencies, soot yield and radiant fractions showed limited success when FDS v.5 was applied to open and wind-free pool fires. However, few substitutions of FDS default models were made, in order to let flame extinction as a combination of slow mixing conditions and radiation cooling and setting flame extinction as the dominant mechanism for soot mass leakage across the flame. FDS simulations performed with these modifications showed more accuracy.

This author used for the simulations square approximations for the pool fires, defining a characteristic dimension of the square burners (H), and performing simulations for fires from $H = 0.4\ m$ to $H = 40\ m$ of characteristic dimension size. This article denoted that the increased importance of smaller flames and smaller length scales at larger pool diameters in order to obtain realistic flame heights are translated into higher computational grid requirements. However, grid requirement for LES of large-scale pool fires was proposed to be as high as condition reflected by equation *(3.24)* expresses:

$$\frac{H}{\delta_x} \geq 300 \tag{3.24}$$

Combustion efficiency, soot yield and radiant fraction were studied for pool fires of different diameters. Radiant fraction decreases with the pool size from an approximate 50% when the characteristic dimension size is 0.4 m to less than 20% when this dimension is 40 m, while combustion efficiency scarcely decreased with the diameter, from 100% until an approximate 95% in the fires of 0.4 m and 40 m respectively); soot yield did not vary with the pool diameter.

3.2.4 Chen, Dembele, Wen and Tam (2009)

Chen, Dembele, Wen and Tam simulated a LNG spill in a lake as 14 m diameter pool in a computational domain of 100×100×100 m (Chen et al., 2009). As required computational capacity was high, the domain was divided into several meshes to facilitate parallel computing

on multi-processor computers, and grid size for the fire and surroundings was finer than for the rest of the domain. Their results of a comparison between experimental and simulation data of centreline temperatures in the pool fire showed a similar tendency as experimental data by McCaffrey (McCaffrey, 1975), and showed that it is incorrect to extrapolate laboratory-scale experiments results to large-scale pool fires, as radiation decrease with the fire size must be contemplated.

3.2.5 Nielsen (2013)

Nielsen thesis in Aalborg University (Nielsen, 2013) dealt with a very wide validation study of FDS (v. 5) capacities for indoor pool fires. Aware of the restriction of FDS to create only rectangular geometry obstacles, a same pool fire was simulated through a pool with the same surface area, a pool with an equivalent circumference and another one with the same hydraulic diameter. Results showed that pool with the equivalent circumference of the original circular fire gave the best results. This denoted that despite the simplification of pool fires to square surfaces performed by most of authors, circular surfaces provide better results. However, in this study, an additional accuracy study of square equivalent of originally circular pools will be carried out.

A domain study was also performed, according to velocity profiles in a door of a compartment. The results concluded that domain should be extended about the equivalent distance of the door height beyond the door of the simulated room.

This author, found for all comparisons performed even though FDS may under or over predict parameters (because properties of involved materials, geometry or other factors may not be identical in real experiment and FDS simulation), it reproduces the increase and decrease in the parameter at approximately the same time as the real experiment. FDS is expected to provide, then, good relative results (which should indicate if tested values are increased or decreased) in a sensitivity study. Despite the over and under prediction of some parameters, difference between FDS and experimental data did not reach the 10% in steady state and the 20% in transitory regimes. Exceptionally, a high discrepancy of 45% between experimental and FDS data was observed during the fire extinction of one of the performed comparisons.

Despite of confirming the capability of FDS to provide good results within a relatively small uncertainty interval, flame length was much higher than expected in one of the studied cases. This error was supposed to be committed because of a higher HRR, from the fire, which created a higher temperature in the top of the room and then created a stepper gradient between the top and bottom of the domain.

3.2.6 Kelsey, Gant and McNally (2014)

In 2014, Kelsey, Gant and McNally published an article after performing a severe sensitivity study of different parameters in the behaviour of liquefied natural gas (LNG) pool fires in FDS v.6 (Kelsey et al., 2014).

Experimental design contemplated the variation of different parameters, which were supposed to cause effect on the flame height and air entrainment simulation results. The modified parameters were the pool fire diameter, the burning rate, the radiative fraction, the grid

resolution and the turbulence model (the authors used both Smagorinsky and Deardorff methods).

These authors decided to use a domain of 3×3×8 m^3 and different values of $D^*/\delta x$ in a rank from 16 to 40; pool fire diameters ranged from 10 to 100 m, burning rate ranged from 0.05 to 0.5 kg/(m^2·s) and radiative fraction ranged from (0.2 to 0.35). The sensitivity analysis showed that the fire diameter has a dominant effect on both flame height and entrainment velocity. The influence of the other input parameters differed, depending upon which model output was analysed: the flame height was almost completely dependent on fire diameter and burning rate, while the entrainment velocity was sensitive to the mesh resolution and turbulence model. In finer meshes, the predictions of the air entrainment velocity from the Smagorinsky and Deardorff turbulence models became almost identical. This behaviour is consistent with the fact that a greater proportion of the turbulence energy should be resolved with a finer grid.

The variable, which affected most both flame height and air entrainment, was pool diameter, followed by burning rate in air entrainment. The other varied parameters had little influence.

3.2.7 Pachera, Brunello, Raciti and Castelli (2015)

Recently, in 2015, Pachera, Brunello, Raciti and Castelli used FDS v. 6 to simulate an experiment carried out previously by the Technical Research Institute of Finland (Pachera et al., 2015), where a pool fire of 4.9 kg of heptane were burned in a room of 10 m wide, 10 m long and 5 m high. The experiment was reproduced with three different grid sizes: coarse (20 mm), medium (13.9 mm) and fine (10.0 mm); the fire was ventilated through an open window. They also used two different ways to predict the amount of fuel used in the reaction: in the first case, mass flow rate was imposed according to the experiments and in a second case, it was calculated through an evaporation model. In both cases, satisfactory results were obtained for temperature distribution and for species concentration. All grid sizes showed results following the same tendency as experimental data; fine and medium mesh simulations over-predicted temperatures and carbon dioxide volume fraction time evolutions, and under predicted oxygen volume fraction time evolution, unlike coarse mesh simulation, which under predicted temperature and carbon dioxide fraction time evolution. Was precisely the coarse mesh simulation, which provided the results were most nearby to the experimental data.

Smoke layer height was also measured for all three-grid sizes, showing a very scarce difference between real data and FDS simulations data and between the three cell dimensions. Both initial state and steady state (after 600 s) were, then, good predicted.

For data obtained through the added evaporation model, as the default turbulent mixing model could be too fast, a calibration of maximum heat release rate per unit volume was performed using coarse mesh (which showed the best results and spent the minimum time), finding a good approximation to reality with HRRPUV limited to 700 kW/m^2.

4 Experimental scenario description

4.1 Installations description

In this project, different experiences performed by Chatris, Muñoz and Ferrero in their respective PhD thesis will be reproduced with FDS simulations. In order to build the simulation scenario and judge the experimental results, it is essential to know how the installation was were the experiments were carried out. Experimental place will be described according to the information provided by these authors.

The experiments were performed between 1999 and 2006 at the specialized centre *Can Padró*, at the outskirts of Sant Vicenç de Castellet, province of Barcelona. This location is provided with different outdoors concentric pools of different diameters (initially 1.5, 3, 4 and also 5 and 6 m since an enlargement that took place between 2003 and 2004) with walls made of concrete, as Figure 4.1 shows. These delimiter walls had a width of 12 cm in all cases and a height that varied from 21 cm in the smaller pool to 44 cm in the most external circumference. In pools of small areas liquids must not leave the most concentric region and in the case of pools with larger areas, liquids must occupy the most external regions, but also the inner areas. These pools were filled with water until its level arrived near the total height of the delimiter walls to be finally marked up with a fine layer of fuel.

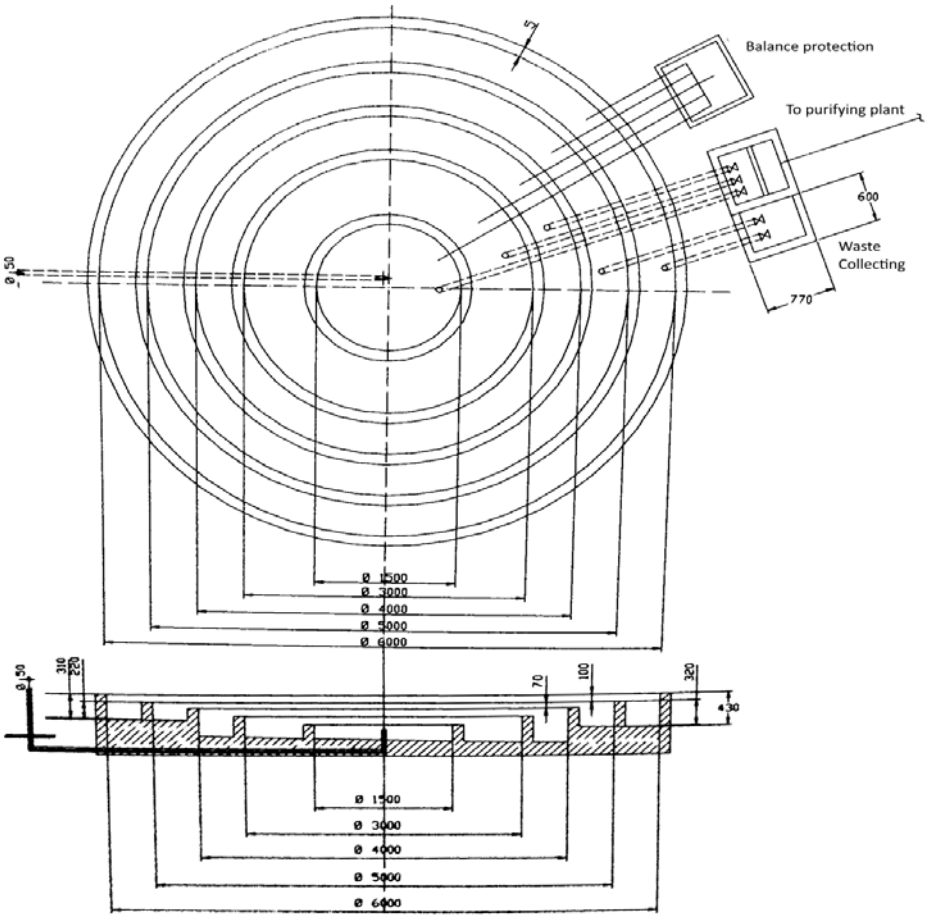

Figure 4.1 Scheme of concentric concrete pools installation. Dimensions indicated in millimetres.

4.2 Measurement of temperatures

4.2.1 Contact method

Temperatures inside the flame were taken by different K type thermocouples set at the axis of the central pool. Thermocouples were fixed in ceramic bars, which had to offer excellent mechanical properties of resistance against high temperatures. Bars laid over different steel profiles attached to an electrical-type metal tower that was divided into two stretches: one of 8 meters height and an extension of 4 additional meters height and was placed at 4 m from the most external pool. The tower was based in a support structure of 1.2x1.2x1.5 m^3 and the whole structure was coated with antioxidant paint and with a with a Spraywool-F recovering. Properties of this coating are properly described in (Chatris, 2001).

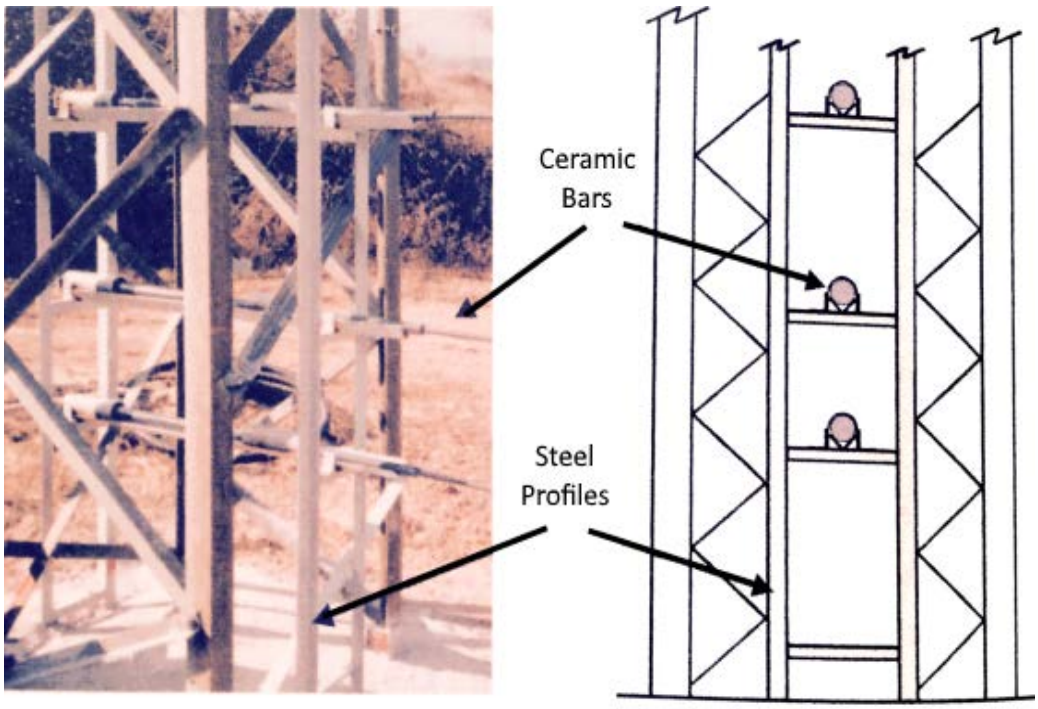

Figure 4.2 Thermocouple support structure detail (ceramic bars and steel profiles)

In these experiences, thermocouples, isolated with an Inconel 600 coating in order to resist temperatures around 1200 ˚C, were set along different axial and radial positions, which varied with the experiments, inside and outside the flame region, and even inside the mass of water laying under the fuel. Chatris only used 14 thermocouples with the similar features, while Ferrero used 32 devices of different bead diameters with different characteristics according to the location where they were located.

While Chatris set thermocouples all along the whole tower height, Muñoz and Ferrero divided the study temperatures into three zones (Ferrero, 2006):

- A region inside the liquids, water and fuel.
- A region of continuous flame, in which flame shedding does not appear.
- An intermittent flame region, in which flame oscillates.

In FOC_03 project data, used by Muñoz and Ferrero, temperatures corresponding to radial positions were only measured in the continuous flame region. In order to set thermocouples in positions out of the pool axis, an additional structure was used. This structure was composed by two metallic towers with basis, placed 1 m away from the most external pool; that had different subjection elements every 10 cm, which allowed setting wires, where thermocouples were placed. A special paint coat and an additional coating of rockwool was applied in order to protect the towers from the action of flames. In the edges of the structure, a system of weights and pulleys counteracted the effect of the thermal dilatation.

As Ferrero explains in his thesis, thermocouples used in continuous flame region presented a bead diameter of 1 mm and 1.5 mm while thermocouples in intermittent zone had a bead diameter of 3 mm and therefore, had a higher response time, as controlling instantaneous values when the thermocouple is found alternatively in contact with flame and smoke. Devices set inside the liquid were provided with a special coating and had bead diameters of 1 mm in order to provide a fast response. Schemes indicating the position of thermocouples in continuous and intermittent flame region are shown in Figure 4.3 and Figure 4.4 right respectively.

In all experiments performed by Chatris, Muñoz and Ferrero, thermocouples were made of the same materials. Positive and negative thermoelements were made of cromel and alumel, respectively, whose chemical composition is specified in Table 4.1 (Ferrero, 2006).

Table 4.1. Chemical composition of positive and negative elements of thermocouples.

Chemical Composition	KP-Cromel	KN-Alumel
Ni	90%	95%
Cr	10%	-
Al	-	2%
Mn	-	2%
Si	-	1%

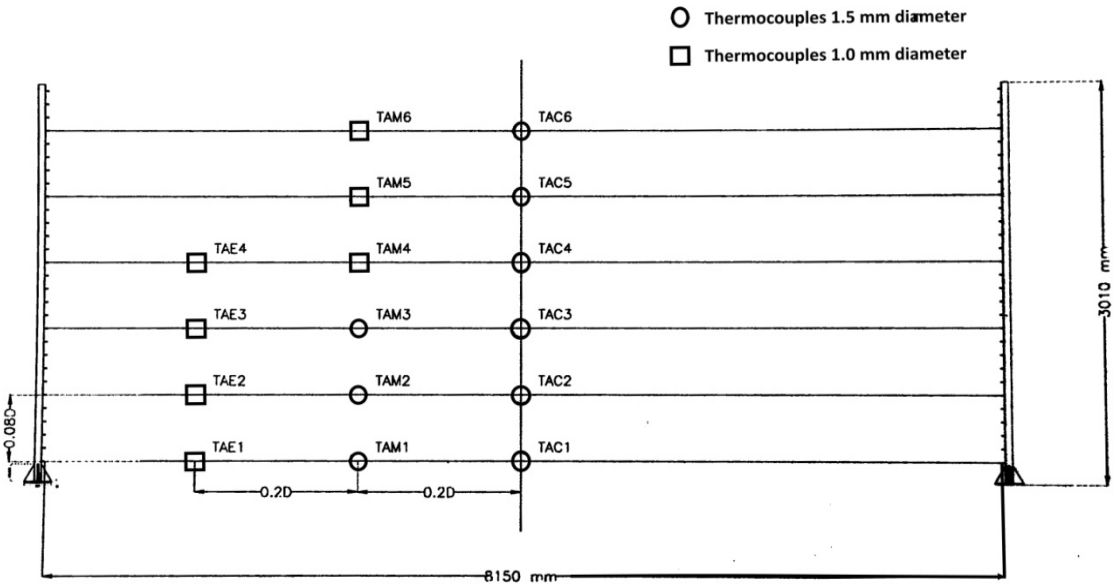

Figure 4.3 Scheme of thermocouples position in continuous flame zone used in FOC_03 campaign experiments.

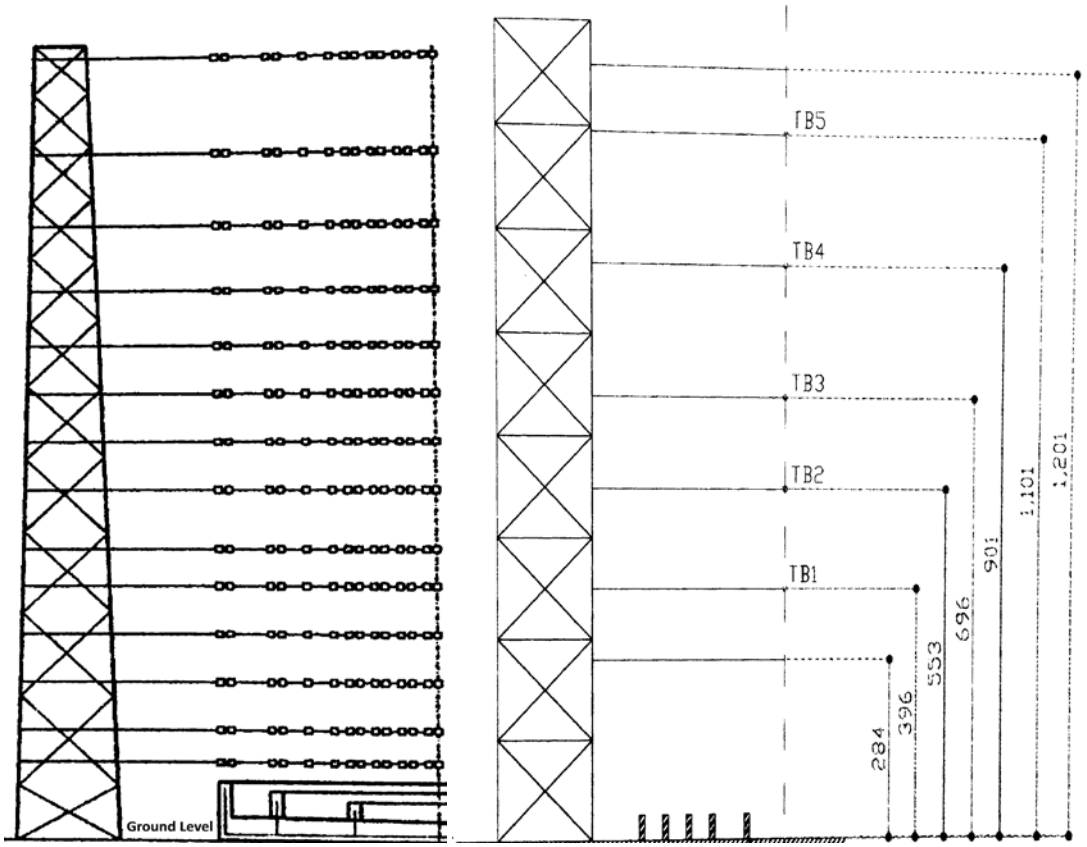

Figure 4.4 Scheme of thermocouples placed along the tower in Chatris (left) and Muñoz/Ferrero experiences (right).

4.2.2 Thermographic camera method

Additionally to the direct method for measurement of temperatures, these were also obtained by analysing images extracted from films recorded by a thermographic camera working in infrared spectrum, which had a vision field of 24º×18º at a minimum zoom distance of 0.5 m. This method is not explained further, as it cannot be reproduced with FDS and therefore, will not be considered in the studies of the present project.

Temperatures measured through thermocouples (maximum values near 1000 ˚C for a pool fire of 4 m diameter) were significantly lower than values measured from the images caught by thermographic camera (maximum values near 1250 ˚C for a pool fire of 4 m diameter). Both techniques were used as complementary, as thermography permitted to establish a complete characterization of flame surface temperatures and thermocouples took measures inside the flame.

4.3 Measurement of other variables

4.3.1 Mass burning rate

Burning rate was determined as a mass loss rate of fuel, showed by the shrinking of the level of fuel along the experiments. Variations of fuel layer thickness were related to the loss of weight detected by a balance, away from the zone where fire was provoked, which weighed a recipient connected to the pool by flexible and rigid tubes, as Figure 4.5 shows.

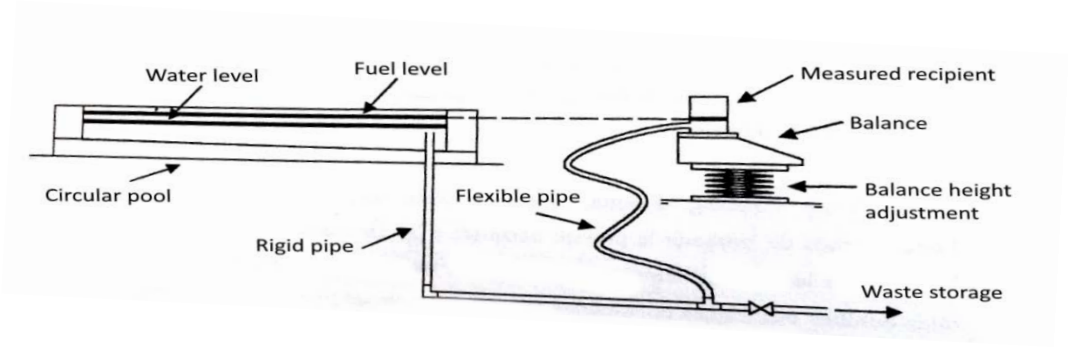

Figure 4.5 Burning rate measurement scheme.

This technique is not further detailed as burning rate will be defined in FDS simulations (see section 5.2) as a constant value corresponding to the steady state fuel mass loss rate per unit area measured in the experiments.

4.3.2 Thermal radiation

In order to determine radiation, Muñoz and Ferrero installed three radiometers *Schmidt-Boelter* thermopiles. Two of them were flux transductors model 64-2-16 (measurement range from 0 to 23 kW/m^2) and the other one was a dual sensor that measures total heat release and radiation heat transfer, model 64-20T-20R(S) (measurement range from 0 to 227 kW/m^2). The transductors were placed away from the fire, in order to measure only the radiation heat. The dual sensor was used to measure the heat flux that arrived to the fuel surface and was placed, so, inside the pool.

However, radiation devices used by Muñoz cannot be reproduced in FDS as the simulation domain needs to be quite narrow in order to avoid an excessive computational expense (see section 6.2). Therefore, radiation measurement systems will not be further detailed.

4.3.3 Ambient conditions

Environmental conditions were measured with the help of a meteorological station Davis Instruments *GrowWeather,* which was placed at 14 m from the pool axis by Chatris, at 25 m by Muñoz and at 40 m by Ferrero. This device could determine air and ground temperatures, wind speed, solar radiation, atmospheric pressure, humidity and dew point. This device stores data automatically every 30 minutes, but with the help of the software *FireAll*, it could register data every second.

Before starting the experimentation, the data station registered data every 30 minutes, in order to know how the wind speed behaved along the day and then, find the optimal hours to perform the experiences. The predominant direction of wind was found to be from west to east during the day and from east to west during the night. The best hours to perform the experiments were found to be during morning.

While experiences were carried out, however, meteorological station registered data with its maximum speed, in order to determine the exact evolution of the meteorological variables in the development of the fire.

4.3.4 Flame lengths and inclinations

Flame contour definition currently accepted was proposed by Cowley and Johnson in 1991, as the region in which products of combustion emit light in the visual spectrum (Cowley et al., 1991). Flame length was considered, then, the highest point of the flame contour.

Muñoz and Ferrero used video cameras recordings in order to study the time evolution of flame geometries and observe in which instants flame is out of the set thermocouples due to the action of wind, and then, judge which punctual measures can be eliminated from the study. These films were also useful to control empirically the fire behaviour and permit the analysis of the part of the flame, which is covered by smoke. In the case of Ferrero, sound tracks of the videos were also useful to determine the instant when the boilover occurs.

As flames are three-dimensional bodies, two cameras were disposed perpendicularly between them, and one of the devices was orthogonal to the dominant direction of wind. However, if wind speed was not exactly perpendicular to the camera, flame lengths and inclinations observed in images could be corrected if the angle between the wind direction and the normal to the vision line was known.

Cameras provided 25 frames per second, which were stored in files of extension .jpg that were loaded to Matlab®, which converts them to matrices of dimensions equal to the image sizes. Muñoz designed a Matlab® program that allows the user to determine flame length of every frame by selecting manually the highest point of the flame contour.

4.4 Experimental results by Chatris (2001)

Chatris designed different experiences considering pool fires of different diameters (1.5, 3.0 and 4.0 m), different fuels (gasoline and diesel) and with thermocouples set at different axial and radial positions, measured respectively from the fuel layer surface and from the pool axis respectively, as explained in the last section. Table 4.2 summarizes the features of every experience.

The different experiences were performed during the first hours of morning. This condition guaranteed the experiments reproducibility, in presence of scarce wind. As the geographical emplacement where these experiments were carried out usually suffers strong winds of variable direction, some adverse phenomena occurred, as displacement of the flame to a region out of the measurement range of thermocouples, and therefore, some of these experiences were repeated.

Due to safety measures, the performance of the different experiences was carried through three independent phases, one for each pool diameter. The pool size that was studied first was 1.5 m and after performing all experiments featuring this diameter, pool dimensions were increased. Every time that pool diameter was changed, a preliminary test was carried out using diesel oil (PREFOC1, 2 and 3), in order to put into practice all actuation logistics.

According to Chatris conclusions presented in his thesis, temperatures appeared in the pool fire which had the biggest diameter, and that this value was registered approximately at the axial position corresponding to the third part of the flame average height. Time evolution of

temperatures and of mass loss rates allowed dividing the fires into different stages (an initial transitory regime, a stationary regime in which all parameters remained approximately constant and a final transitory regime, which corresponded to the fire burnout).

Chatris presented its data in different folders, but the notation of its data is different from what is indicated in the table below. Every folder contained 14 files called from TP1 to TP14, which are supposed to indicate the temperature values registered by every thermocouple. Some experiments had more than one folder: for example, experiment FOC2 was divided into four different folders (FOC2, FOC2_R, FOC2_S, FOC2_T, and FOC2_U) and FOC1 into three folders. It was not possible to identify what the notation R, S, T and U means, but probably, these letters could refer to different radial positions for thermocouples. As specific positions of thermocouples, as well as time scale, could not be identified, only three figures indicating registered values for the case of gasoline are shown below. In order to be able to plot caught temperatures versus time, a time scale was chosen, supposing that temperature values are registered each 0.1 seconds, according to fire duration data indicated in the thesis (140-160 s).

Although most of thermocouples cannot be assigned to a concrete axial position, figures below help to find between which ranks of values found data comprises. Higher temperatures are caught by TP12 thermocouple in all cases and show similar maximum values (near 930 ˚C), which is supposed to be at the centre of the continuous flame region, while flame does not arrive to TP14 (pink curve).

Table 4.2. List of all experiments performed by Chatris during the development of his PhD thesis.

Experiment name	Fuel	Pool diameter [m]	Thermocouple axial positions [cm]	Thermocouple radial positions [cm]
PREFOC.1	Diesel	1.5	60.5, 94.5, 144.5, 194.5, 244.5	0
FOC.1	Diesel	1.5	60.5, 144.5, 244.5	0, 25, 50, 75
FOC.2	Gasoline	1.5	60.5, 144.5, 244.5	0, 25, 50, 75
FOC.3	Diesel	1.5	94.5, 194.5, 283.0	10, 35, 60, 85
FOC.4	Gasoline	1.5	94.5, 194.5, 283.0	10, 35, 60, 85
PREFOC.2	Diesel	3.0	60.5, 144.5, 445.0	0, 50, 100, 150
FOC.5	Diesel	3.0	60.5, 144.5, 445.0	0, 50, 100, 150
FOC.6	Gasoline	3.0	60.5, 144.5, 445.0	0, 50, 100, 150
FOC.7	Diesel	3.0	94.5, 283.0, 552.0	25, 75, 125, 160
FOC.8	Gasoline	3.0	94.5, 283.0, 552.0	25, 75, 125, 160
PREFOC.3	Diesel	4.0	60.5, 194.5, 445.0, 620.0	0, 100, 200
FOC.9	Diesel	4.0	60.5, 194.5, 445.0, 620.0	0, 100, 200
FOC.10	Gasoline	4.0	60.5, 194.5, 445.0, 620.0	0, 100, 200
FOC.11	Diesel	4.0	94.5, 283.0, 495.0, 794.5	50, 150, 210
FOC.12	Gasoline	4.0	94.5, 283.0, 495.0, 794.5	50, 150, 210

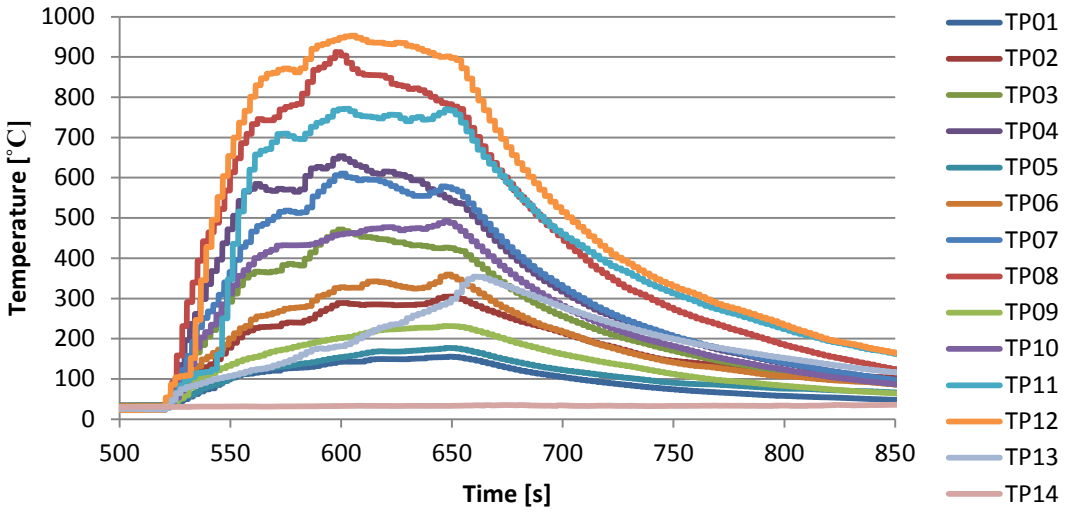

Figure 4.6 Time evolution of temperatures at different axial positions for FOC2 experiment.

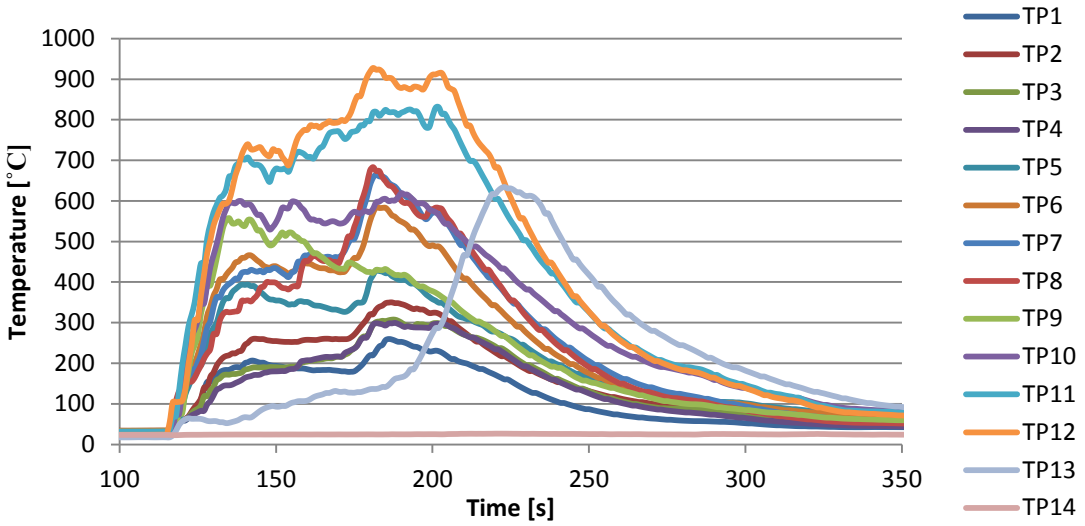

Figure 4.7 Time evolution of temperatures at different axial positions for FOC2_R experiment.

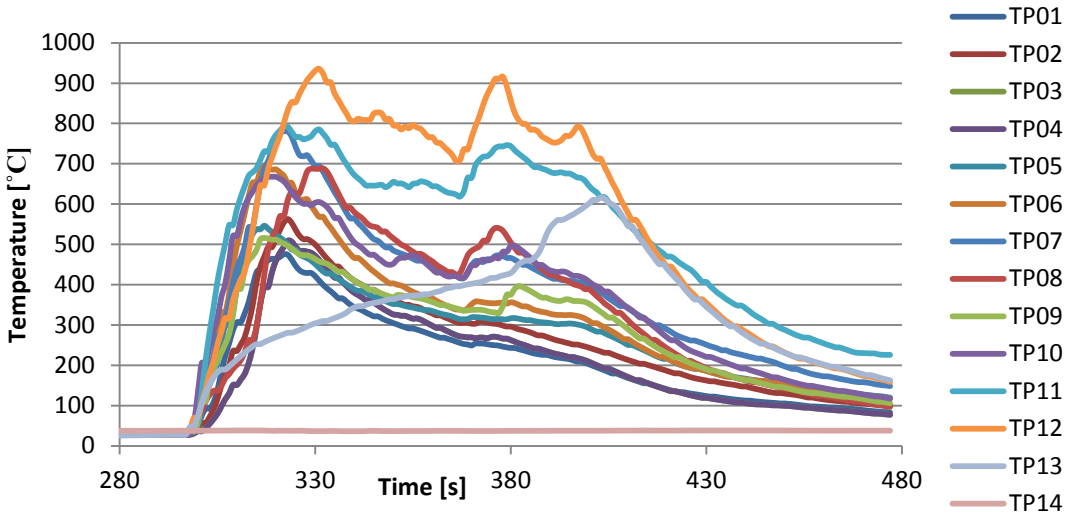

Figure 4.8 Time evolution of temperatures at different axial positions for FOC2_S experiment.

4.5 Experimental results by Muñoz (2005) and Ferrero (2006)

Muñoz and Ferrero used for the elaboration of his thesis data obtained years before by Chatris, as well as results provided by their own experiences, in an experimental data collecting project known as FOC_03, for which thermocouples registered new values every 0.5 seconds. All experiments performed in FOC_03 project are listed in Table 4.3. However, position of radiometers has not been specified, as it cannot be simulated in this project.

Due to lack of computational capacity, only the smallest pool size will be considered (1.5 m), which would correspond to FOC3_21 and FOC3_22 experiments.

Table 4.3. List of the different experiments carried out during the FOC_03 data collecting campaign.

Experiment Name	Fuel	Pool Diameter [m]	Fuel layer thickness [cm]	Fuel Density [kg/m^3]	Fire Duration [s]
FOC3_01_D3	Diesel	3	1.27	840	256.5
FOC3_02_D3	Diesel	3	1.50	840	306
FOC3_02_D3	Diesel	3	1.50	840	306
FOC3_03_G3	Gasoline	3	2.00	752.5	272
FOC3_03_G3	Gasoline	3	2.00	752.5	272
FOC3_04_D3	Diesel	3	2.00	840	436
FOC3_05_D3	Diesel	3	2.49	840	518
FOC3_05_D3	Diesel	3	2.49	840	518
FOC3_06_G6	Gasoline	6	1.56	752.5	311
FOC3_07_D6	Diesel	6	1.50	840	342
FOC3_07_D6	Diesel	6	1.50	840	342
FOC3_08_G5	Gasoline	5	1.50	752.5	169
FOC3_08_G5	Gasoline	5	1.50	752.5	169
FOC3_09_D5	Diesel	5	1.50	840	314
FOC3_09_D5	Diesel	5	1.50	840	314
FOC3_10_D5	Diesel	5	2.00	840	442.99
FOC3_10_D5	Diesel	5	2.00	840	442.99
FOC3_11_D5	Diesel	5	2.00	840	389
FOC3_12_D6	Diesel	6	2.00	840	436.56
FOC3_13_G4	Gasoline	4	1.50	752.5	205
FOC3_13_G4	Gasoline	4	1.50	752.5	205
FOC3_14_D4	Diesel	4	1.50	840	296
FOC3_14_D4	Diesel	4	1.50	840	296
FOC3_15_D4	Diesel	4	1.50	840	399
FOC3_15_D4	Diesel	4	1.50	840	399
FOC3_16_D4	Diesel	4	2.50	840	511.73
FOC3_16_D4	Diesel	4	2.50	840	511.73
FOC3_17_G3	Gasoline	3	1.50	752.5	200
FOC3_18_D3	Diesel	3	1.20	840	247.8
FOC3_19_M3	Mixture	3	2.00	796.25	269.54
FOC3_20_D3	Diesel	3	1.20	840	236.95
FOC3_20_D3	Diesel	3	1.20	840	236.95
Foc3_21_G15	Gasoline	1.5	1.81	752.5	275
Foc3_22_D15	Diesel	1.5	1.98	840	411

FOC3_21 experimental results

This experiment was carried out the day 21th July of 2004, at 9:31 h. The average ambient conditions during the experience were:

- Ambient temperature: 20.61 ˚C
- Atmospheric pressure: 995.57 hPa
- Solar radiation: 383 W
- Relative humidity: 91%

Comparison of time evolution of temperatures at different axial positions, for every radial position of thermocouples in the case of continuous fire zone, and axial positions in the case of intermittent zone, are presented in the following graphics. Notice that data corresponding to the time instants when the combustion had not been begun yet or fire had already been suppressed has been eliminated from the plot and axis have been adjusted to data referring to fire development.

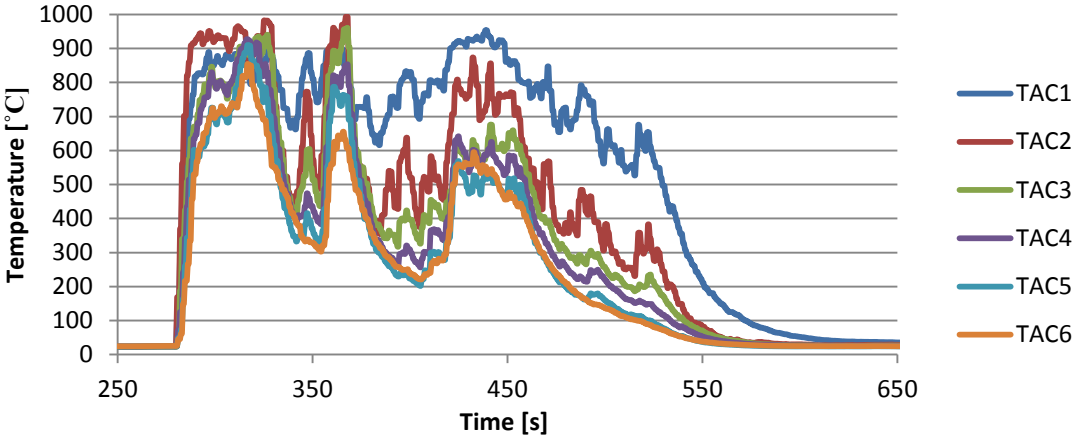

Figure 4.9 Time evolution of temperatures at the pool axis in the continuous flame region.

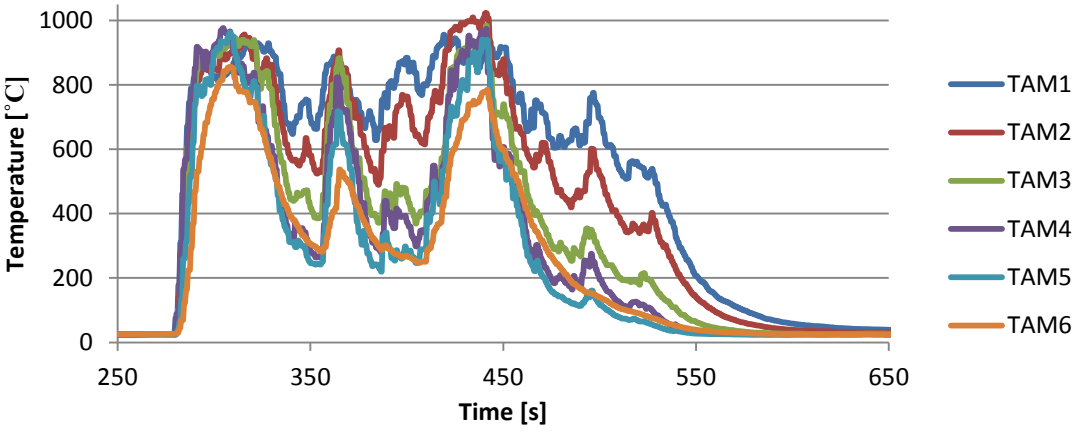

Figure 4.10 Time evolution of temperatures at a radial distance of 30 cm from the pool axis in the continuous flame region.

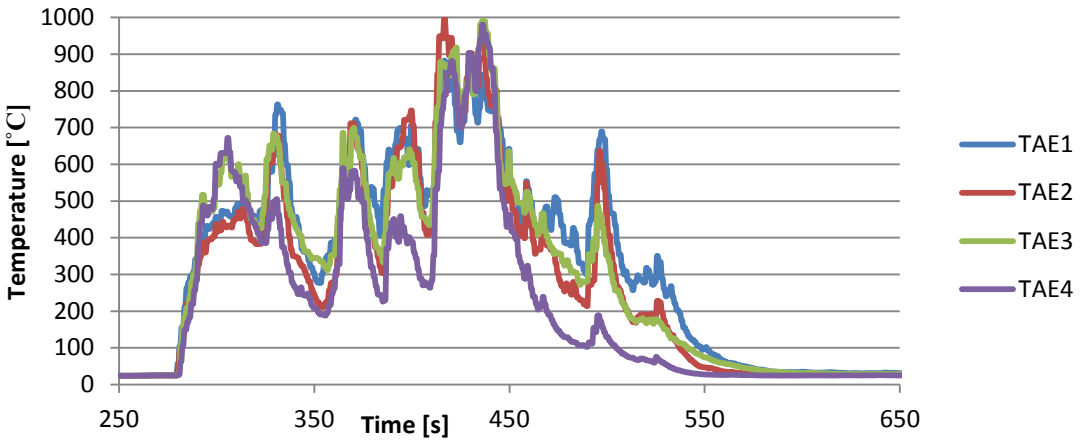

Figure 4.11 Time evolution of temperatures at a radial distance of 60 cm from the pool axis in the continuous flame region.

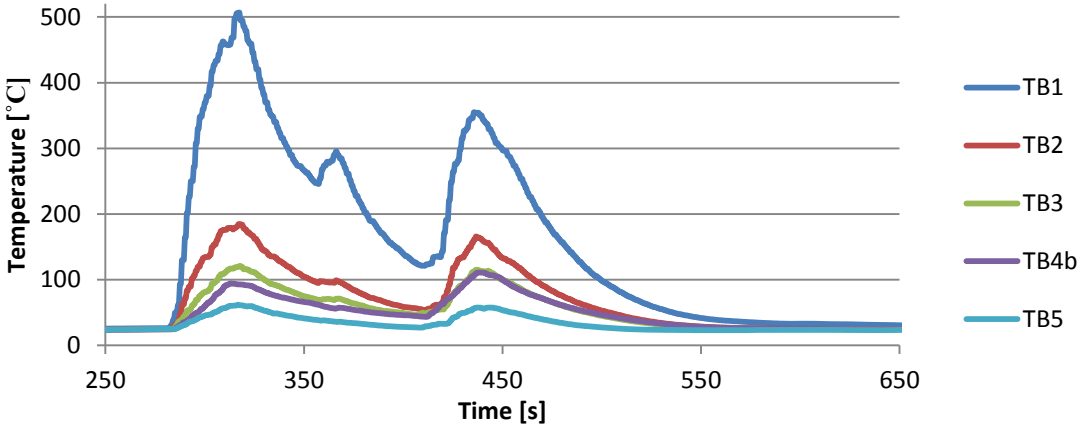

Figure 4.12 Time evolution of temperatures at the pool axis in the intermittent flame region.

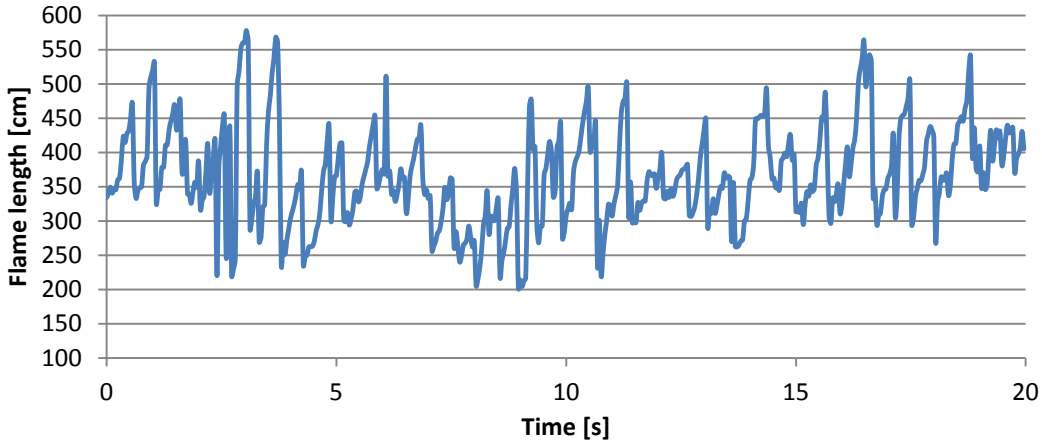

Figure 4.13 Time evolution of flame lengths during 20 seconds once the stationary regime is reached.

FOC3_22 experimental results

This experiment was carried out the day 21th July of 2004, at 10:05 h. The average ambient conditions during the experience were:

- Ambient temperature: 21.72 ˚C
- Atmospheric pressure: 995.57 hPa
- Solar radiation: 465 W
- Relative humidity: 91%

Comparison of time evolution of temperatures at different axial positions, for every radial position of thermocouples in the case of continuous fire zone, and axial positions in the case of intermittent zone, are presented in the following graphics. Notice that data corresponding to the time instants when the combustion had not been begun yet or fire had already been suppressed has been eliminated from the plot and axis have been adjusted to data referring to fire development.

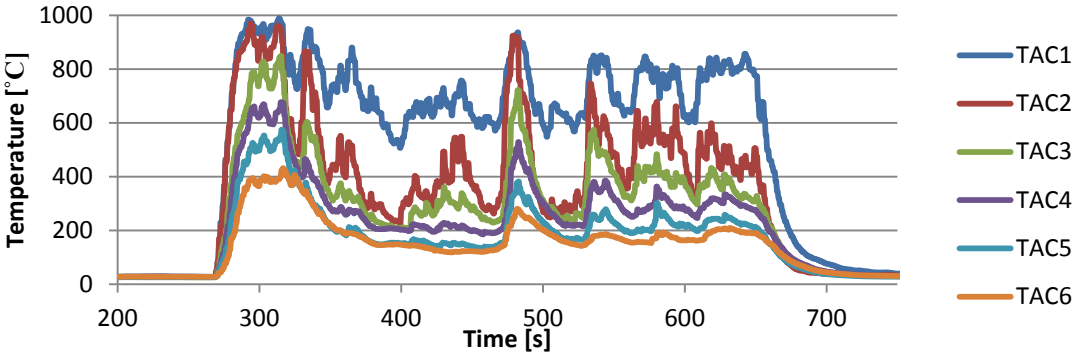

Figure 4.14 Time evolution of temperatures at the pool axis in the continuous flame region.

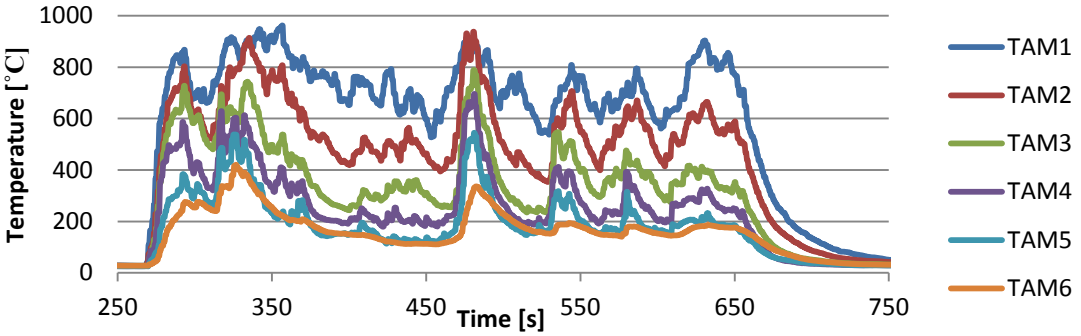

Figure 4.15 Time evolution of temperatures at a radial distance of 30 cm from the pool axis in the continuous flame region.

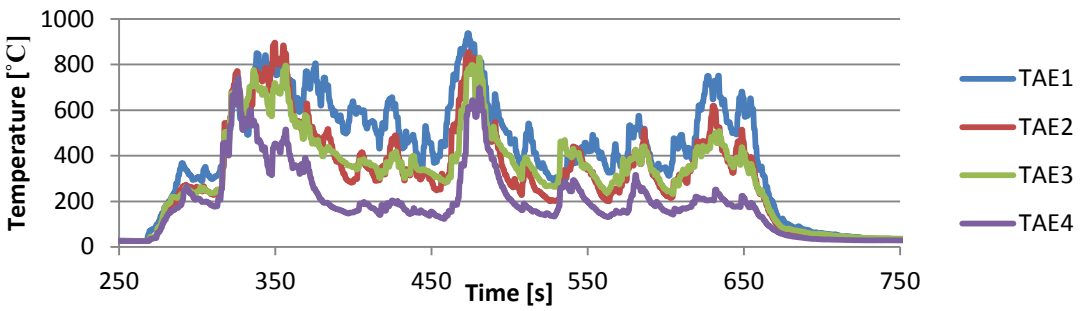

Figure 4.16 Time evolution of temperatures at a radial distance of 60 cm from the pool axis in the continuous flame region.

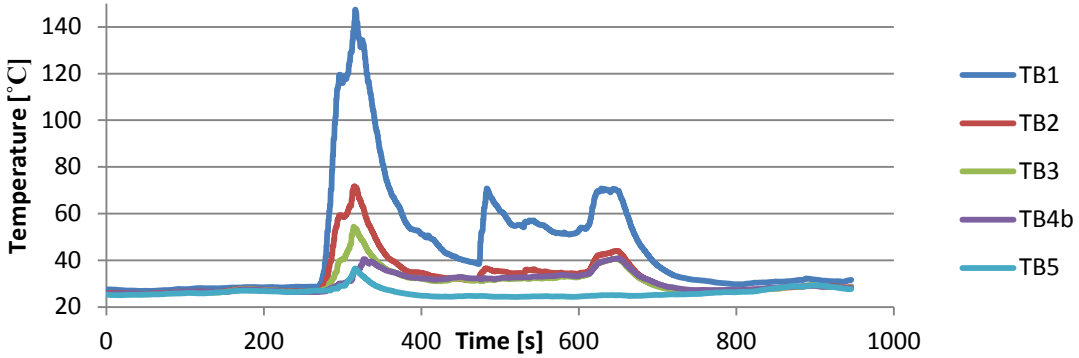

Figure 4.17 Time evolution of temperatures at the pool axis in the intermittent flame region.

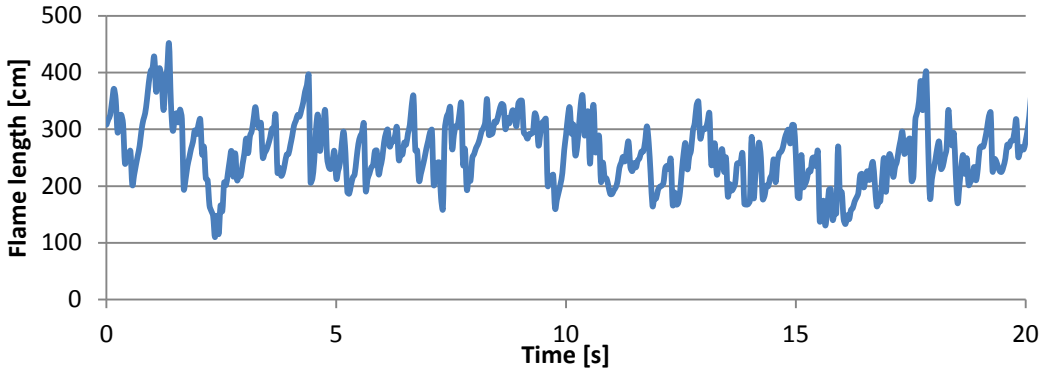

Figure 4.18 Time evolution of flame lengths during 20 seconds once the stationary regime is reached.

5 Definition of experimental scenario in FDS

5.1 Obstacles and ventilations

The experimental scenario has been modelled in FDS as a circular pool placed at the centre of a prismatic domain (with H height larger than D depth and W width, which have the same longitude) with a concrete floor at the $Z = 0$ plain (from 0 to 0.03125 m) and ventilations at the $X = 0$, $X = D$, $Y = 0$ and $Y = W$ plains. Due to the necessity of building cubic or prismatic obstacles in FDS, the pool was modelled through joining different prismatic objects, as Figure 5.1 shows. The pool is made of a liquid water mass that occupied from 1 (coarse grid size) to 5 cells height (fine grid size), placed under a fuel layer that occupied a single cell, and the whole circular contour is surrounded by a wall of concrete, that occupied a single cell. However, thickness used for calculations in FDS is not given with the number of cells, but with a surface option called *thickness* (Mcgrattan et al., 2015b). Fuel layer thickness and water mass depth were set to 2 and 18.75 cm height respectively and concrete wall width was set to 12 cm.

The initial pool was circular, as the scenario defined for FDS simulation was tried to be the most similar as possible to real experimental scenario. However, since many authors who simulated pool fires, given the difficulty to create non-rectilinear obstacles in FDS, used square approximations instead of circular pools, a pool shape study was performed, building scenarios with square pools centred at the simulation domain and setting the same *thickness* for the present obstacles.

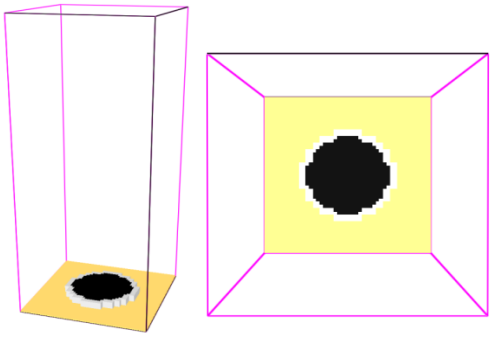

Figure 5.1 General and top views of a sample pool fire simulation.

5.2 Fuels and materials involved in the simulation

The fuels used in experimental pool fires were gasoline and diesel, whose exact chemical composition was unknown, as these fuels are a mixture of different hydrocarbons and no composition analysis were held. However, FDS needs to know the chemical composition of the fuels involved in the simulations, so equivalent chemical formulas were chosen, according to bibliography suggestions: C_7H_{14} for gasoline and $C_{16}H_{28}$ for diesel (Montes et al., 2014).

As exact composition of the fuels was not known, reactions of pyrolysis and therefore, of combustion could not be specified to FDS. This is the reason why burning rate had to be specified through fuel mass loss rate per unit area (MLRPUA) instead of being calculated from the reaction chemical kinetics parameters. Fortunately, mass loss rates per unit area were well

specified in the consulted thesis; MLRPUA chosen values for the simulations were proposed by Rew et al. (1997), as these were very similar to averaged values of MLRPUA registered in Chatris and Muñoz experiments.

Physical and chemical average properties of the fuels used by Chatris, Muñoz and Ferrero (Gasoline Repsol E98 unleaded and Diesel Repsol e+) were obtained from technical characteristics data sheets available at Repsol website.

Properties of concrete (Pachera et al, 2015), water (Perry et al., 2008) and fuels are summarized in Table 5.1.

Table 5.1. Chemical and physical properties of the materials involved in the simulations.

Substance	Units	Concrete	Water	Gasoline	Diesel
Boiling temperature	˚C	-	100	94	305
Conductivity	W/(m·K)	1.4	0.6063	0.116	0.116
Density	Kg/m^3	2307	994.7	709	833
Emissivity	-	-	-	0.75	0.75
Heat of combustion	KJ/kg	-	-	46816	43960
Heat of vaporization	KJ/kg	-	2435.1	349	250.8
Specific heat	KJ/(kg·K)	0.658	1.8639	2.22	3.05
MLRPUA	kg/(m^2·s)	-	-	0.067	0.054

As radiative fraction does not depend on the fuel in the case of hydrocarbon pool fires, according to Muñoz, a same value will be used for gasoline and gasoil. For the first studies, used value will be 0.35, which uses FDS by default, as this is the value that FDS developers recommend for a small-medium scale pool fire (Mcgrattan et al., 2000). However, as the equation (*2.6*) suggests, default value that FDS establishes for radiative fraction could be larger than the values that experimental data presents, and this is the reason why varying this parameter will be considered in the sensitivity analysis.

Ambient condition that FDS establishes by default were used for the first simulations (study of domain, symmetry, mesh and pool shape) as experimental ambient conditions were not available yet (ambient temperature of 20 ˚C, atmospheric pressure, null wind speed and 40% of relative humidity). However, these were replaced for experimental ambient conditions when files containing experimental conditions and measurements were received (sensitivity study).

5.3 Measurement of variables in FDS

5.3.1 Temperatures

Temperatures have been obtained through the help of different thermocouples, which have been set at the centre of the computational domain and at the same axial positions as Muñoz and Ferrero placed their devices.

FDS thermocouples present by default a bead diameter of 1 mm, the default bead emissivity is 0.85 and by default, FDS considers nickel density and specific heat for thermocouples, which will be accepted, considering that this is the controlling component, as Table 4.1 shows. Thermocouples used in simulations presented the same bead diameters as real

thermocouples used in FOC_03 campaign; however, for chapter 6 simulations, default bead diameters were used, as the function that allows changing this parameter had not been discovered yet.

Data provided by thermocouples (and other measurement devices) is stored in FDS v.6 in a file called *filename_devc.csv* created automatically in the same directory as the run simulation. This file, which can be opened with Microsoft Excel®, presents the data of different devices separated with commas, and different instants of time in different lines. A total amount of 1000 values corresponding to different time steps are registered in the *devc* file. Then time scale is relative; for example, if the total simulated time is 200 s, each value is registered, approximately every 0.2 seconds.

Additionally to thermocouples, slices[5], which show temperatures as different colours in the $X = 1.5$ m and $Y = 1.5$ m plains were added; this allows controlling the instantaneous temperature values in each moment of this simulation in Smokeview for any point of the plain. However, the data provided by a slice file is stored with a complex binary encryption that impedes its usage. Unfortunately, slices do not provide information on the temperatures inside the liquid, as it is set as an obstacle and thermocouples inside obstacles do not provide information either.

5.3.2 Flame lengths

Unfortunately, FDS does not offer a direct way to obtain flame length with the help of a device and is not given either by any output file. Despite Ferrero considered flame contour as the region in which products of combustion emit light in the visible rank of the spectrum, this definition could not be used for the determination of flame contour, as FDS does not provide wavelengths of emitted light. In order to determine the maximum height a flame reaches, two definitions were used.

Temperature slices method

Solid bodies which behave as a black body emit perceptible light for the human eye when their temperature is over 798 K (Mahan, 2002), which means 525 ˚C (*Draper point*), and therefore, zones which present a temperature value over this quantity will be considered flame. Is it possible to compile all registered values over a selected maximum as a single value, and set these equal as the specified quantity in a Smokeview slice, by modifying the option *slice bound data*, found in *file bounds* option in dialogs menu (Figure 5.2 left). Using this method, maximum temperatures were turned to 525 ˚C, so all regions over this temperature showed this value in the slice. By clicking over the legend of the slice, values surrounding selection are shown as a black region in the slice (Figure 5.2 right); then, after clicking over the value of 525 ˚C, all zones of the considered flame contour were shown as a black shape.

As flames are three-dimensional objects and wind could push the fire out of the studied slice, and fire length could seem smaller than what it actually is. This is why another slice, orthogonal to the first one, was set in order to simulate the two video cameras set orthogonally in experiences of FOC_03 project. Two sets of flame lengths (one per slice) were calculated, and the correct result was considered the maximum value between the duplet that corresponded to the same time step. Figure 5.3 left shows the same fire at the same time step seen from the

[5] Device parameters can be controlled with the DEVC namelist group.
Slice file parameters refer can be controlled with the SLCF namelist group.

frontal and lateral slices respectively, from which it is possible to see that without the help of a side slice; flame height would have been underestimated.

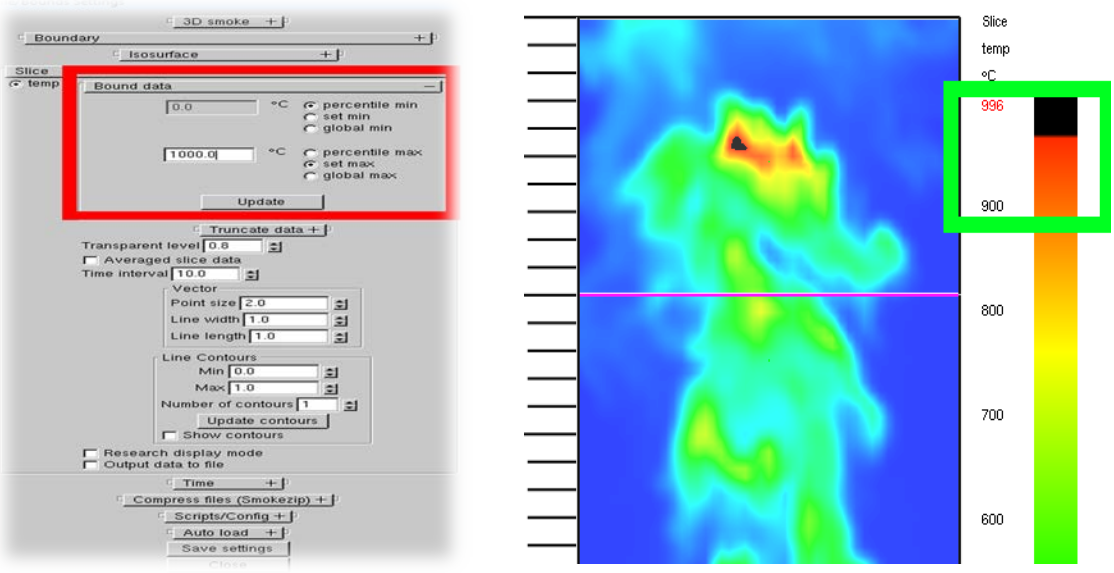

Figure 5.2 Left-View of the bound data menu for setting desired maximum slice temperature. Right-Temperature colour scale.

Once every animation was prepared, the metric were activated and the view was changed to a frontal (for the frontal slice) or a side view (for the lateral slice) of the fire. With the correct perspective prepared, the Smokeview animation was rendered, setting 5 frames per second. Images obtained from rendering were stored in *.png* format and had dimension of 480x882 pixels.

This method has proved to be accurate in these time steps when slices are inside the whole flame contour. However, despite the usage of two orthogonal slices in positions X=1.5 and Y=1.5, flame height values are sometimes underestimated when flame edges are pushed out of both slices.

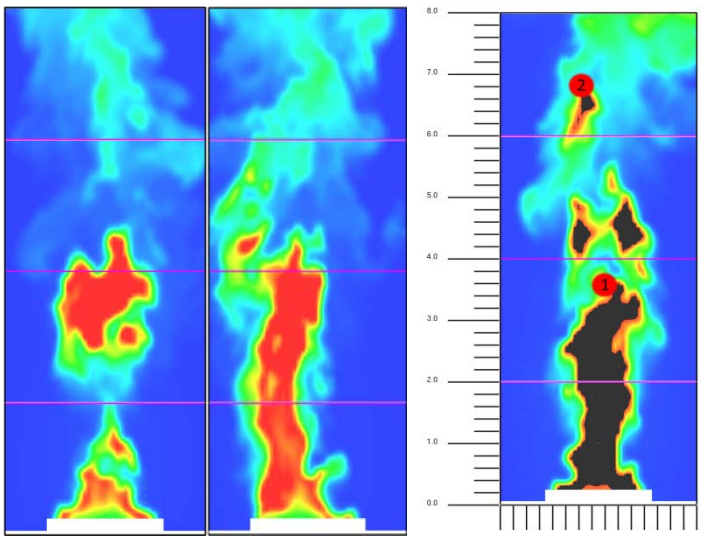

Figure 5.3 Left-View of both Y=1.5 (left) and X=1.5 slices (right). Right - Case with presence of flamelets.

Heat release rate per unit volume (HRRPUV) method

In order to find a definition of flame that does not underestimate flame contours when flame is not straight, flame was additionally defined as the region emitting energy over 100 kW/m^3 (value that cannot be reached only by heat transport) (Orloff et al., 1982), which could be seen in Smokeview by loading the HRRPUV in 3D Smoke menu. The bound, which by default is 200 kW/m^3, was changed in dialogs menu. In order to make the fire shape more visible, fire colour was set to red and the smoke was hidden by setting at 1.0 the option *smoke albedo*. From these images, flame lengths data were extracted in the same way as in the case of images showing temperatures.

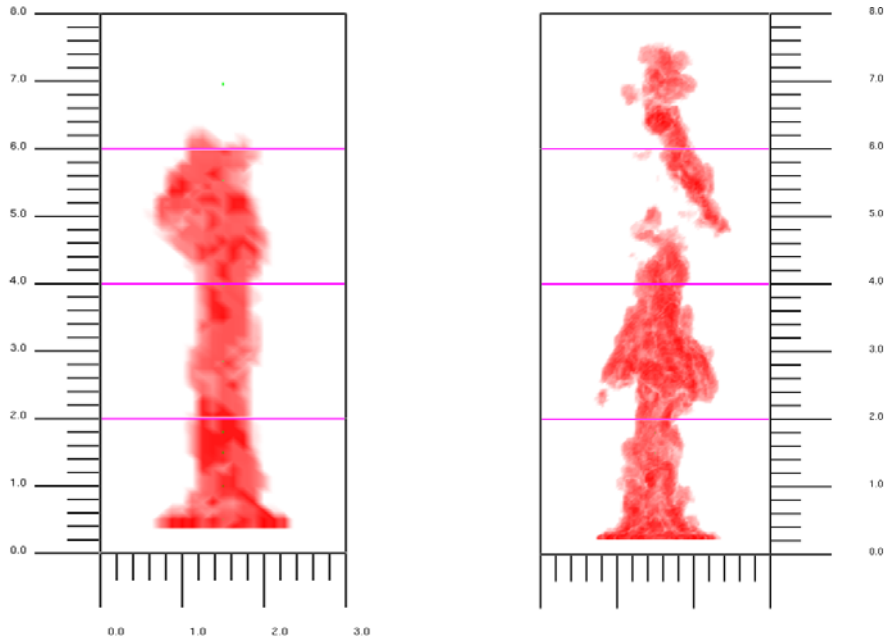

Figure 5.4 Aspect of images analyzed for the determination of flame length using the HRRPUV method

As this method allows considering all three dimensions of the flame, this replaced the initially chosen method for the estimation of flame lengths. However, the initial definition that uses Draper point will be used to confirm that flame does not exist in a determined radial position if temperature values caught by thermocouples (in '*filename'_devc.csv*) set at this position do not reach 525 ˚C.

5.3.3 Heat release rate and radiation

As computational restrictions imply the use of a narrow simulation domain (see section 6.2), radiometers cannot be set as these require being at a reasonable distance from the fire. This restriction impeded to collect radiation data from radiometers as Muñoz did in his thesis.

However, FDS simulations provide an output file called '*filename'_hrr.csv* which contains the heat release rate, the mass loss rate and the heats transferred by convection, by radiation and by conduction among other parameters related to the heat transfer for every time steps, that is every 0.2 s for simulations of 50 s.

Heat release rate per unit volume can be shown in a Smokeview animation, as explained in last section.

5.3.4 Flame shedding

Following the same criterion as Ferrero, flame shedding was determined as the relation between the number of peaks (Np) comprised in a given time interval (Δt), as expressed in equation *(5.1)*. In the case shown in Figure 5.5, there are 6 significant relative minimums (are more than 75 cm larger than the previous relative maximums) in a time interval of 5 s, then, vortex shedding is 1.2 s^{-1}. If flame shedding varies during the simulation period, average values will be used.

$$f = \frac{N_p}{\Delta t} \tag{5.1}$$

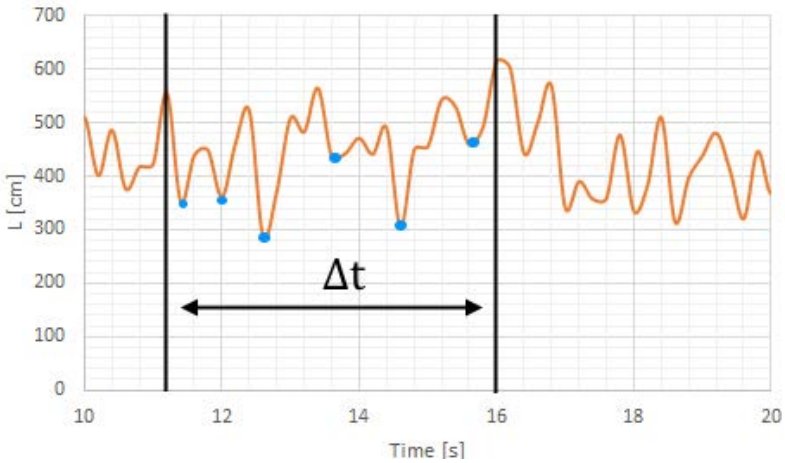

Figure 5.5 Determination of vortex shedding for simulation 3 in absence of wind (section 7.2.3).

6 Simulation Emplacement: domain and mesh studies

6.1 Background

The first matter to consider when a simulation will be started is to find the most suitable grid size that gathers accuracy and scarce computing expense. In order to give an approximate idea of how large should each cell be in simulations involving buoyant plumes, FDS User's Guide (McGrattan et al., 2015b) proposes a non-dimensional expression $D^*/\delta x$ that relates the nominal size of a single mesh cell δx and D^*, which is a characteristic fire diameter. This diameter can be estimated when the total heat release rate of the fire ($\dot{Q}$) is known, according to the following expression:

$$D^* = \left(\frac{\dot{Q}}{\rho_\infty c_{p_\infty} T_\infty \sqrt{g}} \right)^{\frac{2}{5}} \tag{6.1}$$

Heat release rate for a circular shape pool fire can be determined once mass loss rate of fuel per unit area, fuel combustion enthalpy, pool diameter and combustion efficiency[6] are known, according to equation (*6.2*):

$$\dot{Q} = \eta \frac{\dot{m}'' \cdot \Delta H_c \cdot \pi \cdot D^2}{4} \tag{6.2}$$

A validation study sponsored by the U.S. Nuclear Regulatory Commission (2007) ranged values of $D^*/\delta x$ from 4 (coarse cells) to 16 (fine cells) in order to find an equilibrium between results accuracy and computation time. However, a more recent study performed by Chung and Devaud (Chung et al., 2008) recognized a $D^*/\delta x$ =40 as the suitable value that assures the best equilibrium between accuracy and computational time.

However, in the case of pool fires, which often have a fuel layer under 2 cm height, it is necessary to use finer cells in order to represent a layer which is thin enough (although mass calculations related to fuel layer thickness are based in the value indicated to FDS with *thickness* option, a good approximation of cell size to real thickness was sought), such as the condition proposed by Arnaud (2008) reflects in equation *(3.24)* for large scale pool fires. As fulfilling this condition may suppose a huge requirement of computational capacity, especially when pool fires are modelled in a relatively wide domain, it is generally necessary to create at least two different meshes: a fine cell sized mesh for the thin fuel layer (that allows to reach a realistic thickness, as these are under 2 cm height, without the necessity to recur to sub-grid features) and another mesh with coarser cells for the rest of the domain in order to ensure that computational time is not excessive. Due to the necessity of optimization of the available time, studies of domain and meshing were performed.

For the following emplacement studies, thermocouples were set at 0.5, 1.0, 1.5, 1.8, 2.84, 3.96, 5.53, and 6.96 m height, trying to use similar positions as used by Muñoz and Ferrero. Fuel layer thickness was set as a unique mesh cell, as well as concrete pool walls, unlike the

[6] Ratio between effective heat of combustion and total heat provided by chemical reaction. All combustion efficiencies will be considered 100% for the calculation of $D^*/\delta x$.

case of water mass laying below the fuel, thickness of which occupied different number of cells, as the same volume of liquid water was tried to reach in all cases.

6.2 Study of Domain

In order to determine the effect of the domain size in the simulation results, multiple simulations of the same gasoline pool fire of 1.5 m of diameter were carried out. Different domains were considered: 4×4×8 m^3, 3×3×8 m^3, 3×3×6 m^3, 2×2×8 m^3, 2×2×6 m^3 and 2×2×4 m^3. A first study has tried to simulate the geometries that are most approximate to reality. However, this implied dividing the domain into different meshes, and, according to FDS User Guide (Mcgrattan et al., 2015b), the information exchange between meshes is not as good as between cells in a same mesh. That is why another study of domain was carried out with a single mesh divided into coarse cells (see appendix A.2).

The computational domain was divided into four meshes: the region from 0 to 0.5 meters high was divided into two different meshes of the same size with, very small cubical cells (3.25 cm, in order to achieve a fuel layer thin enough formed by a whole cell), and the region from 0.5 m to the top of the domain was also divided into two different meshes of the same size, with coarser cubical cells (12.5 cm) in order to assure a reasonable calculation time. In these experiments, different thermocouples were located inside and outside the liquid in the axis of the fire, imitating the position of the devices that were present in the experimental studies of Chatris and Muñoz in Can Padró. The fires were simulated during a period of 200 s, which was chosen as large in order to dispose of a consistent sample of temperatures corresponding to steady state.

The temperature evolution caught by all the thermocouples was compared for these domains at heights of 0.5 m, 1.5 m, 2.84 m and 3.96 m, finding that differences between these different cases exist, although most of them are not significant. Temperature evolution graphical data for this study is given below:

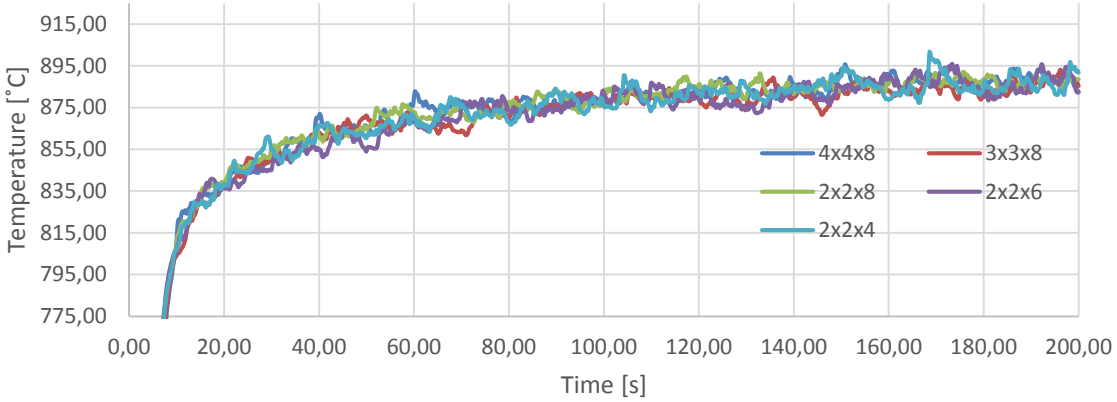

Figure 6.1 Time evolution of temperatures of different domains caught by thermocouple at $z = 0.50$ m

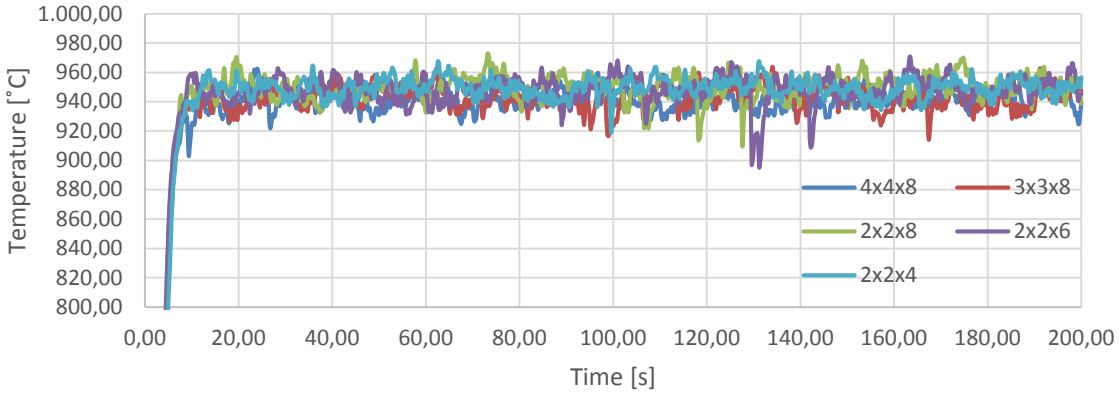

Figure 6.2 Time evolution of temperatures of different domains caught by thermocouple at $z = 1.50$ m

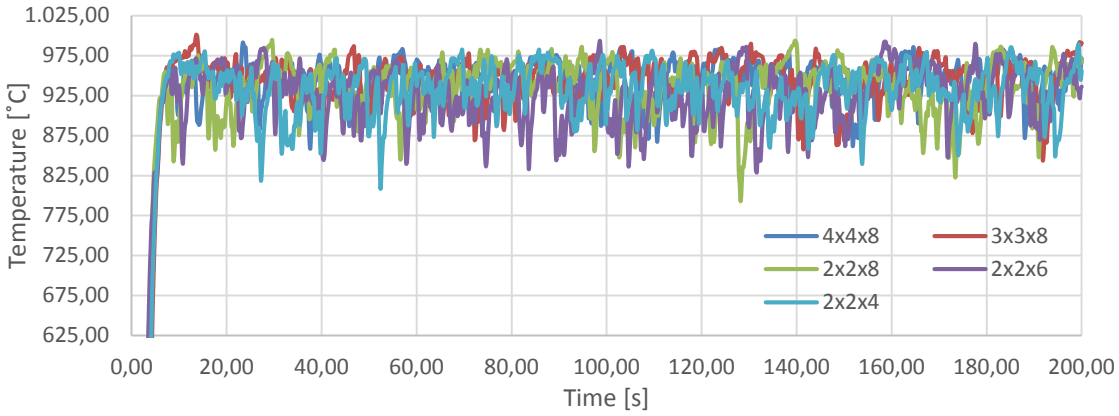

Figure 6.3 Temperature evolution of different domains caught by thermocouple at $z = 2.84$ m

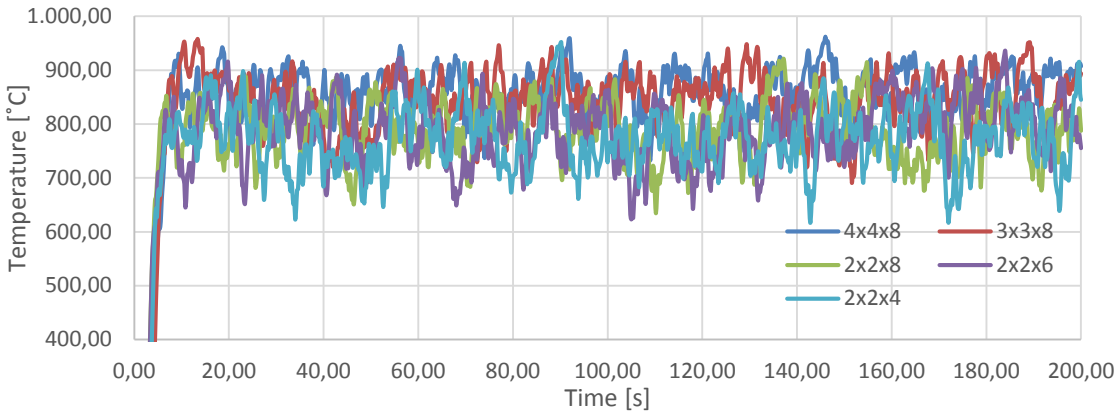

Figure 6.4 Temperature evolution of different domains caught by thermocouple at $z = 3.96$ m

As shown in the previous figures, stationary regime is reached at the same time by all the studied domains. However, temperature evolution may vary in different domains once fire has arrived to stationary. In Figure 6.1, value oscillations are scarcely perceptible, and 2×2×4 m^3 domain draws a profile with temperatures a bit higher than other domains when this state is reached in low z thermocouple positions, as Table 6.1 reflects. Nevertheless, when the z position of the thermocouple is increased, temperatures show more oscillations and other domains show higher temperatures during the rest of the stationary, letting these other domains (especially larger ones) to register larger maximum values. The magnitude of variations does not coincide between domains, as can be seen at Table 6.1.

Table 6.1. Mean temperatures and corresponding standard deviation registered during the simulation.

Average temperatures, ˚C (standard deviation)						
z	4×4×8	3×3×8	3×3×6	2×2×8	2×2×6	2×2×4
0.50 m	874.78 (15.76)	872.12 (15.99)	874.85 (15.52)	872.42 (16.69)	873.53 (16.17)	888.66 (13.77)
1.50 m	941.46 (6.72)	942.88 (7.60)	942.87 (8.04)	949.77 (8.24)	948.11 (8.98)	949.66 (6.19)
2.84 m	946.07 (22.68)	946.00 (24.64)	949.76 (21.18)	936.12 (31.29)	927.93 (32.51)	933.97 (28.90)
3.96 m	863.71 (39.42)	847.01 (50.29)	863.35 (43.41)	790.82 (51.42)	791.12 (57.44)	774.31 (56.97)

The marked difference between average temperature at z=3.96 m of 4×4×8, 3×3×8 and 3×3×6 m^3 and the rest of domains show that when fire is closed in a narrow control volume, results of temperatures read at thermocouples away enough from the fire bottom are not very reliable.

In addition, Table 6.1 also shows higher standard deviation values for the sets of temperatures corresponding to simulation performed with domains of 2×2×8, 2×2×6 and 2×2×4 m^3 for equal z-axis positions. It is logical to see that standard deviation is higher for these z-axis positions where temperature evolution shows more oscillations, according to last figures.

Mean temperatures and standard deviations were from calculated samples of 1950 values, once values registered before reaching the steady state of temperature had been removed.

Table 6.2. Maximum temperatures reached during the simulation period

Maximum temperatures						
z	4×4×8	3×3×8	3×3×6	2×2×8	2×2×6	2×2×4
0.50 m	895.77 ˚C	893.11 ˚C	892.06 ˚C	895.94 ˚C	901.54 ˚C	908.57 ˚C
1.50 m	962.63 ˚C	963.70 ˚C	969.75 ˚C	972.86 ˚C	970.94 ˚C	967.70 ˚C
2.84 m	990.94 ˚C	1000.94 ˚C	991.85 ˚C	994.13 ˚C	993.16 ˚C	989.10 ˚C
3.96 m	962.00 ˚C	957.71 ˚C	964.88 ˚C	920.68 ˚C	935.55 ˚C	951.58 ˚C

By watching Smokeview animations, is it possible to appreciate qualitatively that Flame heights are higher than expected in all cases, reaching a mean flame length of 6 m, and maximum values over 7 m height. These inaccurate lengths may be due to the fact that mesh in the region up from 0.5 m height was divided into too coarse cells. However, how grid size effects on flame length will be studied in the mesh study. Domains under 8 m height will be discarded, as whole flame cannot be studied.

Comparing temperatures registered by thermocouple set at $z = 0.5$ with experimental data by Muñoz and Ferrero (Figure 6.5) is possible to appreciate that real data experiences more value oscillations than simulated data, which is almost completely constant. This shows that all temperatures measured at this position are practically equal for all simulated cases. However, another case will be studied in order to check the FDS predictive capability.

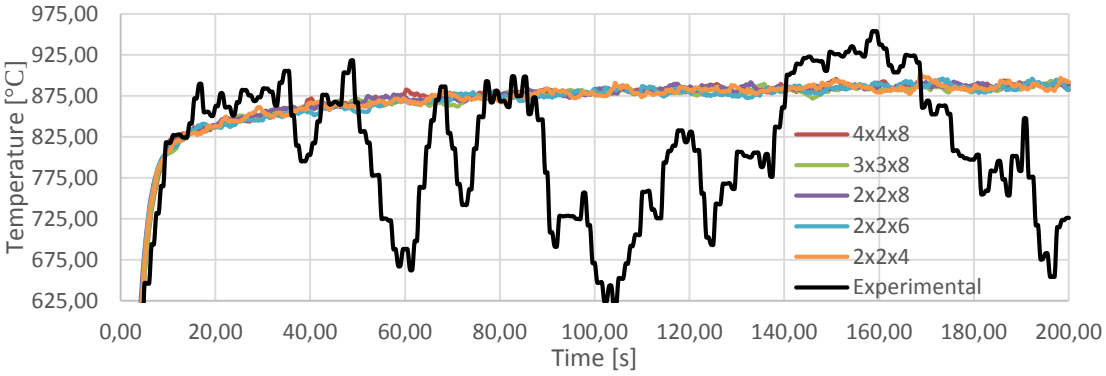

Figure 6.5 Comparison between experimental data collected (FOC_03) and FDS simulation results.

As Figure 6.2 shows, maximum temperature values given by FDS thermocouple at $z = 1.5$, (located about 0.3 m above fire basis) for a 1.5 m diameter gasoline fire, are very close to the maximum temperature results obtained by Chatris (near 930 ˚C) and by Muñoz and Ferrero in FOC_03 project with real thermocouples in the continuous flame region.

Figure 6.6 shows the comparison between the maximum temperatures reached at any position of simulated fires, for those domains where flame length is not cut, with Chatris largest temperature set (registered by TP12).

Figure 6.7 is an interval plot generated with Minitab®, which indicates mean values and standard deviations of every data set, and shows that 3×3×8 m^3 domain is the most approximate in mean to experimental data. An ANOVA analysis carried out with only 30 selected values of each data set (temperatures obtained at $z = 1.5$ m for all three studied domains and Chatris experimental data) because experimental temperatures were not registered with the same frequency as FDS simulation data performs its calculations. Real fires did not last as much time as simulated fires (which are infinite because no reaction models were specified and, instead a constant fuel mass loss rate was set) and time scales are different. However, all 30 values belong to steady state.

Results of ANOVA statistical analysis (setting a significance value of α=0.05), for which was considered as null hypothesis that all three data sets are equal (and then, as alternative hypothesis that at least, one of these is different), showed a p-value of 0.146 and therefore, null hypothesis could not be refused and all four data sets were considered not to be significantly different.

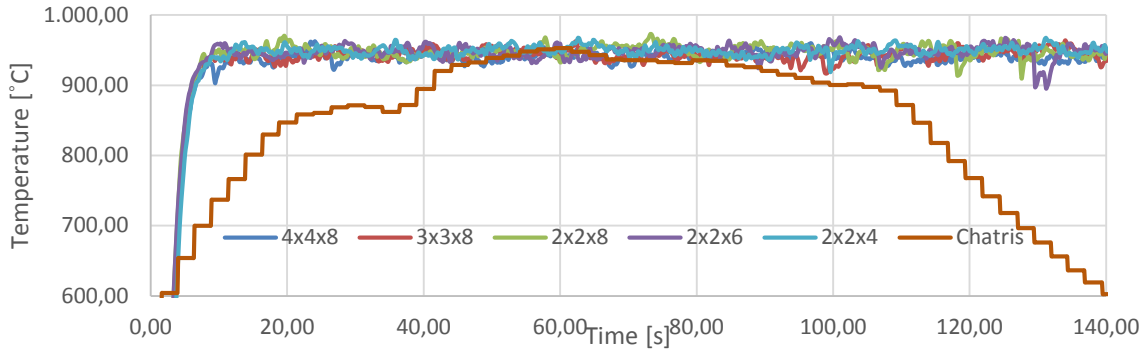

Figure 6.6 Comparison between experimental data collected by Chatris and FDS simulation results.

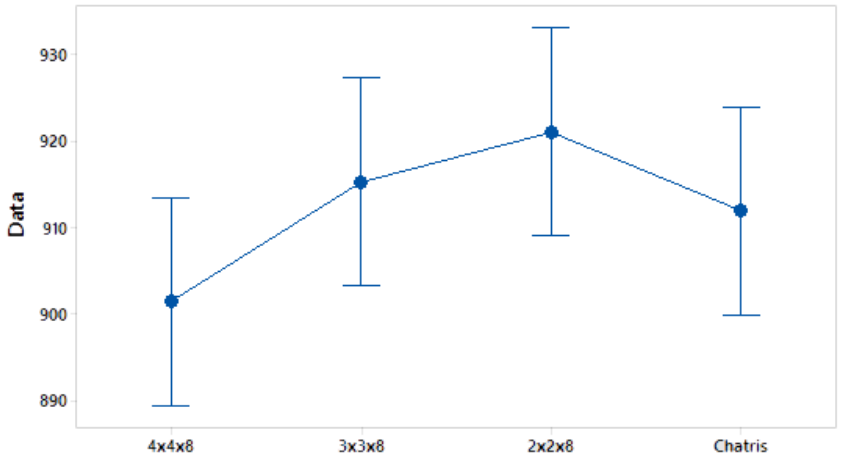

Figure 6.7 Interval plot showing means and standard deviation of all studied domains

Results are practically identical, finding exclusively a difference on the time required in order to reach the steady state, which is near 30 s in the experimental fire and near 10 s for the simulation results given by FDS, as can be observed in the figure. However, this difference between times cannot be considered significant and is probably due to the fact that fuel starts burning from zero seconds time, when in the reality, exist a time elapsed between the first contact of ignition source and fuel and the beginning of the combustion reaction.

Therefore, these results can be validated, and most accurate results can be considered these that are nearer experimental measures and have less variability. Anyway, chosen properties of fuels or of reaction for this first study may differ from real data and this could explain some discrepancies between simulation and registered experimental data.

According to this study, **3×3×8 domain will be chosen as the most proper one**, because it is the smallest domain whose results are near the expected, has relatively small standard deviation and whose flame is not cut by the control volume.

6.3 Symmetry study

The first study of domain was performed with the region where the pool is found divided into two different meshes by the Y direction (left of Figure 6.8), due to the necessity of dividing the domain in different meshes with similar number of cells per mesh, according to the available computation capacity. A question that may come to mind is: Could this division influence the simulation results?

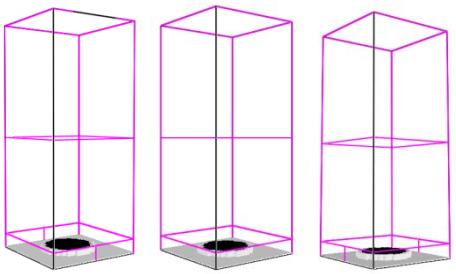

Figure 6.8 Mesh divisions in different partition studies for 3×3×8 m^3 domain

In order to find an answer to that question, two additional simulations were run for the 3×3×8 m^3 domain: one of them with only three meshes (the mesh where pool of gasoline was located was not divided into two meshes, as central domain of Figure 6.8 shows), and another one splitting the pool region into two meshes, but in the X direction (as Figure 6.8 right shows). Simulation with flame split in the Z direction was not considered, because of the non-symmetry.

The results showed small differences in the time required to reach the steady state in each simulation. Figure 6.9 shows that this time is about two second decimals higher in the case of the simulation whose pool is not split. Differences between splitting the pool region by the Y or the X axis are not significant. However, Figure 6.10 does not show the same tendency.

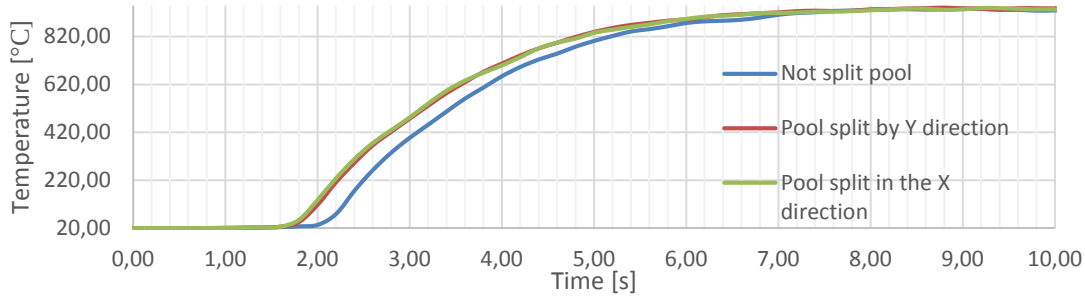

Figure 6.9 Time evolution of temperatures caught by thermocouple at z=1.50 m

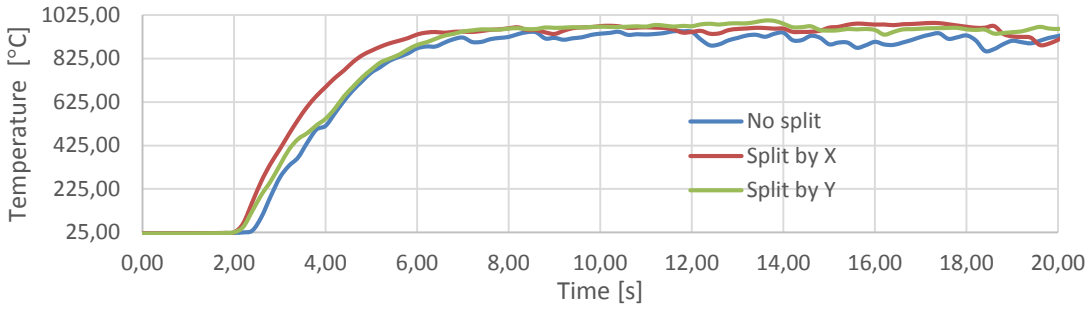

Figure 6.10 Time evolution of temperatures caught by thermocouple at z=2.84 m

Heat release rate was also compared for these different cases. There were no appreciable differences among the obtained results: all three simulations took the same amount of time in getting into the steady state, and heat release rate fluctuations through the studied time period seem completely random, as can be observed in Figure 6.11.

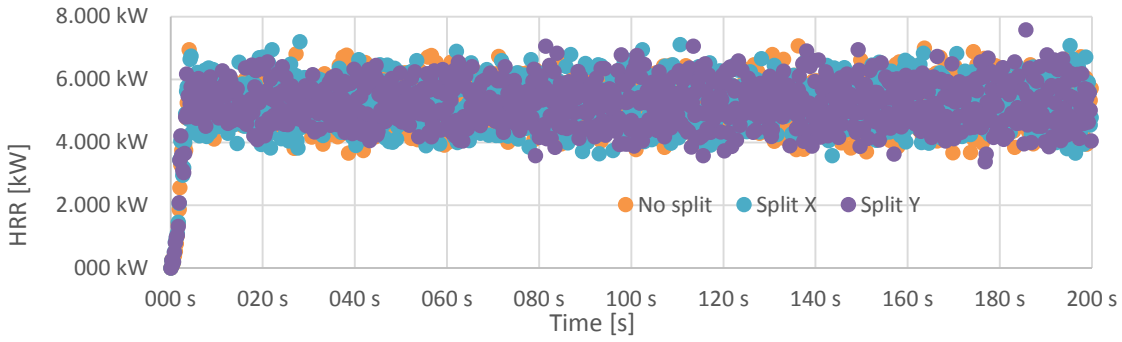

Figure 6.11 Time evolution of heat release rates for different simulations of this study

Mass loss rates per unit area were also compared in the three cases. They expend exactly the same time amount (90 s) in reaching the same final value of MLRPUA.

These results help to prove that differences between these three simulations are basically random, and, therefore, splitting the pool through X or Y axis will not cause significant errors. The pool region will be divided, then, when it is required in order to decrease the computational expense, or even will be only considered half domain for these simulations, which are especially computationally expensive.

6.4 Study of mesh

Once the studied domain had been fixed to 3×3×8 m^3, a mesh study was carried out in order to determine which is the most recommendable grid size that provides accurate results and spends the least possible time in the calculations.

In order not to modify the geometry parameters of the FDS files written formerly, proposed grid sizes used cubical cells with size values that were multiples of the cell dimensions chosen in the study of domain, so chosen values of δx were 3.1250, 6.2500 and 12.5000 cm.

As simulations are run in a 4-cored computer, domains of all simulations were divided into four different meshes of 3x3x2 m^3.

Despite the intention of modifying geometry the least possible, some obstacles had to be re-sized in the simulations that used a larger grid size, in order to let all obstacles to occupy an integer number of cells, but always trying to keep the water pool depth near the desired value of 16 cm and making the fuel layer thickness as thin as possible. For example, fuel layer thickness is 6.25 m high if grid size is 6.25 cm, but 12.5 cm if grid size is 12.5 cm. Water pool depths and fuel layers thickness are summarized in Table 6.3:

Table 6.3. Summary of different parameters corresponding to the different mesh resolutions

Grid size [cm]	$D^*/\delta x$	Number of cells	Water pool thickness [cm]	Fuel layer thickness [cm]	Computational time [s]
3.125	60.862	2,359,296	15.625	3.125	346702.04
6.250	30.431	294,912	12.500	6.250	11059.36
12.500	15.215	36,864	12.500	12.500	777.38

From data in Table 6.3, is it possible to find a parabolic relation between number of cells in the simulation and the total computational time, represented in Figure 6.12.

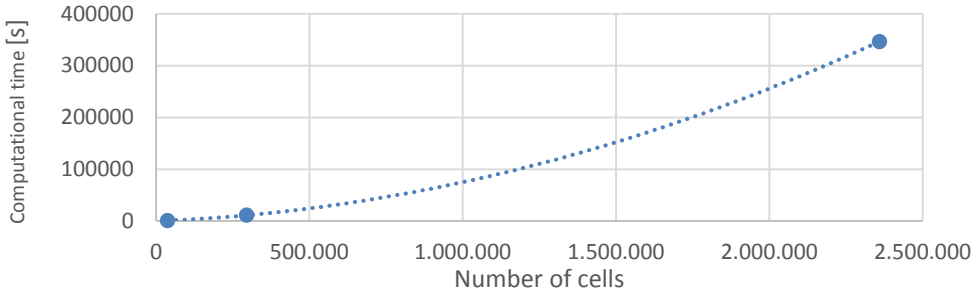

Figure 6.12 Changes in computational domain time according to total number of simulated cells.

As Table 6.3 shows, parameter $D^*/\delta x$ values are considerably higher than recommended values by US Nuclear Regulatory Commission (2007), and fine grid size is even higher than value proposed by Chung and Devaud (Chung et al., 2008). These cell width values are small (as obstacles width was intended to be set as similar as possible to user-specified thickness), and may oscillate between 1 and 2 cm. However, computational restrictions of CERTEC computers did not allow a cell size finer than 0.0325. Time evolution of temperatures registered by thermocouples at z=0.5, 1.5, 2.84, 3.96 and 5.53 m height are compared below for the different grid resolutions. Experimental temperatures from FOC_03 project have also been plotted for the heights in which there were thermocouples.

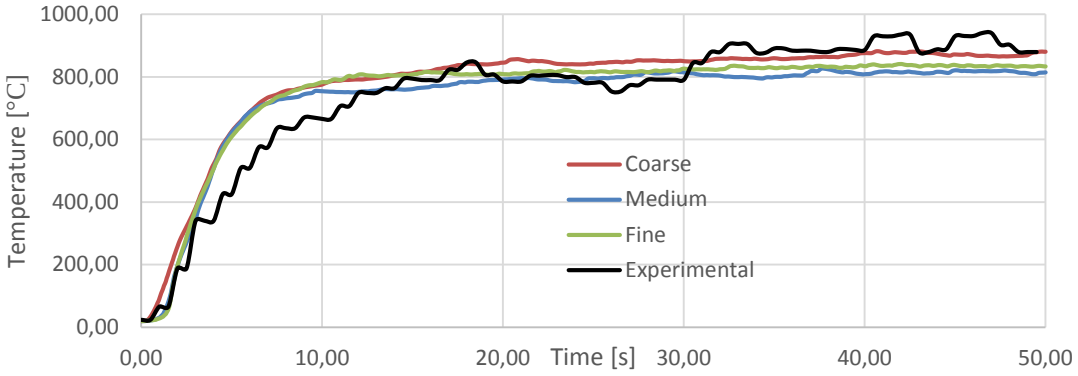

Figure 6.13 Temperature evolution of different domains caught by thermocouple at $z = 0.50$ m.

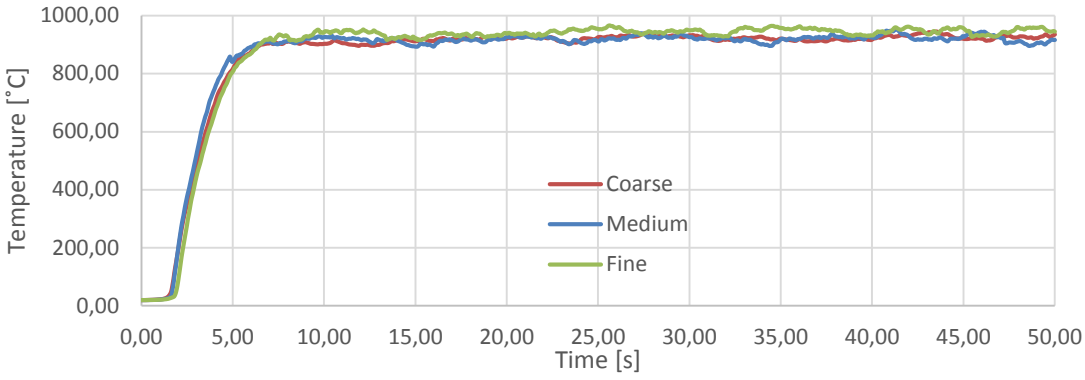

Figure 6.14 Temperature evolution of different domains caught by thermocouple at $z = 1.50$ m.

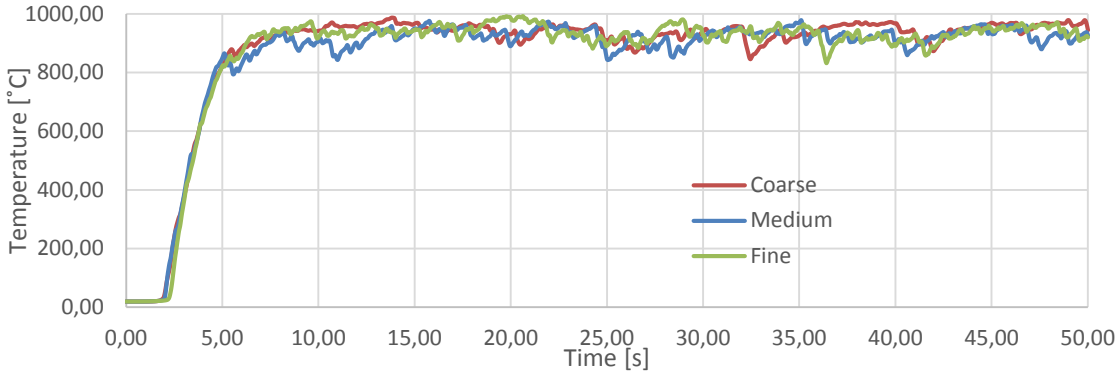

Figure 6.15 Temperature evolution of different domains caught by thermocouple at $z = 2.84$ m.

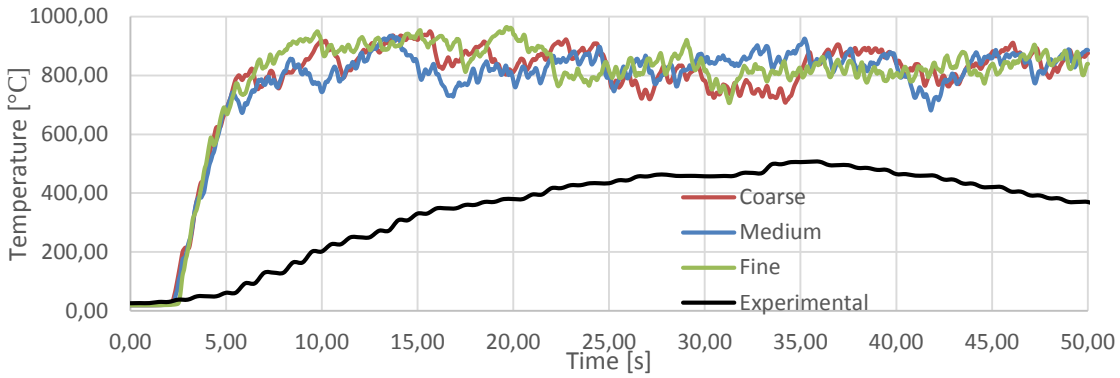

Figure 6.16 Temperature evolution of different domains caught by thermocouple at $z = 3.96$ m.

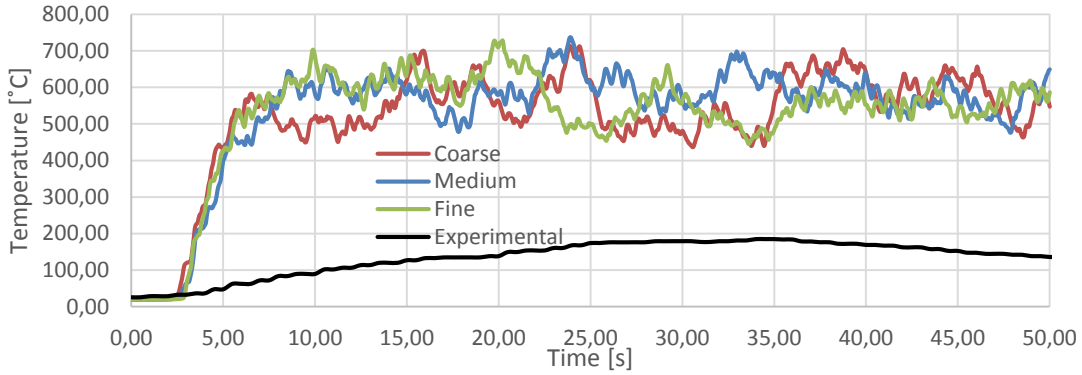

Figure 6.17 Temperature evolution of different domains caught by thermocouple at $z = 5.53$ m.

Temperatures caught by thermocouple set at 0.5 meters height show a similar fire growth tendency (until $t = 10$ s). However, stationary behaviour is different for all domains, as can be seen at Figure 6.13, where coarse grid size simulation shows the highest temperatures, followed by fine grid resolution and finally medium simulation.

Temperature sets registered thanks to thermocouple placed at z=1.50 m (Figure 6.14) show a similar behaviour during all simulation period, although fine grid sized simulation clearly seems to reach the highest temperatures.

In addition to the visual inspection of temperature time evolutions, ANOVA hypothesis test studies were carried out using Minitab® and setting a significance level of α=0.05, in order to determine if different data sets of 1950 values (which represent temperatures at steady state)

are equal (null hypothesis) or are different (alternative hypothesis). If the p-value obtained from the ANOVA analysis is larger than 0.05, the null hypothesis cannot be refused and therefore, there is not an statistically significant difference between data sets; otherwise, null hypothesis will be refused and therefore, studied data sets will be considered different.

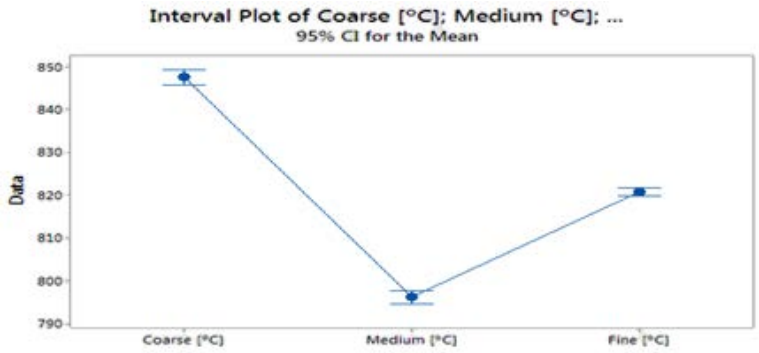

Figure 6.18 Mean and standard deviation presented by each grid size related temperature set at $z = 0.50$ m.

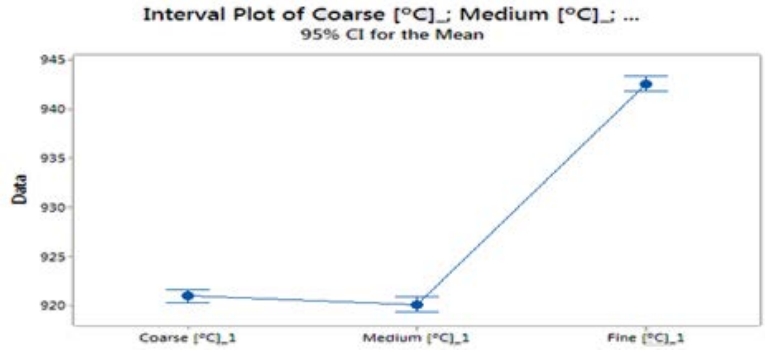

Figure 6.19 Mean and standard deviation presented by each grid size related temperature set at $z = 1.50$ m.

For data sets corresponding to temperatures caught by thermocouple placed at position $z = 0.50$ m height, ANOVA analysis provided a p-value of 0, which means that null hypothesis must be refused (0 is smaller than 0.05), and therefore, the three sets are significantly different. A closer relation between high and medium resolution than between coarse and medium grid size (Figure 6.18) was found. That was the reason why a t-test comparing medium grid size and fine grid size data sets was performed, finding a p-value of 0.012, which is smaller than 0.05 and then, null hypothesis can be refused and these two data sets cannot be considered equal. The performed ANOVA analysis, setting a significance level of α=0.05, provides a p-value of 0, and as this is lower than 0.05, null hypothesis must be refused. As Figure 6.19 shows, means for coarse and medium grid size simulations are practically equal, while mean temperature for fine grid sized simulation is significantly higher.

Last ANOVA analysis performed for the two first thermocouple positions have shown that there is already significant difference between different data sets in the data sets corresponding to the two first z positions. This would force to use the most accurate mesh, which means fine grid size.

Mean temperatures, standard deviations, maximum and temperatures summarized in Table 6.4, while computational times required to finish each simulation can be found in Table 6.3.

Table 6.4. Mean & standard deviation for temperatures registered during the simulation period.

Mean temperatures, ˚C (Standard Deviations)					
z	Coarse	Medium	Fine	% Error Coarse	% Error Medium
0.50 m	850.75 (22.85)	798.39 (19.7)	821.79 (11.52)	+3.52	-2.85
1.50 m	921.66 (9.34)	919.08 (10.89)	942.49 (10.92)	-2.21	-2.48
2.84 m	942.13 (25.97)	926.20 (26.46)	935.62 (26.37)	+0.69	-1.02
3.96 m	837.00 (55.72)	833.60 (44.08)	844.86 (50.73)	-0.93	-1.33
5.53 m	566.23 (68.86)	588.57 (48.07)	566.49 (59.06)	-0.05	+3.90

If results of simulations are compared of experimental results of FOC_03 project, is it possible to appreciate two very important differences between experimental data and simulation results:

- Qualitatively, watching Smokeview simulations is easy to appreciate that flame heights are much higher in simulations than experimental results. Muñoz and Ferrero obtained a mean flame height of 3.65 m for gasoline pool fires, while simulated fires provide results over 4 m height in all cases. This data can be confirmed as temperatures of experimental data shown in Figure 6.16 and Figure 6.17, are much lower for real data, what means that flame heights scarcely reach (for $z = 3.96$ m) or do not reach (for $z = 5.53$ m) this positions in the real data, but in simulations do.

- The central region attached to the pool surface provides temperatures that are significantly smaller than experimental data from FOC_03. Figure 6.20 shows, marked as a black region, temperatures over 830 ˚C in slices placed at $Y = 1.5$ m position for the same instant of time of all three simulations. As is it possible to see, purple horizontal line shows that temperature caught for this time step by thermocouple TAC1 is clearly under-estimated in the case of medium and coarse grid sizes.

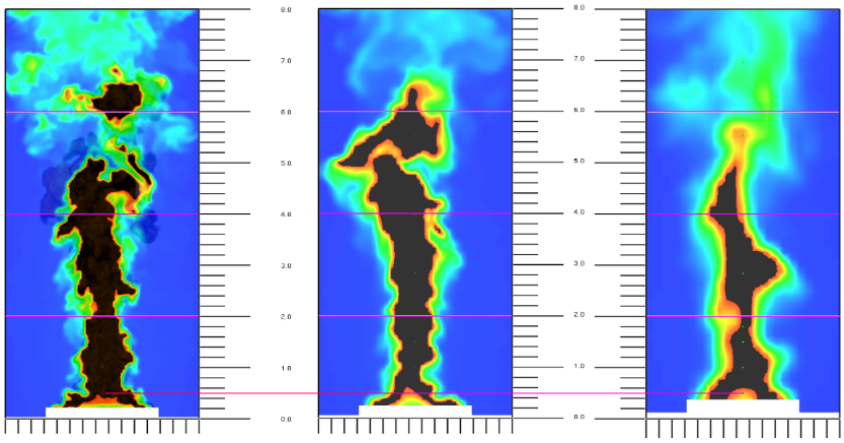

Figure 6.20 Regions over 830 ºC for simulations. From left to right: fine, medium & coarse grid sizes.

Differences between registered temperatures that belong to the continuous flame region of the simulated fire seem to be minimal for the three grid sizes. For example, as in the temperature sets collected by thermocouple at z=1.5 m, lowest mean temperature (medium grid size) is T=919.08 ˚C and the supposed correct mean temperature is T=942.5 ˚C, the committed error is -2.48 %.

In quantitatively analysis of flame heights is possible to see that all three simulated grid resolutions provide flame lengths centred near the value of 5 m, which is significantly over results found experimentally by Muñoz. It is also possible to check that flame shedding is similar for all simulations and also for experimental data, as it varies only with the pool diameter. Summarized data is presented in Table 6.5.

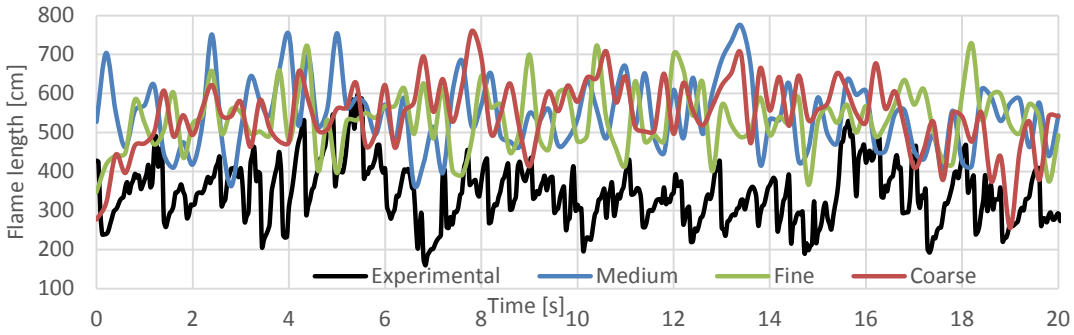

Figure 6.21 Comparison between experimental and simulation data obtained for all different grid sizes.

Table 6.5. Summary of flame heights quantitative study for different grid sizes.

	Coarse	Medium	Fine	Experimental
Maximum length [cm]	759.80	774.59	728.53	598.60
Minimum length [cm]	255.06	367.32	366.27	159.40
Max-Min [cm]	504.74	407.27	362.26	439.20
Mean length [cm]	555.11	538.06	540.85	343.95
Standard Deviation	90.41	85.19	80.97	76.25

All three simulations register similar mean flame length values, which are 2 m over experimental data obtained for FOC_03 project. Maximum registered flame heights are similar for all the studied cases, while minimum value registered value in the simulation using coarse grid is significantly smaller than values found for medium and fine grid size simulations. For the interval of registered values, the simulation that presents the most approximate data to experimental value is medium grid size simulation.

As fine mesh results are more approximated to reality, this should be the chosen grid size. Unfortunately, choosing the fine grid size would also imply a very considerable increase of the computational time, as Figure 6.12 reflects. Due to time restrictions, this size cannot be chosen.

In order to avoid an unnecessary exceed of computational time, **grid size chosen for the sensitivity study will be medium**, that is 6.25 cm, and results will be considered inside a range of ±5% the mean values, which is completely acceptable considering that this grid size last about the 3% of what a fine grid-sized simulation would. Medium grid size is chosen instead of coarse due to the possibility of simulating a thinner fuel layer thickness, which is more approximate to reality.

6.5 Proposed corrections

Before performing domain and mesh studies, different chemical and physical properties for the different materials involved in the simulation (indicated in Table 5.1) were chosen after looking at different bibliographical resources. However, flames seen in the study of domain and mesh simulations reached even seven meters height, while, according to empirical correlations as Heskestad (equation (*2.8*)), flame lengths in a pool fire are about two times the pool diameter. Although many authors have noticed to see larger flame lengths in FDS simulation results than predicted by empirical correlations, especially when coarse cells are used, these exaggerated differences between FDS data and expected results cannot be random. This is the reason why specified properties of fuel were revised, finding two errors:

- The selected flame emissivity was 0.75, as an arbitrary value. However, as equation (*2.3*) indicates, flame thermal emissivity for hydrocarbon pool fires is usually near 0.9; solving this equation for a pool fire of 1.5 m diameter, emissivity is 0.9167. If emissivity is increased, radiation heat flux also increases due to a higher energy release to the surroundings.

- Heat of combustion of gasoline and diesel was taken from Repsol technical datasheets. After looking through Microsoft Excel® files containing experimental data of Chatris and Muñoz, smaller heat of combustion values were found. This is due to the fact that combustion heats provided by Repsol are specified in higher heating value (which considers the heat provided by the condensation of the produced water steam); while FDS input heat of combustion must be specified in lower heating value, which does not contemplate the extra provided energy as result of water steam condensation, and therefore, is significantly smaller than higher heating value, so released energy amount will decrease. LHV (given in KJ/kg) can be obtained from HHV (given in KJ/kg) and the percentage of hydrogen composition fraction mass through the equation (*6.3*) (thanks to Josep Arnaldos Viger), finding the values of 43676.28 for gasoline and for diesel.

$$LHV = HHV - 219.78 \cdot H\% \tag{6.3}$$

Some of the less computationally expensive experiments have been repeated with the new conditions of emissivity and heat of combustion. Comparison between results with current and former data are shown below for a gasoline pool fire of 3×3×8 m^3 domain and medium mesh, as it is the most illustrating case.

From the results of time evolution of temperature obtained with the new properties and old temperature results, a correction parameter has been calculated as the mean value of the set of corrections belonging to each time step, which have been calculated as follows:

$$Correction\ Parameter\ at\ step\ n = \frac{Modern\ data\ value\ at\ time\ step\ n}{Former\ data\ value\ at\ time\ step\ n} \tag{6.4}$$

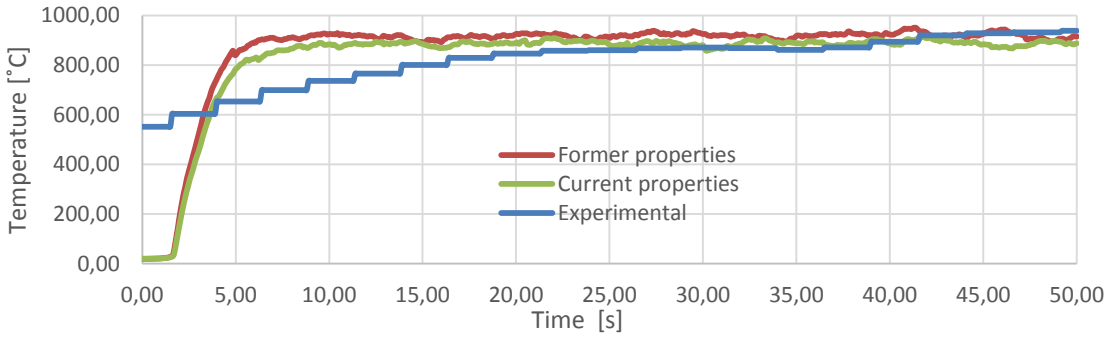

Figure 6.22 Variations on time evolution of temperatures due to changes in fuel properties.

Temperature evolution of experiment with former data seems to register higher results (mean temperature: 920 ˚C) than with current values (mean temperature: 889 ˚C). Experimental data, from Chatris experiments reach higher values, which arrive to a mean that is near 930 ˚C than data simulate using a medium grid size. Error using current emissivity and heat of combustion values would suppose less than 4.5 % and error using former properties would suppose less than 1.4 %.

This mean correction parameter for all calculated cases according to equation (*6.4*) is around 0.97 for the thermocouples set inside the flame. Supposing that in case of repeating the fine mesh simulation with the corrected emissivity and heat of combustion, the correction parameter remains in 0.97, mean flame temperature that is obtained by the multiplication of the mean temperature of 942.5 would be 914.2 ˚C, which means an error of less than 2% with experimental mean temperature.

Despite these corrections, flame heights are still very high. Another factor that is not considered in simulations carried out so far is wind speed, which plays an important role in the determination of flame height through some empirical correlations with the form of equation (*2.10*). Wind speed is one of the most important parameters (together with cell width and fluid density) for the determination of the hydrodynamic behaviour of the fire in FDS, as fluid velocity appears directly in mass, moment, species and energy conservation equations (equations (*3.3*) to (*3.6*)), but also indirectly, as flow parameters such as viscosity or fluid diffusivity also depend on fluids velocity. This is the reason why wind speed effect on simulation results will be studied in next chapter.

7 Square equivalent pools accuracy study

7.1 Background

Different authors mentioned in the summary of all the previous validation work for FDS have used pool fires of square shape, as not rectilinear geometry is not thought to be used in the building up the scenarios of FDS simulations. Although authors like Nielsen (2013) checked the accuracy of these square shape pools compared to the proper circular pools, many of them did not mention how good is information obtained from a simulation of an square equivalent (Figure 7.1 left) of a circular pool fire, compared to results obtained directly from using the circular geometry (Figure 7.1 right).

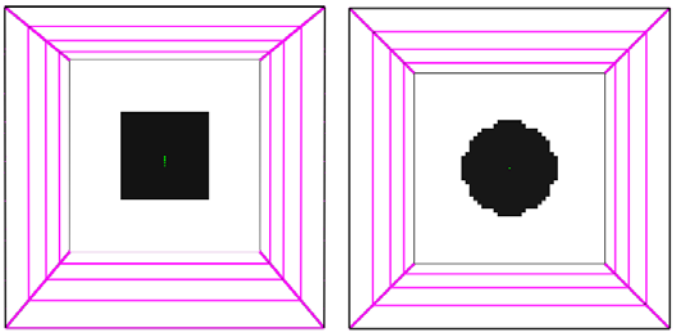

Figure 7.1 Sights of square (left) and circular (right) pool fires seen from the top of the domain.

As studied pools have 1.5 m diameter, their area should be approximately 1.767 m^2, but as an exact geometry cannot be reproduced with the chosen grid resolution, the used pool surface has an area of 1.69 m^2. For a 3×3×8 domain using cubical cells of 0.0625 m, the most approximate area to theoretical value can be achieved by using 22 cells per side of the square (11 on each side of the symmetry axis, as the fire must be centred in the domain, which means an area of 1.89 m^2). However, is it also important to find how a square pool fire with less surface than original circular pool behaves, and then, square with the immediate area value under 1.77 (that is, 1.56 m^2 using 20 cells per side of the square) will be also be tested. Experiments are summarized in Table 7.1:

Table 7.1. Summary of all the experiments carried out for the accuracy study of square pools.

Experiment nº	Pool shape	Fuel	Number of pool cells	Total pool area (m^2)
1	Circle	Gasoline	432	1.69
2	Square	Gasoline	484	1.89
3	Square	Gasoline	400	1.56
4	Circle	Diesel	432	1.69
5	Square	Diesel	484	1.89
6	Square	Diesel	400	1.56

7.2 Gasoline in absence of wind

7.2.1 Temperatures at the pool axis

In order to check how approximating a circular pool fire with a rectangular geometry may vary simulation results, temperatures measured by thermocouples set at the pool axis and placed at z=1 m, z=1.8 m and z=4 m were compared for the simulation results of experiments 1, 2 and 3. As Figure 7.2 and Figure 7.3 show, square pool shapes provide higher temperatures than circular shapes in those points inside continuous flame region. However, in the points which are generally out of the flame, as Figure 7.4 shows, temperatures registered in the results of circular pool fire may exceed the corresponding values on the square pool shape fires.

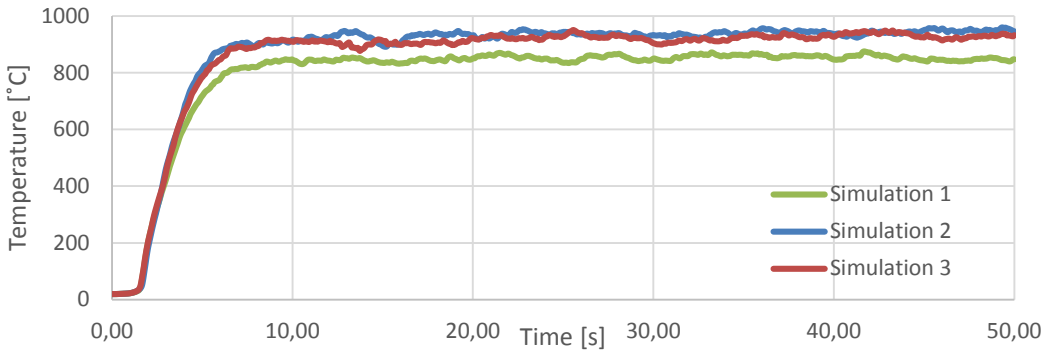

Figure 7.2 Temperature evolution of different simulations caught by thermocouple at z=1.0 m.

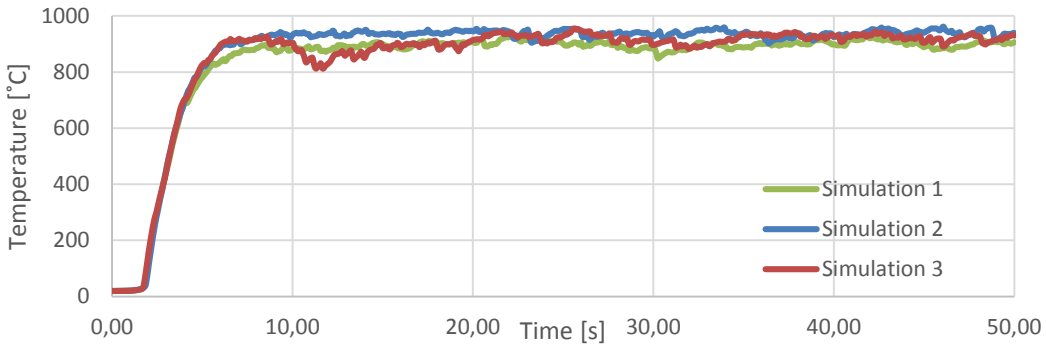

Figure 7.3 Temperature evolution of different simulations caught by thermocouple at z=1.8 m.

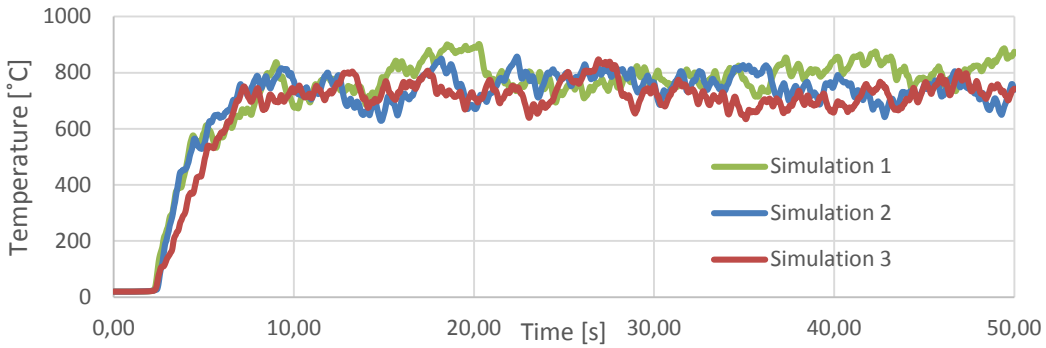

Figure 7.4 Temperature evolution of different simulations caught by thermocouple at z=4.0 m.

In low axial positions (between 0.3 and 0.9 meters height), temperatures are significantly higher for square shape pool fires that for the circular pool fire, and these first present better similarity with experimental data from FOC_03 project (red curve).

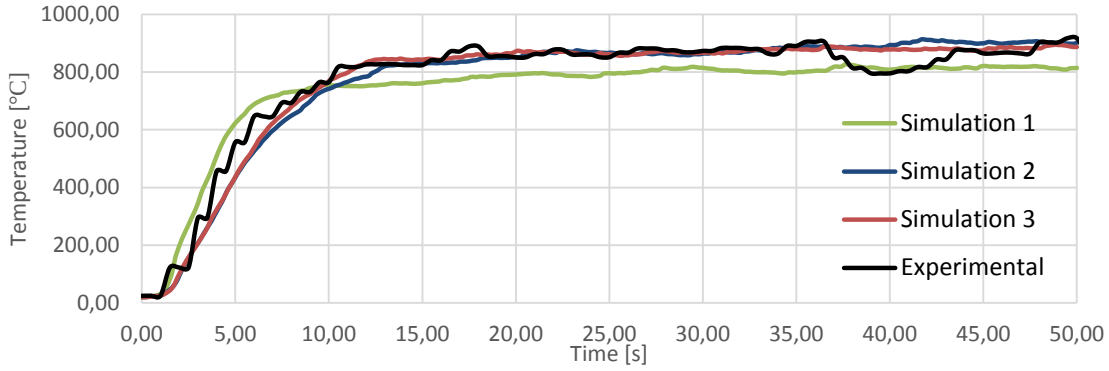

Figure 7.5 Temperature evolution of different simulations caught by thermocouple set a pool axis and z=0.5 m.

By watching Smokeview animations, is it easy to see that region attached to pool surface reaches higher temperatures in the case of square shape pool fires. Figure 7.6 shows information from temperatures provided by the slice set at Y=1.5 m with temperature values over 830 ˚C marked as a black zone in animations corresponding to experiments 1 and 2 respectively.

As Figure 7.6 shows, 2.5 seconds after the ignition beginning, the zone which lays next to the pool surface is still colder than region placed few centimetres higher, as air entrainment rate is smaller in the case of circular pool fire, and then, as fuel mass disappearance rate (as is it controlled by the limiting reactant) and then, total heat release rate produced in the combustion and therefore temperature. However, after 25 seconds, this region has almost disappeared, and 50 seconds after the fire beginning, that zone no longer exists.

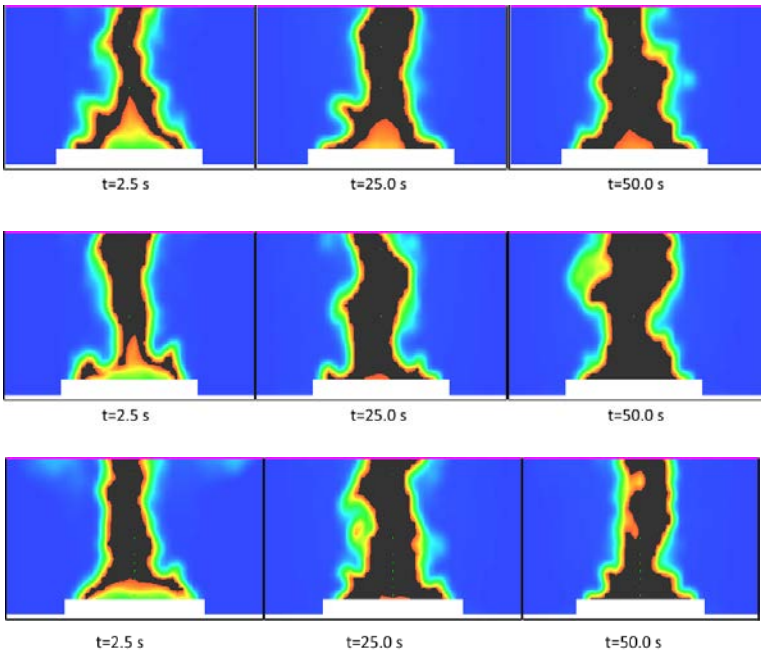

Figure 7.6 Qualitative analysis of evolution of temperatures at the downfire region for circular (up) and square (centre, sim.2 and down, sim.3) pool fires.

Looking at mean temperatures, which are summarized in Table 7.2, is it possible to see that between two square pool fire simulations, the simulation with more number of elements (nº 2) provides higher temperature values than the simulation which represents the pool with a smaller surface area (nº 3).

Flame heights are over predicted, as thermocouple set at radial position z=4 m registers temperatures significantly higher for the case of experimental results from FOC_03 project. Time evolution of flame heights for each simulation is analysed in next section.

Table 7.2. Mean and standard deviation for temperatures registered during the simulation period.

Mean temperatures [˚C]				
Experiment	**1**	**2**	**3**	**Experimental**
$z = 0.5$	802.68	876.21	872.06	862.56
$z = 1.0$	847.82	932.37	918.01	-
$z = 1.8$	895.804	934.91	910.18	-
$z = 4.0$	780.924	748.076	722.83	392.02

7.2.2 Temperatures out of the pool axis

Additionally to the study of temperatures caught at the centre of the flame, temperatures registered by thermocouples placed at 0.3 and 0.6 axial positions from the pool axis were also be studied. Comparison of time evolution of temperatures at different positions for circular (simulation 1) and square (simulation 3) pool fire simulations, and the experimental data from FOC_03 project are presented from Figure 7.7 to Figure 7.10.

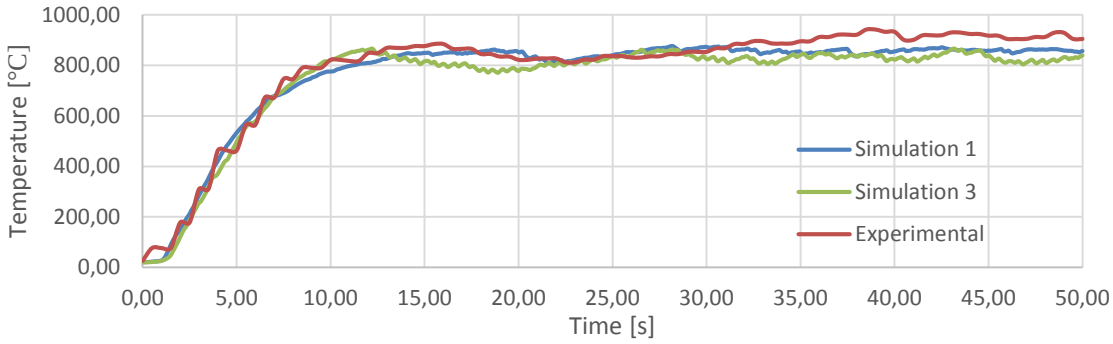

Figure 7.7 Time evolution of temperatures registered at 0.3 m from the pool axis and at 0.5 m height.

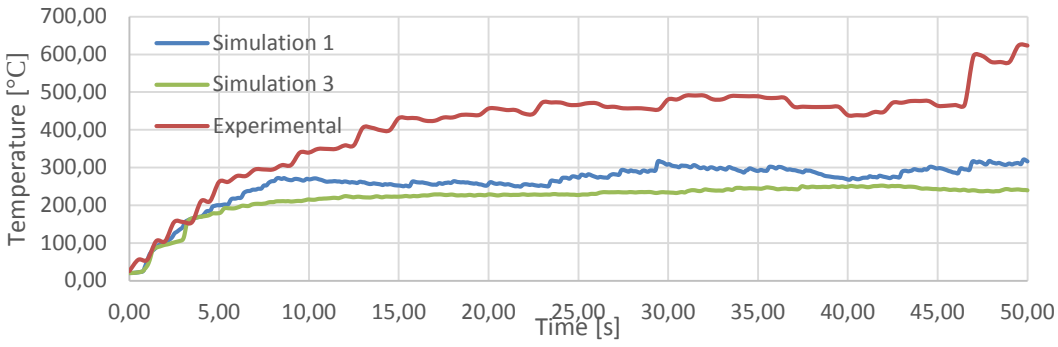

Figure 7.8 Time evolution of temperatures registered at 0.6 m from the pool axis and at 0.5 m height.

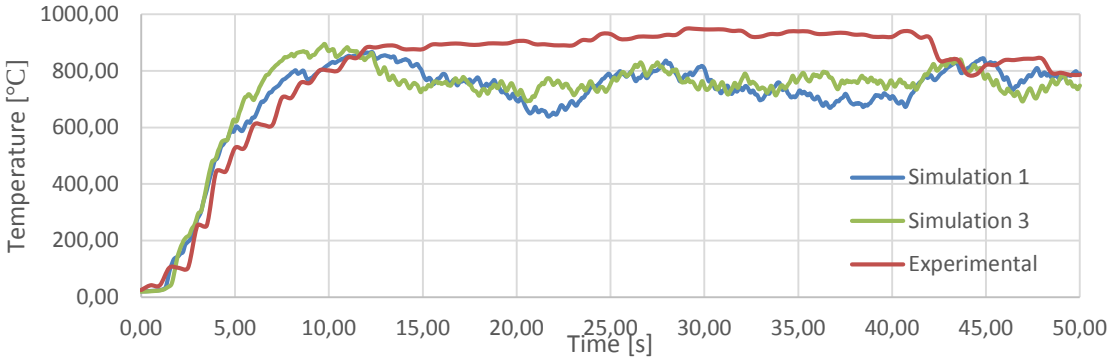

Figure 7.9 Time evolution of temperatures registered at 0.3 m from the pool axis and at 0.8 m height.

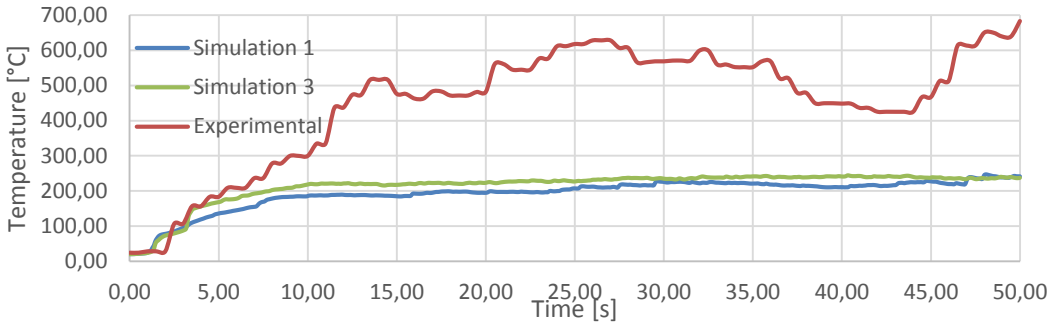

Figure 7.10 Time evolution of temperatures registered at 0.6 m from the pool axis and at 0.8 m height.

These results show that accuracy of simulated data decreases with the axial and the radial position, especially with the first one. Notice that data from simulation 2 has not been plotted, as simulation 3 provided results that were more nearby to reality than simulation 2 and this chapter is focused in the effect of different pool shapes on results.

7.2.3 Flame length

Fluid velocity has showed to be, together with the computational cell width, one of the most affective parameters in FDS hydrodynamics calculations, as plays an important role directly in FDS hydrodynamic governing equations, but also in the determination of other parameters, such as dynamic viscosity or subgrid scale kinetic energy. In addition, increasing wind speed (which is low and shows random directions by default in FDS simulations) would reinforce the variation of air entrainment caused by the change of pool shape. This is the reason why effect of pool geometry on flame length, inclination angles and flame shedding will be studied.

Figure 7.11 shows the time evolution of flame heights during 20 seconds since the stationary regime is reached. Most of measured lengths are comprised between the values of 400 and 600 cm, but circular pool fire simulation, as shown, presents the data set with higher values, and therefore, the most inaccurate, as experimental flame heights of gasoline pool fire presented a mean value under 3500 cm. All simulations show flame shedding considerably similar to experimental measurements.

Data set corresponding to simulation number 3 does not reach values as extreme as the other two simulations and, in addition, presents the smallest mean value, and therefore, presents the data that is more approximated to experimental results obtained by Muñoz and Ferrero, as Table 7.3 shows.

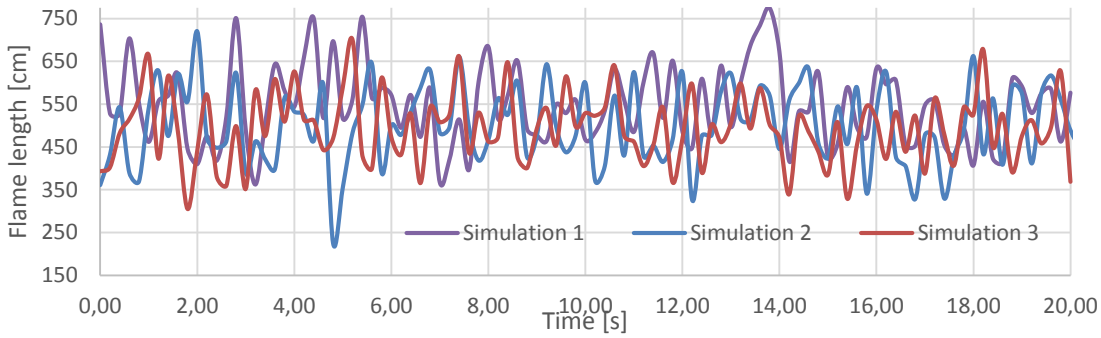

Figure 7.11 Time evolution of flame lengths measured during 20 s since steady state is reached.

Table 7.3. Summary of flame heights measurement study according to the pool study.

	Simulation 1	Simulation 2	Simulation 3	Experimental
Maximum length [cm]	774.59	719.85	700.84	598.60
Minimum length [cm]	367.32	271.59	328.23	159.40
Max-Min [cm]	407.27	448.26	372.60	439.20
Mean length [cm]	538.06	507.76	498.85	343.95
Standard Deviation	85.19	86.47	79.71	76.25
Flame shedding [s^{-1}]	1.36	1.38	1.20	1.36

As flame lengths measurement is not direct and requires a significant amount of time, next flame height studies as a function of pool shape will only consider simulation 3 pool sizes to represent a square pool fire.

7.3 Gasoline with presence of wind

7.3.1 Temperatures

Probably, as Nielsen reports (see section 3.2.5), the difference of temperatures between square and circular shape pools simulation results showed in Table 7.1 is due to the effect of air entrainment, as contact between external airflows and flame is expected to be better in circular fires. This is the reason why three new simulations were performed, setting wind flows in the x direction with speed of u=2 m/s and u=4 m/s. Results of these simulations are given below.

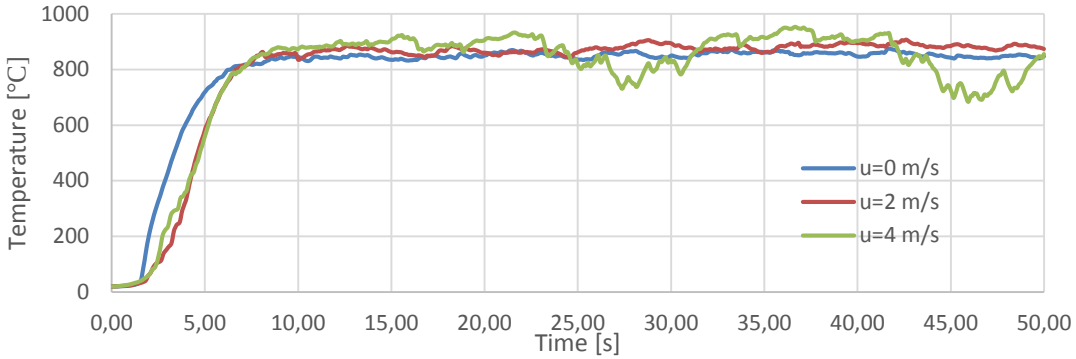

Figure 7.12 Time evolution of temperatures caught by thermocouple set at z=1 m for simulation nº1.

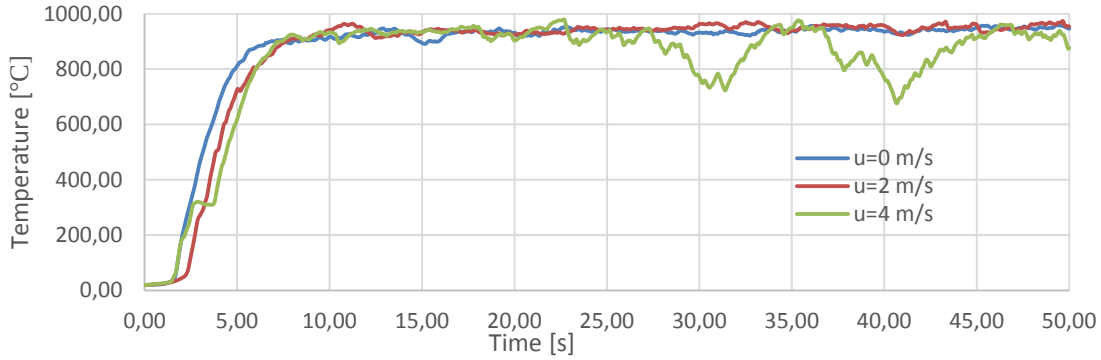

Figure 7.13 Time evolution of temperatures caught by thermocouple set at z=1 m for simulation nº2.

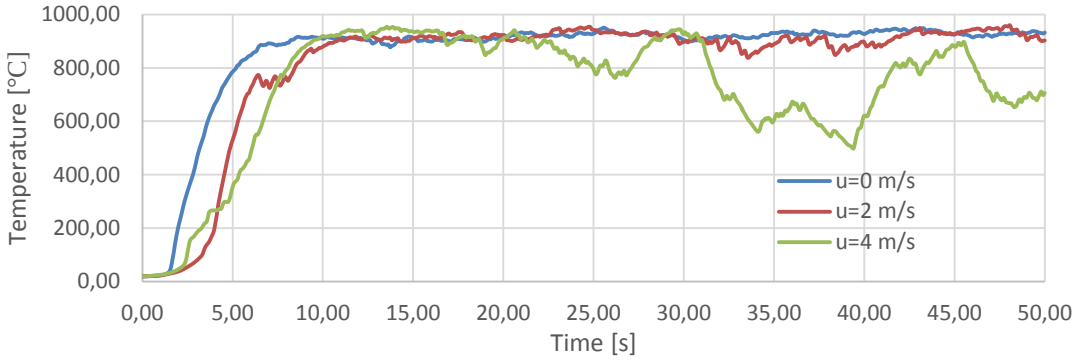

Figure 7.14 Time evolution of temperatures caught by thermocouple set at z=1 m for simulation nº3.

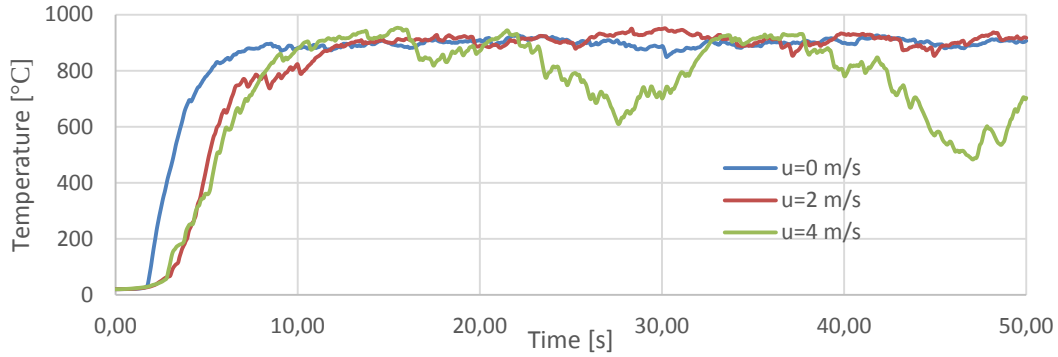

Figure 7.15 Time evolution of temperatures caught by thermocouple set at z=1.8 m for simulation 1.

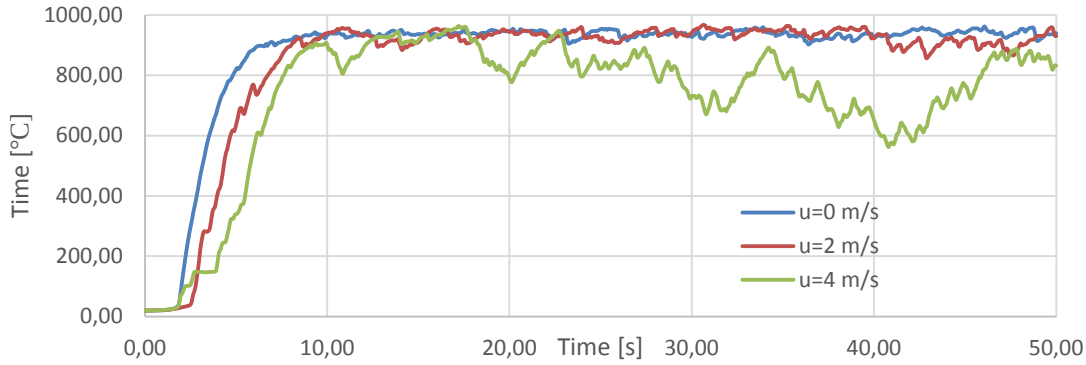

Figure 7.16 Time evolution of temperatures caught by thermocouple set at z=1.8 m for simulation 2.

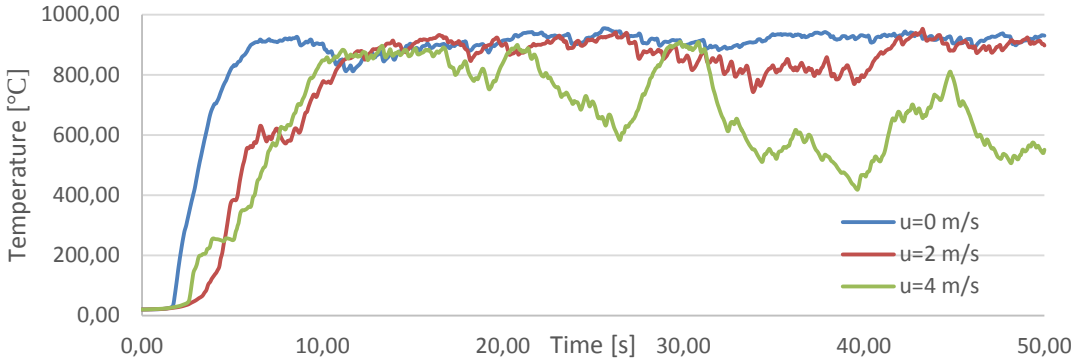

Figure 7.17 Time evolution of temperatures caught by thermocouple set at z=1.8 m for simulation 3.

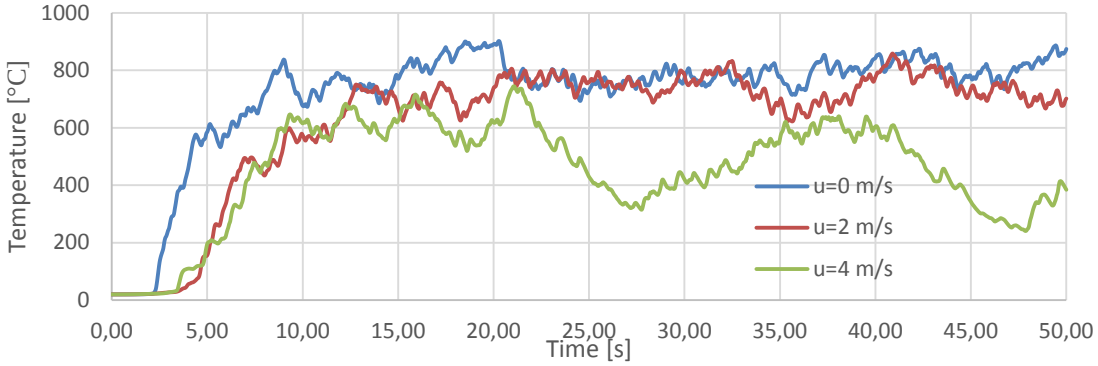

Figure 7.18 Time evolution of temperatures caught by thermocouple set at z=4 m for simulation 1.

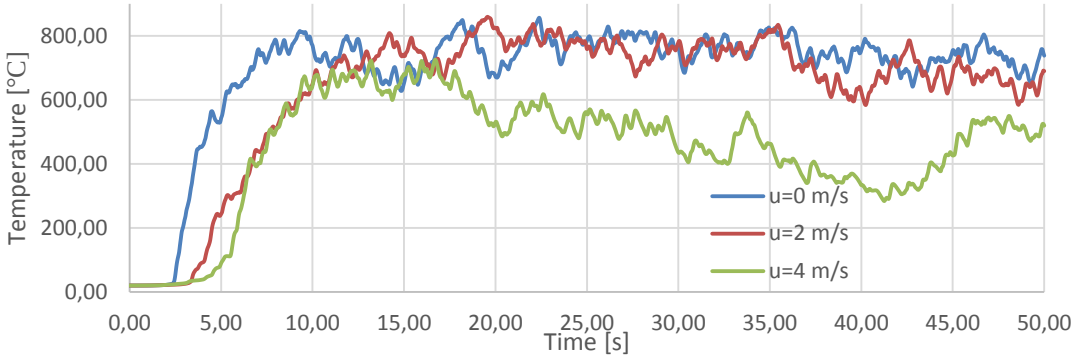

Figure 7.19 Time evolution of temperatures caught by thermocouple set at z=4 m for simulation 2.

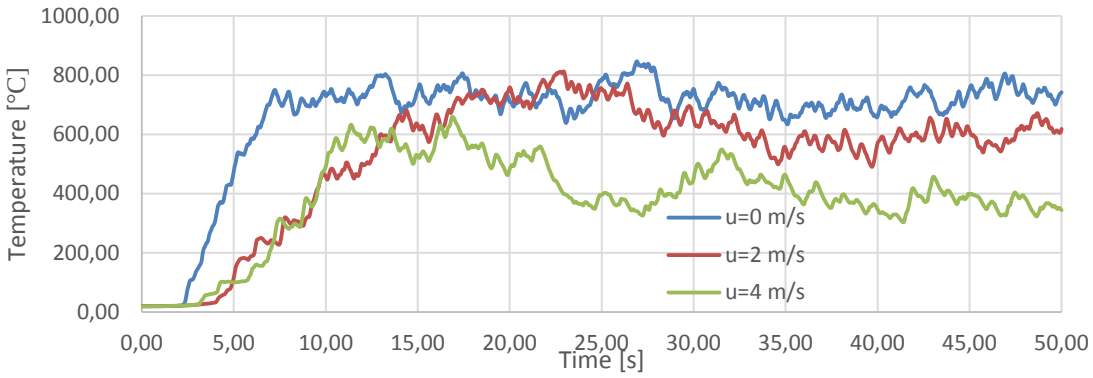

Figure 7.20 Time evolution of temperatures caught by thermocouple set at z=4 m for simulation 3.

From Figure 7.12 to Figure 7.20, it is possible to see that time required to reach the steady state of temperatures is higher with presence of wind, and that wind speed of 2 m/s does not change significantly the stationary temperatures registered by thermocouples set at 1 and 1.8 m height z positions, in experiments nº1 and nº2 but it does in case of nº3.

When wind speed is increased to 4 m/s, different low-value peaks appear in the time evolution of temperatures, which are not important in the case of the circular pool fire at z= 1 m height, as Figure 7.12 shows, but grow as the measured axial position increases, especially after 30 s of the fire beginning, until this circular shape pool fire reaches the lowest registered temperature through all studied cases (near 300 ˚C). Square shape pool fires show more peaks than the circular pool, and follow the same tendency of showing lower temperatures as axial position and wind speed increase. For wind speed of 4 m/s, temperatures registered by thermocouple set at z=4 m in square shape pool fires reach their maximum about 15 seconds after the fire begins and do not recover this value in all the considered simulation period.

The simulation that presents a time evolution of temperatures most affected by the wind is undoubtedly nº3, which reaches the lowest temperature of most of analysed cases. Simulation nº2 follows a similar pattern for time evolution of temperatures (but does not reach so low values), which could be explained as they both present a square shape.

7.3.2 Flame lengths

In presence of a non-negligible wind speed, this pushes the flames, which provokes the inclination of the whole flame, especially when the stationary regime is not established yet. Considering flame heights as highest values found in the Y coordinate would imply a considerable error when all the body that constitutes the flame is inclined, as case shown in Figure 7.21, where flame length and flame angle are calculated from a Smokeview animation screenshot of region emitting more than 100 kW/m^3.

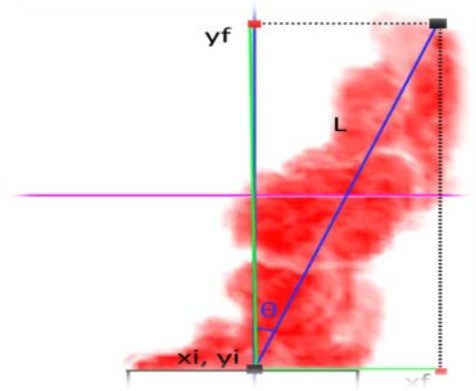

Flame length

$$L = \sqrt{(y_f - y_i)^2 + (x_f - x_i)^2} \quad (7.1)$$

Flame inclination angle

$$\theta = \tan^{-1}\frac{(x_f - x_i)}{(y_f - y_i)} \quad (7.2)$$

Figure 7.21 Flame lengths and flame angles calculation method from a Smokeview screenshot.

Time evolution of flame lengths and inclination angles for circular (experiment 1) and square (experiment 3) pool fires when wind blows from west to east with velocity of 2 m/s are compared in Figure 7.22 and Figure 7.23 respectively. Comparison of pool geometry effect on flame lengths and inclination angles when wind speed is 4 m/s (also from east to east) can be seen in Figure 7.24 and Figure 7.25.

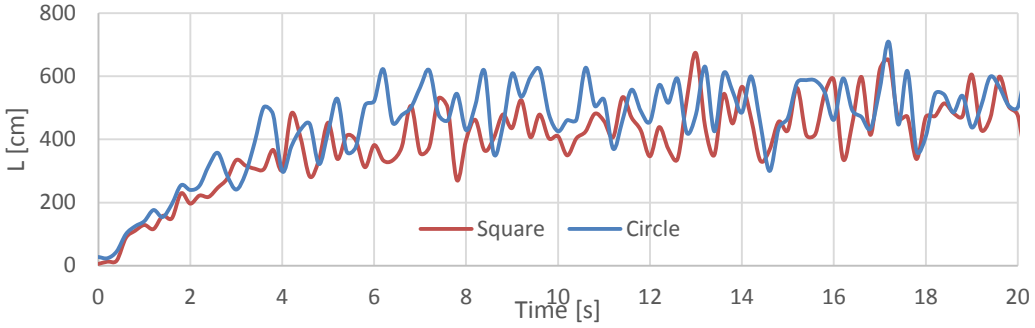

Figure 7.22 Time evolution of flame lengths during the first 20 s of simulation, w.s.=2 m/s.

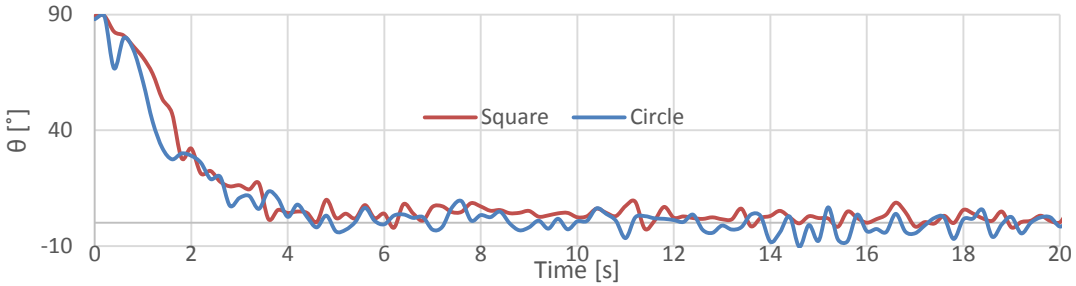

Figure 7.23 Time evolution of inclination angles during the first 20 s of simulation, w.s.=2 m/s.

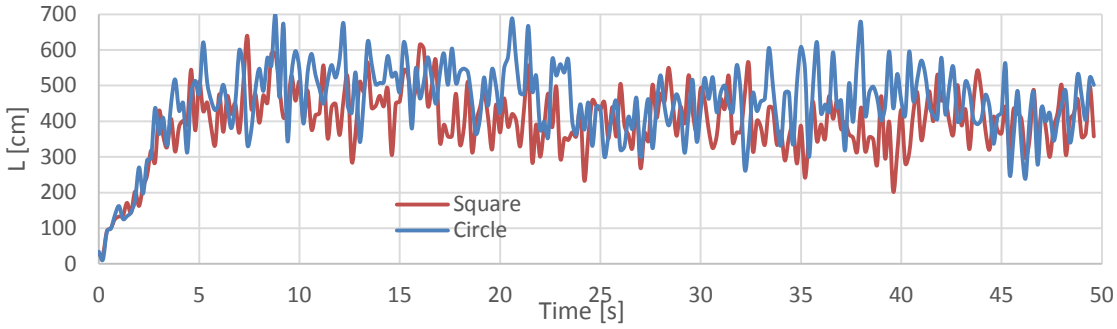

Figure 7.24 Time evolution of flame lengths during the first 50 s of simulation, w.s.=4 m/s.

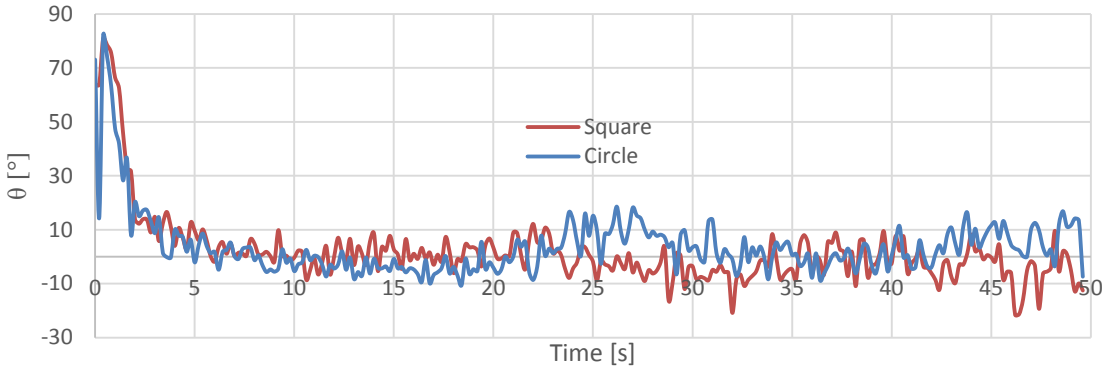

Figure 7.25 Time evolution of inclination angles during the first 50 s of simulation, w.s.=4 m/s.

Time chosen maximum plotted values are different when wind speed varies, as at approximately 25 or 30 seconds from the ignition beginning, flames observed in Smokeview animations look more pressed by the effect of wind, showing generally smaller flame lengths and larger flame widths. This can be observed in Figure 7.25 as a discrete increase of the

amplitude of the oscillations that inclination angle suffers. After 22 seconds approximately since the ignition begins, the wind inclines the flame in the opposite direction as initially in the case of circular pool, whose fire initially presents positive inclination angles (flame inclined to east) and from this moment fort, flames are inclined mainly in the opposite direction.

The main conclusion, regarding pool shape effect on the sensitivity of wind speed on flame height, is that square pool fires show lower heights but similar inclination angles, fact that can be attributed to smaller temperature and HRRPUV values, which can be translated into a better refrigeration, and therefore, a better interaction between wind and fuel vapours, which are pushed out of the source of ignition by wind. The fact that temperatures registered by thermocouple set at z=4 m height show a larger difference when wind is introduced in simulation 3 than in simulation 1 reinforces this conclusion, as difference between flame heights from Table 7.3 and Table 7.4 are more remarkable in the case of square shape pool fires.

Time evolution of inclination angles follows the same pattern in both simulations that represent a same value of wind speed: at the first seconds after the ignition of fuel begins, flame inclination is near 90º, as feedback mechanism has not been established yet. However, 4 seconds after the ignition beginning, inclination angles and flame lengths reach a steady state, which is preserved until the fire suppression occurs[7].

Table 7.4. Summary of study regarding flame lengths determination in gasoline pool fires of different shapes.

Flame lengths and inclination angles for different pool geometries and wind speed values				
	Wind speed = 2 m/s		Wind speed = 4 m/s	
Pool shape	**Circle**	**Square**	**Circle**	**Square**
L_{max} [cm]	734.59	673.65	698.48	639.04
L_{min} [cm]	299.96	270.90	240.14	203.03
$L_{max} - L_{min}$ [cm]	434.62	402.74	458.34	436.01
L_{mean} [cm]	513.89	459.05	470.16	413.86
$Standard\ deviation\ of\ L$	81.32	87.59	87.71	76.23
θ_{max} [°]	9.77	8.51	18.56	12.18
θ_{min} [°]	-10.33	-3.10	-10.62	-21.50
θ_{mean} (abs.) [°]	3.37	2.50	5.20	4.79
$Standard\ deviation\ of\ \theta$	9.77	8.51	6.43	6.08

From Table 7.4, is it possible to appreciate that mean values of flame lengths decrease with the wind intensity, while inclination angles are increased, as expected. Mean flame lengths variation when wind speed is increased is more important in the case square pool fires, while flames inclination increment is more exaggerated for the case of circular pool fires. Largest difference between standard deviations when wind intensity is incremented is presented by square pool shape, in flame length as circular pool deviations scarcely varied when wind intensity was increased. Finally, is it important to point out that standard deviation of the

[7] However, fire suppression will never occur in the studied cases. As a pyrolysis model could not be defined, a constant mass loss rate per unit area controls the formation of fuel vapour that will be ignited. This vaporization rate is constant and is preserved during all simulation time.

inclination angle for circular pool fires suffer a considerably higher increase than for square basis fires. Angles standard deviations decrease with wind speed in both cases, while length standard deviations increase with wind speed in circular pool fires and decrease in square pool fires. In addition, it is possible to appreciate that while maximum flame inclination angle to west (minimum angle) does not vary practically when wind speed is increased in the case of circular pool fires, square pool fires registers a minimum value which is nearly 7 times the minimum reached when wind speed was 2 m/s. Flame shedding could not be measured, as it was extremely variable when wind speed was 4 m/s; however, in the case of wind speed of 2 m/s, both pool geometries showed a vortex shedding value of 1.18 s^{-1}.

Simulation 3 seems to gather in all performed comparisons the values of temperature and flame lengths that are more nearby to experimental data by Muñoz and Ferrero. This is the reason why, in the case of gasoline, pool geometry of simulation 3 will be used for the sensitivity study.

7.4 Diesel in absence of wind

7.4.1 Temperatures at the pool axis

As performed for gasoline pool fires, time evolution of temperatures registered by thermocouples set at low and high axial positions (respectively z=0.5 and z=4.0 m) are compared in figures below.

As time evolution of temperature plots show, in the case of diesel, temperatures are more under predicted by FDS in low axial positions, especially for circular pool shapes, if results are compared to gasoline.

On the other hand, temperatures caught by thermocouples at high axial positions are over predicted, and therefore, flame lengths too. This difference is larger for the circular pool shape fire.

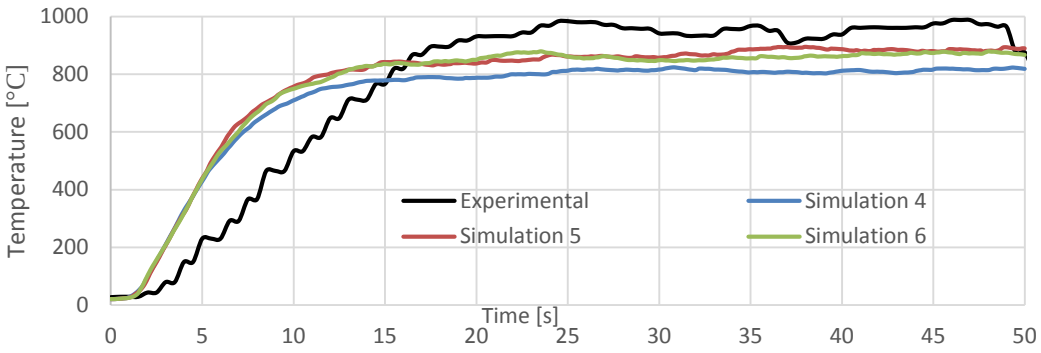

Figure 7.26 Time evolution of temperatures registered at the pool axis and at 0.5 m height.

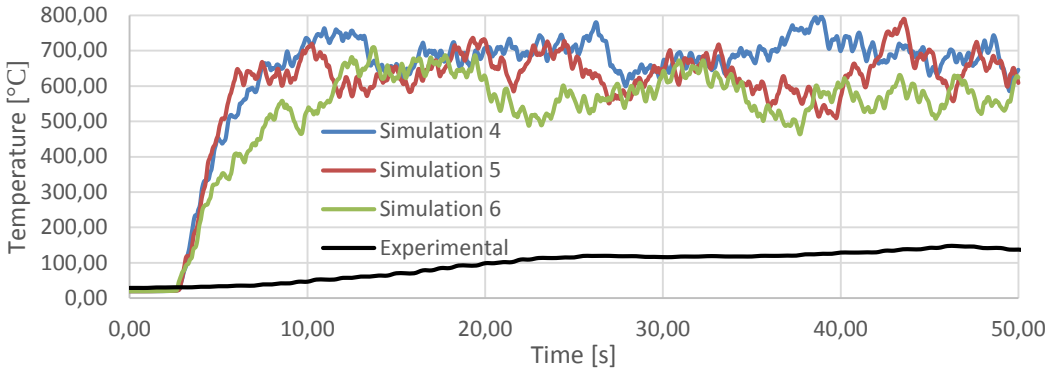

Figure 7.27 Time evolution of temperatures registered at the pool axis and at 4 m height.

7.4.2 Temperatures out of the pool axis

As performed in the case of gasoline, temperatures registered by thermocouples which are set at axial positions z=0.5 and z=0.8 m for two radial positons (50 and 80 cm from the pool axis) will be compared to experimental data from FOC_03 project in order to check the accuracy of simulation data provided by FDS in these positions.

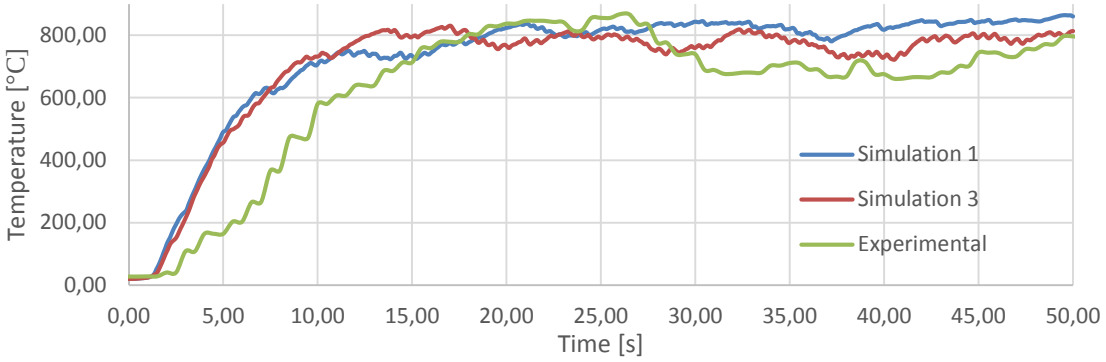

Figure 7.28 Time evolution of temperatures registered at 0.3 m from the pool axis and at z=0.5 m.

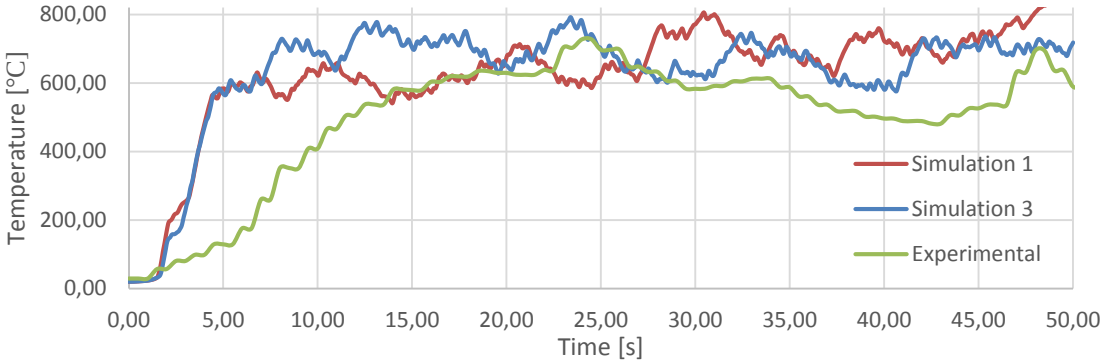

Figure 7.29 Time evolution of temperatures registered at 0.3 m from the pool axis and at z=0.8 m.

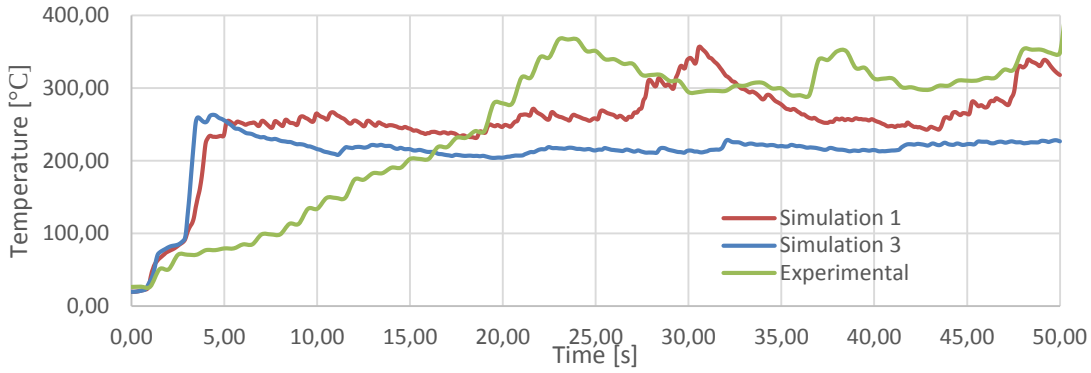

Figure 7.30 Time evolution of temperatures registered at 0.6 m from the pool axis and at z=0.5 m.

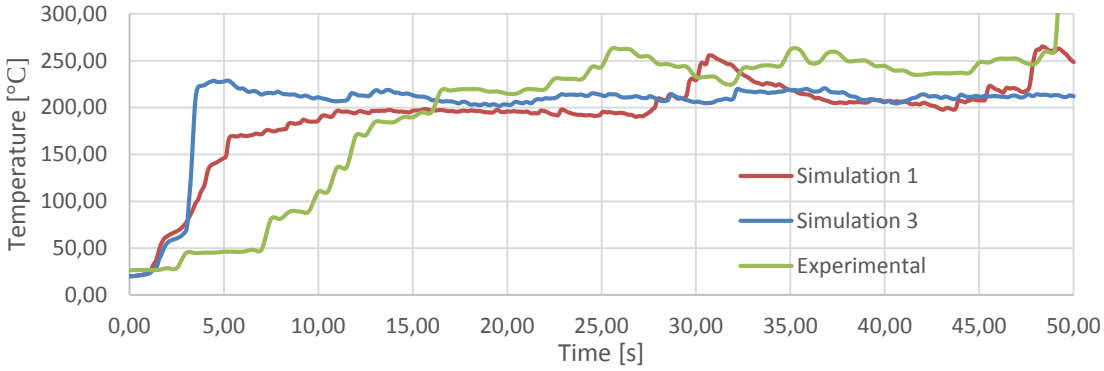

Figure 7.31 Time evolution of temperatures registered at 0.6 m from the pool axis and at z=0.8 m.

Is it possible to appreciate that simulation results of temperatures caught by thermocouples set out of the pool axis are more accurate for the case of diesel than for gasoline. In former plots, simulations reach the stationary temperature practically immediately while experimental fire takes several seconds. Circular pools present larger temperature values in z=0.5 while square pools present larger temperatures in z=0.8 m height. Square pool seems to present results more nearby to experimental data in thermocouples at radial distance of 30 cm from pool axis, while circular fires show more accurate results for measurements taken at radial distance of 60 cm from pool axis.

7.4.3 Flame lengths

As Figure 7.27 showed, central thermocouple set at 4 meters height registers temperatures for simulation 4 (circular pool) which are most of time over 525 ˚C (Draper point), and therefore, is it possible to consider that flame at that height exists. In simulation 6, however, registered values are often 525 ˚C and therefore, is it possible to consider that flame does not exists at this height. Flame heights will be, then, significantly larger for simulation 4 than for simulation 6, as Figure 7.30 shows.

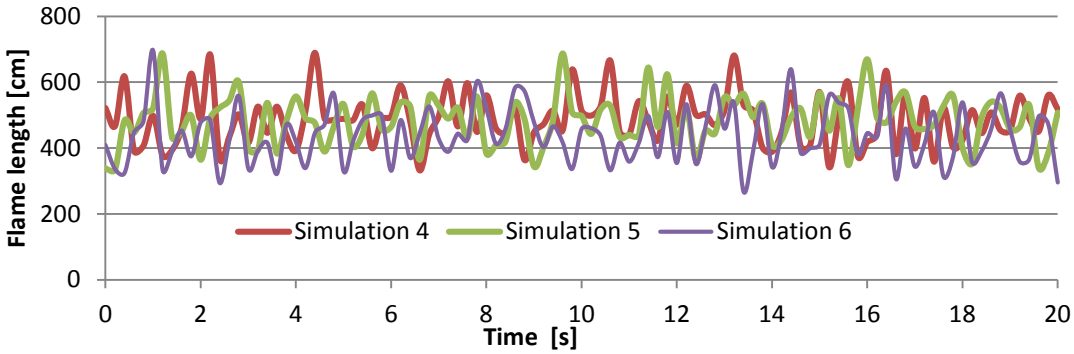

Figure 7.32 Time evolution of flame lengths measured during 20 s since steady state is reached.

Table 7.5. Summary flame lengths measurement study according to the pool geometry.

	Simulation 1	Simulation 2	Simulation 3	Experimental
Maximum length [cm]	689.55	687.01	638.89	450.90
Minimum length [cm]	332.22	339.89	267.73	110.00
Max-Min [cm]	357.34	347.12	371.16	340.90
Mean length [cm]	489.72	484.58	439.44	259.82
Standard Deviation	78.02	72.38	82.00	57.56
Flame shedding [s^{-1}]	1.42	1.33	1.39	1.36

7.5 Diesel in presence of wind

As proceeded in the case of gasoline, effect of wind on gasoline pool fires will be also tested. As temperatures reached at determinate axial positions are directly related to flame lengths, comparison of wind speed effect on temperatures for different cases of wind speed and different pool shapes are not compared.

Looking at Figure 7.33, is it possible to appreciate that when wind speed is 2 m/s, as happened for the case of gasoline, circular pool fires show higher flame length peaks than square pool fires. Regarding to inclination angles, when wind speed is 2 m/s, the time evolution of measured angles follows a similar pattern that gasoline fires followed (initially high angles until the steady state is reached, and then, oscillating values in both directions (right, positive angles and left, negative angles) with low oscillation amplitudes. Square pool fires show scarcely wider oscillation amplitudes than square basis pool fires.

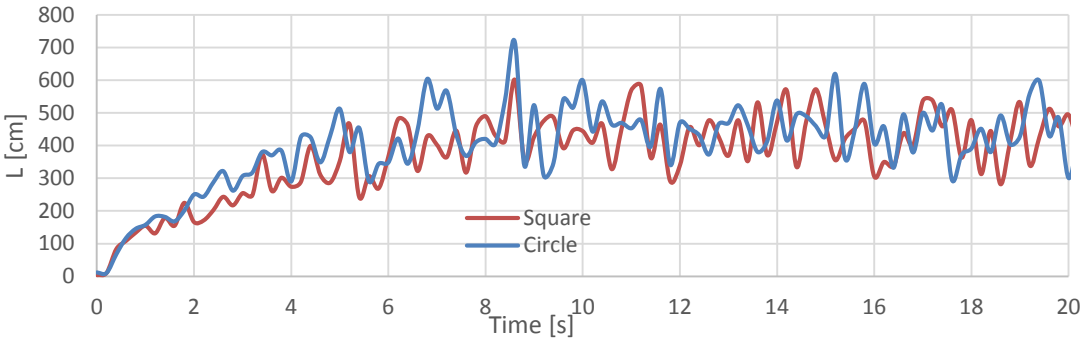

Figure 7.33 Time evolution of flame lengths during the first 20 s of simulation, w.s.= 2 m/s.

ETSEIB

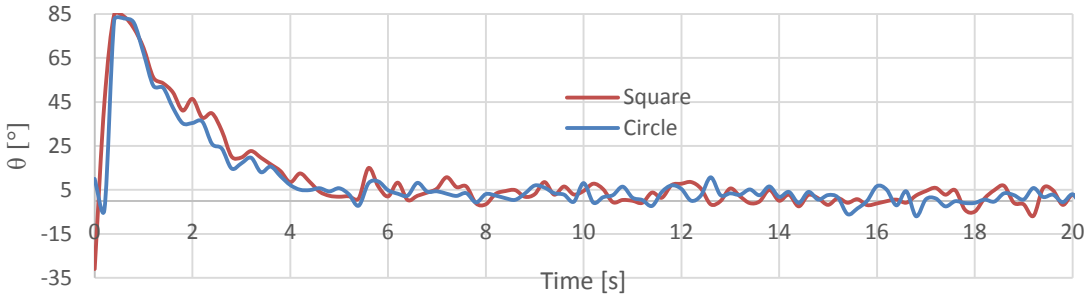

Figure 7.34 Time evolution of inclination angles during the first 20 s of simulation, w.s.= 2 m/s.

Exactly has happened in the case of gasoline, when wind speed is 4 m/s, three periods or stages can be found in the fire behaviour: a fire growth (transitory regime), which lasts approximately 5 seconds, an initial stationary regime until approximately 35 seconds from the ignition beginning, and a stage in which fire is pushed down by wind providing lower flame lengths and larger flame widths. This is the reason why data is registered during 50 seconds instead of 20.

Looking at figures below, is easy to appreciate that circular pool fires register higher maximum values of flame lengths; however, both fires show a similar pattern of time evolution of registered lengths. In the case of angles, circular pool fires are in most of cases inclined by wind to right (show positive inclination angles), while square pools provide fires which are usually inclined to left (negative angles).

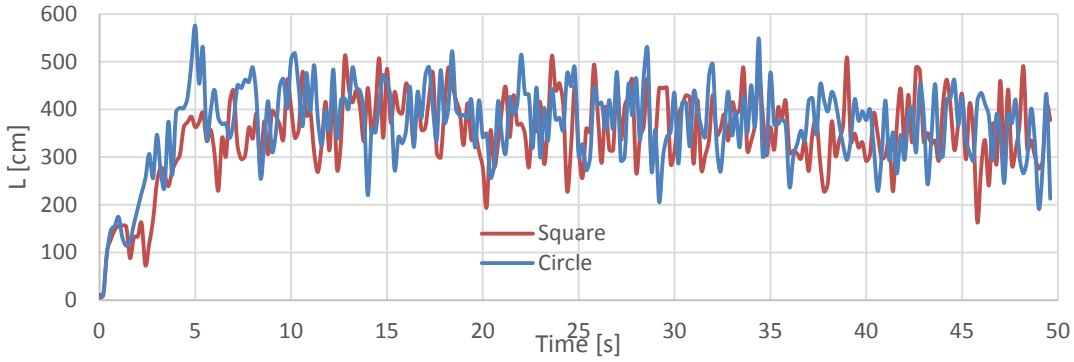

Figure 7.35 Time evolution of flame lengths during the first 50 s of simulation, w.s.= 4 m/s.

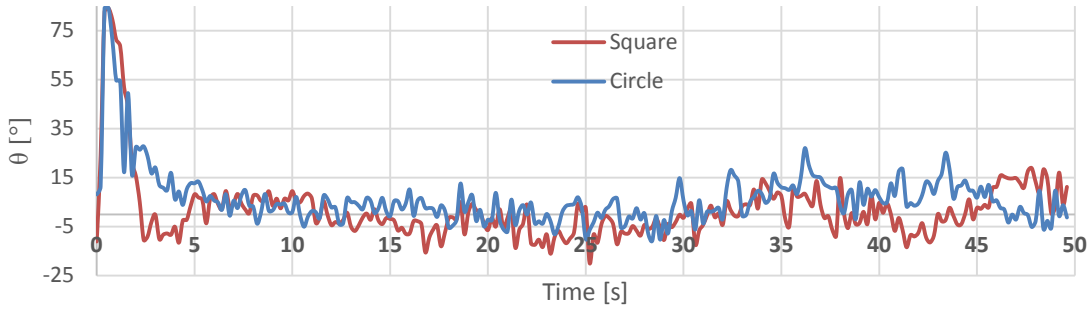

Figure 7.36 Time evolution of inclination angles during the first 50 s of simulation, w.s.= 4 m/s.

Summary of results obtained in the study of different pool shapes effect on flame lengths with different wind speed values are shown in Table 7.6.

Table 7.6. Summary of study regarding flame lengths measurement in diesel pool fires of different shapes.

Flame lengths and inclination angles for different pool geometries and wind speed values				
	Wind speed = 2 m/s		Wind speed = 4 m/s	
Pool shape	**Circle**	**Square**	**Circle**	**Square**
L_{max} [cm]	719.82	602.42	548.82	511.99
L_{min} [cm]	290.95	242.79	192.29	163.56
$L_{max} - L_{min}$ [cm]	428.86	359.63	356.52	348.43
L_{mean} [cm]	453.84	425.97	380.27	363.57
$Standard\ deviation\ of\ L$	86.35	79.00	69.39	66.39
θ_{max} [°]	10.73	14.95	26.98	18.86
θ_{min} [°]	-6.98	-6.85	-10.83	-19.96
θ_{mean} (abs.) [°]	3.13	3.39	6.01	5.98
$Standard\ deviation\ of\ \theta$	10.73	14.95	6.56	7.42

Exactly as happened in the case of gasoline fires, circular pool shapes provide higher maximum flame lengths in both cases of wind speed, although the difference is more remarkable when wind pushes the fire at 2 m/s. Differences between maximum and minimum values decrease with the wind speed, exactly as mean of registered flame heights. As obvious, maximum and minimum absolute values for inclination angles increase with the wind speed, and the mean of absolute values of inclination angles too. Curiously, in this case, standard deviation values decrease when wind speed increases in the case of both studied parameters.

7.6 Discussion

In both cases of gasoline and diesel and in all simulations, temperatures registered by thermocouples set at the pool axis and at z=4 meters height are over predicted by FDS. In general, temperatures registered by thermocouple set at the pool axis and z=0.5 meters height are underestimated, especially in the case of gasoline fires of circular shape, but maximum values registered by FDS thermocouples are similar to experimental maximum temperatures. Regarding thermocouples out of the pool axis, FDS clearly underestimates the caught temperature values. Flame lengths are over predicted in all performed simulations, especially for the circular geometry pool fires.

As Table 7.7 shows, simulation results of mean flame lengths are over all estimations performed by theoretical models described in section 2.3.2. The model that gives the best approximation for the behaviour of simulated data is that which Thomas developed in 1963.

Flame shedding in gasoline pool fires suffers few variations during simulation period, while in the case of gasoil it showed more variability between different time differentials taken for a single simulation, and this is why, averaged shedding values had to be used. Mean vortex shedding values are good predicted in the case of both gasoline and diesel fires, as mean

values are very nearby to experimental measures and also to 1.225 s^{-1}, value given by equation (2.13). This parameter seems not to depend on which is the fuel used.

Table 7.7 Comparison of mean flame lengths provided by FDS, determined experimentally and estimated by theoretical models

Mean flame lengths determined through different methods [m]									
Fuel	Wind speed	Simulation 3	Experimental	Thomas	Moorhouse Cyl.	Mangialavori & Rubino	Pritchard & Binding	Muñoz	Heskestad
Gasoline	0 m/s	4.99	3.44	4.77	3.18	4.08	4.38	3.53	3.76
	2 m/s	4.59	-	4.13	3.07		4.28	3.27	
	4 m/s	4.14	-	3.57	2.98		4.2	3.05	
Diesel	0 m/s	4.39	2.60	4.18	3.00	3.6	4.1	3.25	2.49
	2 m/s	4.26	-	3.52	2.90		4	3.00	
	4 m/s	3.64	-	3.05	2.81		3.92	2.8	

Simulations 3 and 6 have shown the results that are most nearby to experimental data collected by Muñoz and Ferrero in both temperatures and flame lengths. This is the reason why square pool fires with an area slightly lower than experimental fires will be used instead of the original circular fires for the sensitivity study. This shows that, at least for pool diameters of 1.5 m, trying to create circular geometries using different rectangular obstacles in order to achieve the most similar to reality FDS scenario can provide, moreover of the additional effort of creating complex geometries, more inaccurate results that if a single rectangular obstacle is set.

8 Sensitivity study

8.1 Background

In the present study, temperatures at a given position and flame heights may depend on many different FDS input parameters, which are mainly fuel properties and ambient conditions, but also simulation settings, such as radiative fraction. This sensitivity study will indicate how output results vary with fluctuations of these FDS input parameters, and then, how sensitive is response in front of these variations.

In order to perform this analysis, once the studied parameters are chosen, three simulations are performed for each parameter. The first of these simulations is a base case in which square pools fires chosen in chapter 7 are reproduced with the same ambient conditions as the experimental case and in the other two simulations, the studied parameter will be increased and decreased by a 10%. Using the obtained results, the sensitivity coefficient can be calculated according to equation (*8.1*) (Tarragó, 2010):

$$SF = \frac{|F_{+10\%} + F_{-10\%}|}{0.2\ F} \tag{8.1}$$

Where F, $F_{+10\%}$, $F_{-10\%}$ are the mean output values of the base simulation, the simulation in which the studied parameter has been increased in 10% and simulation in which the parameter is decreased in 10%. SF is the relative sensitivity that allows to classify the output response a studied parameter into different categories according to the following criterion (Tarragó, 2010):

- Insensitive, if SF<0.5
- Low sensitivity, if 0.5<SF<1.0
- Moderate sensitivity, if 1.0<SF<2.0
- High sensitivity, if SF>2.0

Due to lack of time, not all the parameters involved in the calculations that FDS performs could be tested. Environmental variables such as air density, air specific heat, and ambient temperature were discarded as their variation between seasons is scarce. The most affected variable of this group would be ambient temperature (given in Kelvin degrees), but, its variation, for example, in equation (*2.9*) for the estimation of flame length (and therefore, the rank of temperatures that thermocouples at high axial positions register), is negligible in comparison with variations of fuel properties.

Fuels are an important source of variability, as these are mixtures of different hydrocarbon fractions and their exact composition is not static. According to empirical correlations detailed in section 2.3.2, the fuel parameters that could affect most the average flame lengths (and then, temperatures registered at hot smoke region), are mass loss rate per unit area and enthalpy of combustion. However, as seen in section 3.1.1, fluid density plays an important role in the determination of hydrodynamic parameters and then, the effect of fuel density on simulation results will also be studied. Since a mass loss rate per unit area has been indicated directly to FDS, parameters related to fuel vaporization such as boiling temperature or heat of vaporization are automatically discarded from this study.

As chosen grid resolution is not as fine as recommended, effect of radiative fraction on simulation results will be also studied, as radiation inside flame zone is affected by this parameter when temperatures are under estimated (see equation (3.23)).

8.2 Results

Simulation results for temperatures registered at pool axis in continuous flame (50 cm from the ground) and hot smoke zones (553 cm from the ground) are presented in tables Table 8.1 and Table 8.2 respectively. These results may show indirectly the mean flame length values (regions over 525˚C are considered flame), and therefore, and due to the complexity of the calculation of specific flame length values and, in addition, to lack of time, these parameters are not directly studied.

Table 8.1 Summary of sensitivity study results for mean temperatures registered at pool axis and axial position z=0.5 m.

		GASOLINE			DIESEL		
Parameter	**Variation**	$T(y=0.0, z=0.5)$	SF	**Sensitivity**	$T(y=0.0, z=0.5)$	SF	**Sensitivity**
MLRPUA [kg/[m²·s)]	-10%	869.66	0.076	Insensitive	832.41	0.054	Low sensitivity
	Base	844.20			844.90		
	+10%	856.82			841.52		
Radiative fraction [-]	-10%	855.86	0.064	Insensitive	834.58	0.018	Insensitive
	Base	844.20			844.90		
	+10%	844.99			837.65		
Heat of combustion [kJ/kg]	-10%	889.11	0.505	Low sensitivity	880.50	0.600	Low sensitivity
	Base	844.20			844.90		
	+10%	803.91			779.17		
Density [kg/m³]	-10%	870.36	0.096	Insensitive	845.95	0.020	Insensitive
	Base	844.20			844.90		
	+10%	854.10			849.31		

Table 8.2 Summary of sensitivity study results for mean temperatures registered at pool axis and axial position z=5.53 m.

		GASOLINE			DIESEL		
Parameter	**Variation**	$T(y=0.0, z=5.53)$	SF	**Sensitivity**	$T(y=0.0, z=5.53)$	SF	**Sensitivity**
MLRPUA [kg/[m²·s)]	-10%	501.26	0.650	Low sensitivity	**421.79**	**1.540**	**Moderate sensitivity**
	Base	462.40			**362.26**		
	+10%	441.16			**310.21**		
Radiative fraction [-]	-10%	509.67	0.389	Insensitive	391.10	0.795	Low sensitivity
	Base	462.40			362.26		
	+10%	473.70			333.53		
Heat of combustion [kJ/kg]	-10%	493.80	0.444	Insensitive	398.62	0.900	Low sensitivity
	Base	462.40			362.26		
	+10%	452.73			333.44		
Density [kg/m³]	-10%	429.79	0.394	Insensitive	369.80	0.075	Insensitive
	Base	462.40			362.26		
	+10%	466.23			375.21		

In the case of temperatures registered by thermocouples set at the pool axis, values are not generally very sensitive. Sensibility coefficients FS for the continuous flame zone are very small, excepting for the case of heat of combustion. For the hot smoke zone, although SF coefficients are larger, registered temperatures seem to be sensitive only to MLRPUA.

Table 8.3 Summary of sensitivity study results for mean temperatures registered 0.5 cm over the ground and at 0.3 m from pool axis.

		GASOLINE			DIESEL		
Parameter	**Variation**	$T(y=0.3, z=0.5)$	SF	**Sensitivity**	$T(y=0.3, z=0.5)$	SF	**Sensitivity**
MLRPUA [kg/[m²·s)]	-10%	807.25	0.127	Insensitive	818.03	0.259	Insensitive
	Base	816.75			800.47		
	+10%	786.56			776.50		
Radiative fraction [-]	-10%	813.60	0.002	Insensitive	779.86	0.009	Insensitive
	Base	816.75			800.47		
	+10%	813.94			778.50		
Heat of combustion [kJ/kg]	-10%	849.49	0.457	Insensitive	806.54	0.412	Insensitive
	Base	816.75			800.47		
	+10%	774.87			740.58		
Density [kg/m³]	-10%	827.51	0.104	Insensitive	813.50	0.060	Insensitive
	Base	816.75			800.47		
	+10%	810.48			823.07		

Table 8.4 Summary of sensitivity study results for mean temperatures registered 0.5 cm over the ground and at 0.6 m from pool axis.

		GASOLINE			DIESEL		
Parameter	**Variation**	$T(y=0.6, z=0.5)$	SF	**Sensitivity**	$T(y=0.6, z=0.5)$	SF	**Sensitivity**
MLRPUA [kg/[m²·s)]	-10%	242.40	0.264	Insensitive	242.05	0.411	Insensitive
	Base	237.26			238.62		
	+10%	229.85			222.45		
Radiative fraction [-]	-10%	252.48	0.778	Low sensitivity	242.98	0.657	Low sensitivity
	Base	237.26			238.62		
	+10%	215.55			211.63		
Heat of combustion [kJ/kg]	-10%	252.50	0.667	Low sensitivity	247.82	0.621	Low sensitivity
	Base	237.26			238.62		
	+10%	220.85			218.20		
Density [kg/m³]	-10%	238.11	0.000	Insensitive	235.29	0.008	Insensitive
	Base	237.26			238.62		
	+10%	238.09			234.90		

Temperatures registered by thermocouples at 30 cm from the pool axis are not sensitive to any of the studied parameters, according to the criterion established. However, in the case of values measured by thermocouple set at 60 cm from the pool axis, is possible to see that all sensitivity factors are increased regarding the previous case, excepting density, whose effect is null for temperatures registered by thermocouple at 60 cm from the axis.

It is logical to find that radiative fraction does not cause sensitive effect in temperatures registered in radial positions near the pool axis, but it does in positions far enough from there (0.6 meters from pool axis), as in these, radiation contributes to energy transport more intensely, as it is out of the direct influence of combustion gases. Heat of combustion also causes more effect in this position that in zones more nearby to pool axis, as Table 8.4 shows.

In all studied cases, simulation results of diesel fires have shown to be more affected when input variables vary, as three variables seem to be insensitive in the case of gasoline while, in the case of diesel, these same variables show to be sensitive (MLRPUA in Table 8.1 and radiative fraction and heat of combustion in Table 8.2).

In general, cases whose output result is sensitive to variations in the input variables, the sensitivity that these show is low. However, in temperatures caught by thermocouple at z=5.53 shows to be moderate sensitive in the case of diesel, as is it possible to see in Table 8.2.

Temperatures registered by thermocouple set 0.5 m over the ground and 0.3 m from the pool axis are not sensitive to any studied parameter, according to Table 8.3.

While MLRPUA and enthalpy of combustion have shown to be the parameters whose variation can affect most the results, especially in high and low axial positions at the pool axis, respectively. Radiative fraction seems to cause significant variations in temperatures registered out of the flame. Density does not affect sensitively any temperature set in any of the studied cases. However, if a finite pyrolysis model had been defined, fuel density could have played an important role on the fire duration, as total fuel mass contained in the pool is computed from pool area defined from geometry, user specified fuel layer thickness and fuel density.

9 Project sustainability study

The environmental impact of this project follows the guidelines indicated in article 7 of Spanish *Ley de Evalución de Impacto Ambiental de Proyectos* (*Ministerio del Medio Ambiente*, 2008).

9.1 Project general description

The realization of this project consists in the validation of Fire Dynamics Simulator in the case of medium scale hydrocarbon pool fires. The sustainability study of this project is given only by the performance of this task.

9.2 Alternatives study

As this project is completely theoretical, there are no alternative solution to its realization.

9.3 Work environment description

This project has been wholly performed at CERTEC offices, placed at chemical engineering department of ETSEIB, UPC (see section 2.5 for more detailed information). The realization of this project has not modified significantly the environmental quality levels.

9.4 Identification of impacts on environment

9.4.1 Evaluation criteria

Environmental impacts that a project may cause on environment can be provoked by three reasons: due to the existence of the project, due to the usage of resources or due to the generation of waste.

The type of effect of impacts may be positive (the development of the project may provide benefits for the science, the society and the environment) or negative (the project may cause damage in environmental, social, economic and other terms).

According to the incidence degree of an impact, these can be divided into direct and indirect impacts.

Finally, in order to value the magnitude of the valuation of a potential environmental impact, according to its degree of environmental compatibility, these can be classified into the following categories:

- **Compatible EI:** Those for which the environment recuperation is immediate and does not require any protective measure.

- **Moderate EI:** Those for which the environment recuperation does not require any protective measure, but recovering the initial environmental conditions may require certain time.

- **Severe EI:** Those for which the recuperation of environmental conditions requires to establish certain protective or corrective measures, in addition to a dilated time.

- **Critical EI:** Those impacts that present a magnitude over the acceptable limit, producing a permanent loss of the environmental conditions quality, without the possibility of recuperation not even with the adoption of protective or corrective measures.

In addition to evaluate the specific impacts of the different cause-effect relations, these are necessary to be valued regarding to project global impact. Global project magnitude will be considered as positive if the global valuation is compatible, moderate or severe, while it will be considered as negative if the global valuation is critical. Impacts caused by project realization are analysed below.

9.4.2 Impact due to the project realization

The impact produced by the performance of this project is positive, as the validation of a fire simulator permits to reduce the number of necessary experiences and therefore, to reduce the emission of contaminant gases products of combustion, but also avoids saving economical and material resources. This project also contributes to determine the behaviour of hydrocarbon fires, and therefore, help in the actuation in front of these accidents, which supposes a benefit for whole society.

9.4.3 Impact due to the usage of resources

There is a direct impact associated to the usage of different resources, especially office material, paper and printer ink. The management of the different wastes is performed according what the normative provided by *Agència Catalana de Residus* requires; then, paper wastes must be deposited into blue containers, printer ink must be taken to an specialized recycling plant and the office material must be thrown into the yellow container of separate collection.

9.4.4 Impact due to emissions

There is an indirect impact related to the usage of electric energy, which is the combustion gases emissions at thermoelectrically centrals. The main contaminant product of the combustion of natural gas is CO_2, responsible of greenhouse effect. As the first simulations were started approximately the 28th September and ended the 15th December, and these were performed by a single computer, which has been open 7 dies per week and 24 hours per day, the time of electrical consumption is of 1896 hours. Supposing that 95% of time computers are in repose and considering that computers have a consumption of 90 W when are active and of 5 W when are in repose (Tarragó, 2010), the total consumption along the whole project is approximately 17.54 kWh.

Emission of CO_2 per produced kWh ratio that OCCC recommends to use for year 2014 (latest published data) is 267 g CO_2/kWh (Oficina Catalana del Canvi Climàtic, 2015). As an approximation, is it possible to consider that all the produced energy is consumed (there are no loses in energy transport); then, the total mass of emitted CO_2 due to the performance of this project is 4.68 kg of CO_2.

9.4.5 Impacts valuation

All impacts derived from this project can be classified as compatible impacts and, therefore, the global impact associated to the whole project too, regarding the predicted corrective measures, which are detailed in next section.

9.5 Predicted measures

The predicted corrective measures in order to minimize the impact of this project on environment are centred basically in the management of the generated waste (paper notations, empty printer cartridges, etc.). Moreover, will it be tried to minimize the consumption of these resources by using documents in electronic format when it is possible and by printing documents by the both sides.

10 Project costs study

All the expenses produced during the realization of this project are classified into two categories: the cost associated to the consumption of material resources and the cost associated to human resources.

The total cost of the project is 6483.401 €. Apportionment of costs is detailed below.

10.1 Material resources cost

The consumption of material resources during the development of this project are basically paper, office material such as pens and folders and ink cartridges for the printer, and the cost associated to the book binding. All this material is supposed to cost a total amount of 60 €.

The project has been wholly developed at CERTEC offices, and therefore, all equipment available in its installations has been used, including computers, books, and specific software, such as Microsoft Office 2010, Minitab® and Matlab®, whose licenses are not included in the project budget, as these were already available at CERTEC and at ETSEIB computer rooms and were not bought specifically for this project. Fire Dynamics Simulator software is free and therefore, it does not require any license.

In the moment of its purchase, the computer used during this project had a cost of 1000 €. Considering the whole computer life as 10 years and that a year has 52 weeks, the computer has a useful life of 520 weeks. The project has lasted 16 weeks of active work in CERTEC, so the usage of the computer due to this project supposes a 3.08 % of its whole useful life, which implies an amortization cost of 30.77 €.

As this project required to perform various simulations, one of the dominant factors which conditions the cost is the price of electricity, which is considered to be approximately 0.15 € for each consumed kWh (“ComparadorLuz”). As this project implies a direct electrical consumption of 17.54 kWh (considering the electrical expense during the work revision as null), the total cost associated to the electrical consumption is 2.631 €.

The total cost related to the usage of material resources is, then, **93.401 €**.

10.2 Human resources cost

In the case of human resources, the costs can be divided into the dedication hours of the engineering student (intern) who has developed this project, who is supposed to have a salary of 10 € per hour and the dedication hours of the two directors of this project, doctors in engineering, who have developed management and counselling tasks, and who are supposed to have a salary of 60 € per hour.

The engineering student has dedicated approximately 6 hours per day all 7 days of the week, what makes 42 hours per week and, considering that this project has been developed along 19 weeks, the total number of hours dedicated to this project are 798, which supposes a cost of 3150 €.

The two doctor engineers have dedicated to this project approximately an hour per week in 15 first weeks and 4 hours per week during the three final weeks, in which memory revision was performed, which makes 27 hours, and therefore, 3240 €.

The total cost of human resources is, then, **6390 €**.

11 Project planning

Is it possible to consider the first day of project the day July 22th 2015, after the first meeting with the professor Eulàlia Planas, who provided the thesis of Miguel Á. Muñoz and J.M. Chatris Riu and bibliographical resources in the field of fire phenomena, as the possibility to access to CERTEC installations. During the months of July, August and September an introduction and a bibliographic research about fire phenomena, pool fires and CFD was performed.

The first days of work at CERTEC installations, several simple example simulations were created and run, in order to know the software works, at the mean time that FDS User's Guide reading took place.

The bulk of the work started after the first simulation scenario was modelled and the domain study started. From then to the end of the work, collection of simulation results, new simulations and simulations planning design were combined with the redaction of this memory. Undoubtedly, the bottleneck of this project have been the simulations. If an input FDS parameter of a simulation was wrong and this had to be repeated, this time delayed the whole project.

The activities chronogram followed during the performance of this project is exposed in Figure 11.1.[8]

In addition to the development of the different sections of this project, a wide revision work has been performed between the days 21th December 2005 and 14th January 2016, which adds three additional weeks of work that was considered for the estimation of the budget in last section.

[8] Notice that black labels in chronogram denote whole project phases.

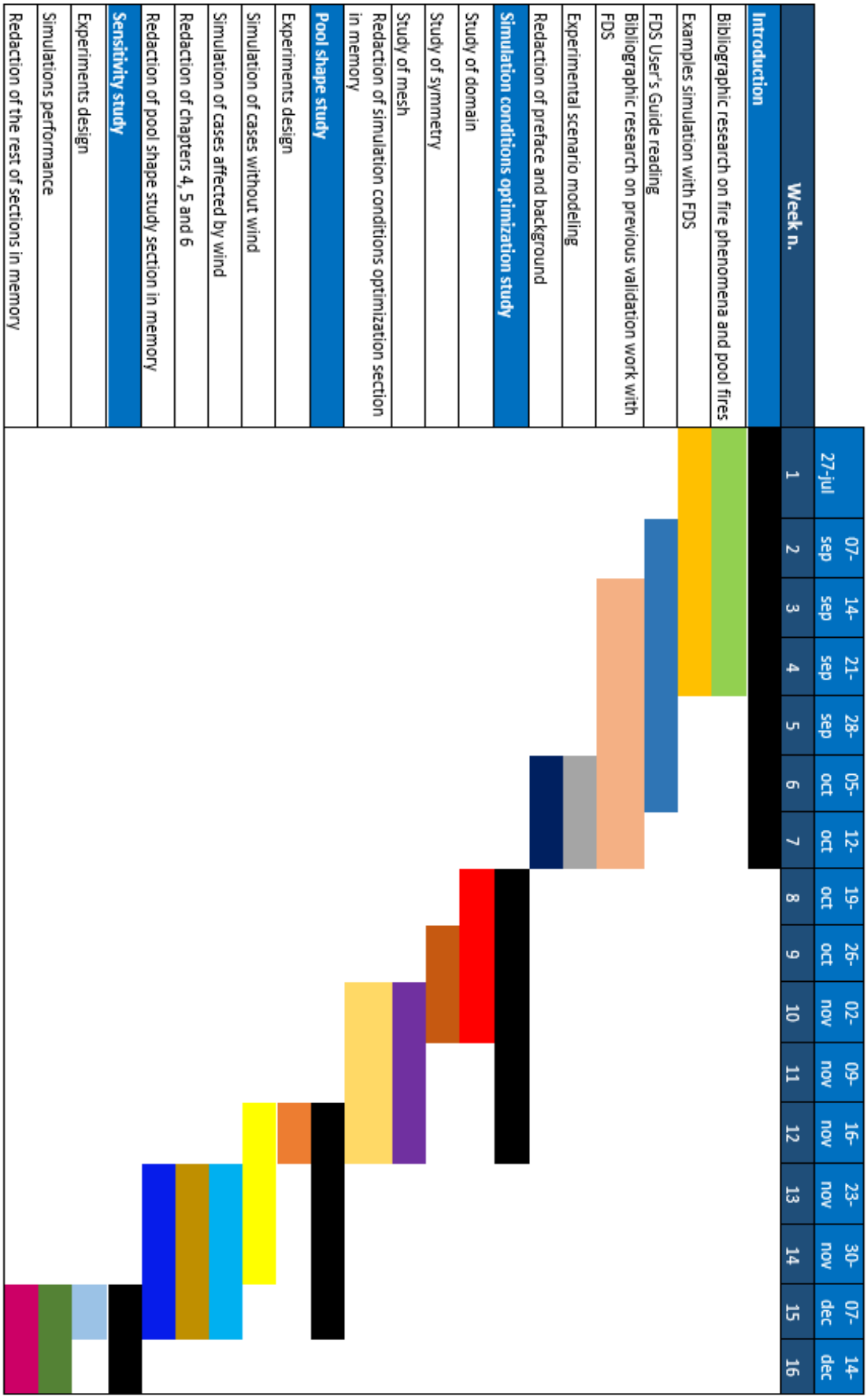

Figure 11.1 Project activities chronogram

12 Conclusions

This project can be divided into three large parts: an introduction part, in which basics about fire phenomena, pool fires and FDS simulation models, as well as previous validation works performed with FDS have been exposed; a study that had as main objective finding the most suitable simulation conditions (domain, mesh, symmetry, pool shape) and a sensitivity study, which indicates which parameters can cause a larger affection to simulation results if there are modified.

Empirical correlations introduced in background section revealed that measured fire features, such as flame lengths, are highly dependent on pool diameter, fuel heat of combustion and mass loss rates, but also on environmental properties, such as wind speed, ambient temperature or air density. Analysis of FDS governing equations showed that critical parameters in the cases contemplated for this project were computational cells width, fluid velocity and density, fuel heat of combustion and radiative fraction. As a constant mass loss rate per unit area was set instead of defining a pyrolysis or fuel vaporization model, this was also considered as a critical variable to be studied in a sensitivity study.

The bibliographic research has shown that Fire Dynamics Simulator is a very useful tool for the prediction of fire behaviour, however, it has several restrictions, such as the difficulty to include in the simulated scenario non rectangular obstacles, the impossibility to measure directly parameters such as flame lengths, which are often over predicted, or the high dependence of several parameters on grid size, which is increased in the case of pool fires.

Unfortunately, simulated times for each fire, chosen domain ($3\times3\times8$ m^3) and chosen grid size (cubical cells of 6.25 cm), were parameters very conditioned by computational resources. Then, an equilibrium between results accuracy and computational time required to perform the simulations had to be found.

In order to simulate pool fires of circular shape, the first simulation attempt tried to represent the physically most nearby to reality scenario, and from these, some simplifications have been implemented according to the results accuracy, compared to experimental data. This means that although set obstacles are provided with the same characteristics as in reality, the simulation results might not be suitable if FDS is not thought for its representation. Square fuel shapes showed to provide results more nearby to reality than approximations to circular pools by combining different rectangular shapes. In addition, creating obstacles with more or less than a cell depth has shown to have no sense, as this is controlled by the *thickness* user-specified option in FDS. For example, the fuel layer thickness may occupy a single cell height, which means 6.25 cm, but the real thickness given to FDS may be 2 cm, according to this option.

While maximum registered temperatures for simulation results are very close to maximum temperatures registered experimentally, continuous flame zone is significantly higher in the case of simulations, where temperatures at the pool axis usually are over 525 ˚C even at 4 meters height. However, and especially in the case of gasoline, temperatures registered by thermocouples at low axial positions (under 0.8 meters height) have shown to be underestimated, as temperatures measured in radial positions out of the pool axis. Temperature heights have been clearly over predicted in all studied cases, but these have shown to decrease with presence of wind. Vortex shedding values for cases with absence of

wind were also studied, showing good agreement between simulated data, experimental data and Pagni theoretical correlation.

Air entrainment has showed to vary according to the pool shape, as downfire region did not reach temperature values in circular simulated pool fire as high as in the case of square shape fires. Air entrainment varies and therefore, fuel vapour mass flux disappearance rate varies and then, heat release rate produced in the fire, which is directly related to temperatures through energy conservation equation, also suffers variations.

The results of sensitivity study showed that heat of combustion is the studied variable whose variation may affect most temperatures registered in low axial positions at the pool axis, while fuel mass loss rate per unit area affects specially the temperature at high axial positions (and therefore, flame lengths). Temperatures measured in the case of diesel fires are more sensitive to input data variations that temperatures registered in gasoline fires.

Radiative fraction affects specially temperatures of these regions that are nearby to the flame but out of it, while fuel density seems not to cause significant effect on registered temperatures.

Analysis of FDS mathematical models revealed that fuel chemical formula is also an important factor in for FDS calculations (stoichiometric factors play a very important role on simple chemistry combustion model, but also for the determination of fluid averaged molar mass). The usage of different turbulence models, especially if coarse grid sizes are used, could also imply sensitive variations on simulations results. Then, testing different validation models under different conditions, using alternative equivalent chemical formulas for the fuels or setting a real fuel composition as a lumped specie could be interesting points to be contemplated in future FDS validation projects.

13 Bibliography

Björklund, A. (2009). Risks in using CFD-codes for analytical fire-based design in buildings with a focus on FDS : s handling of under-ventilated fires.

Blinov, V. ., & Khudiakov, G. N. (1957). Certain laws governing diffusive burning of liquids. *Academiia Nauk*, *113*, 1094–1098.

Chatris Riu, J. M. (2001). *Velocitat de combustió i distribució de temperatures en incendis de bassals d'hidrocarburs*.

Chen, Z. B., Dembele, S., Wen, J. X., & Tam, V. H. Y. (2009). TOWARDS LARGE EDDY SIMULATION OF LNG POOL FIRES, (155), 326–335.

Chung, W., & Devaud, C. B. (2008). Buoyancy – comodels and large eddy simulation applied to a large axisymmetric helium plume. *International Journal for Numerical Methods in Fluids*, *58*(1), 57–89.

Comission, U. N. R. (2007). Verification and Validation of Selected Fire Models for Nuclear Power Plant Applications. Washington DC: NUREG 1824.

ComparadorLuz. (n.d.). Retrieved December 13, 2015, from http://comparadorluz.com/faq/precio-kwh-electricidad

Cowley, L. T., & Johnson, A. D. (1991). Blast and fire engineering project for topside structures. In *Fire loading series*. The Steel Construction Institute.

Deardorff, J. W. (1980). Stratocumulus-capped mixed layers derived from a three-dimensional model. *Boundary-Layer Meteorology*, *18*(4), 495–527.

Ferrero, F. (2006). Incendios de hidrocarburos: Estudio de la formación y evolución del Boilover de capa fina.

Floyd, J. E., McGrattan, K. B., Hostikka, S., & Baum, H. R. (2003). CFD Fire Simulation Using Mixture Fraction Combustion and Finite Volume Radiative Heat Transfer. *Journal of Fire Protection Engineering*, *13*(February 2003), 11 – 36. http://doi.org/10.1177/104239103031494

Hamins, a, & McGrattan, K. (1999). Reduced-scale experiments to characterize the suppression of rack-storage commodity fires. Retrieved from http://fire.nist.gov/bfrlpubs/fire99/art128.html

Hammins, A., & Kashiwagi, T. (1995). Characteristics of Pool Fire Burning. *Fire Resistance of Industrial Fluids*.

Health and Safety Executive. (n.d.). HSE website. Retrieved October 25, 2015, from http://www.hse.gov.uk/offshore/strategy/pool.htm#Background

Heskestad, B. G. (1998). Dynamics of the fire plume. *Philosophical Transactions of the Royal Society A: Mathematical, Physical and Engineering Sciences*, *356*, 2815–2833. http://doi.org/10.1098/rsta.1998.0299

Hietaniemi, J., Hostikka, S., & Vaari, J. (2004). FDS simulation of fire spread – comparison of model results with experimental data. *English*. Retrieved from http://www.vtt.fi/inf/pdf/workingpapers/2004/W4.pdf

Hostikka, S., Mcgrattan, K., & Hamins, a. (2003). Numerical Modeling Of Pool Fires Using Les And Finite Volume Method For Radiation. *Fire Safety Science*, *7*, 383–394. http://doi.org/10.3801/IAFSS.FSS.7-383

Kelsey, A., Gant, S., Mcnally, K., Hill, H., Betteridge, S., Technology, S., … Ch, C. (2014). Application of global sensitivity analysis to FDS simulations of large LNG fire plumes, (159), 1–11.

Kwon, J. W., Dembsey, N. a., & Lautenberger, C. W. (2007). Evaluation of FDS V.4: Upward flame spread. *Fire Technology*, *43*(4), 255–284. http://doi.org/10.1007/s10694-007-0020-x

M. Muñoz Domínguez, A. J. R. de A. M. J. M. P. (2014). *Ingeniería térmica*. Madrid: UNED.

Ma, T. G., & Quintiere, J. G. (2003). Numerical simulation of axi-symmetric fire plumes: Accuracy and limitations. *Fire Safety Journal*, *38*, 467–492. http://doi.org/10.1016/S0379-7112(02)00082-6

Mahan, J. R. (2002). *Radiation heat transfer: a statistical approach* (3rd ed.). New York: John Wiley & Sons.

Mangialavori, G., & Rubino, F. (1992). Experimental Test on Large Hydrocarbon Pool Fire. In *7th Int. Symp. Loss Prev. and Safety Promotion in Process Ind.* (p. 83). Taormina, Italy.

McCaffrey, B. J. (1975). Purely Buoyant Diffusion Flames: Some Experimental Results. Gaithersburg, USA: National Bureau of Standards.

Mcdermott, R., Mcgrattan, K., & Floyd, J. (2011). A Simple Reaction Time Scale for Under-Resolved Fire Dynamics, 809–820. http://doi.org/10.3801/IAF

Mcgrattan, K. B., Baum, H. R., & Hamins, A. (2000). Thermal Radiation from Large Pool Fires Thermal Radiation from Large Pool Fires. *National Institute of Standards and Technology*.

McGrattan, K. B., Hostikka, S., Floyd, J. E., & McDermott, R. (2014). Fire Dynamics Simulator, Technical Reference Guide, Volume 1: Mathematical model, *3*(1018).

McGrattan, K. B., Hostikka, S., Floyd, J. E., McDermott, R., Weinschenk, C., & Overholt, K. (2015a). Sixth Edition Fire Dynamics Simulator Technical Reference Guide Volume 3 : Validation, *3*.

McGrattan, K. B., Hostikka, S., Floyd, J. E., McDermott, R., Weinschenk, C., & Overholt, K. (2015b). Sixth Edition Fire Dynamics Simulator User ' s Guide.

Moorhouse, J. (1982). Scaling Criteria for Pool Fires Derived from Large-scale Experiments. In *I. Chem. Symposium* (Vol. 71, pp. 165–179).

Muñoz, M. Á. (2005). Estudio de los parámetros que intervienen en la modelización de los efectos de grandes incendios de hidrocarburo: geometría y radiación térmica de la llama.

Nielsen, J. G. (2013). *Validation Study of Fire Dynamics Simulator*. Aalborg University.

Oficina Catalana del Canvi Climàtic. (2015). Guia pràctica per al càlcul d'emissions de gasos amb efecte d'hivernacle (GEH). Generalitat de Catalunya. Retrieved from http://canviclimatic.gencat.cat/web/.content/home/redueix_emissions/guia_de_calcul_demissions_de_co2/150301_Guia-practica-calcul-emissions_sense-canvis_CA_v3.pdf

Orloff, L., & De Ris, J. (1982). Froude modeling of pool fires. *In Symposium (International) on Combustion*, *19*(1), 885–895.

Pachera, M., Brunello, P., & Castelli, M. R. (2015). Validation of Fire Dynamic Simulator (FDS) for Pool Fire in Large Enclosures.

Pagni, P. J. (1989). *Pool fire vortex shedding frequencies* (No. 89).

Perry, R. H., Green, D. W., & Maloney, J. O. (2008). *Perry's Chemical Engineers' Handbook* (8th ed.). New York: McGraw Hill.

Pritchard, M. J., & Binding, T. M. (1992). A New Approach for Predicting Thermal-Radiation Levels from Hydrocarbon Pool Fires. In *Proceeding of the Symp. on Major Hazards Onshore and Offshore* (pp. 491–505).

Quintiere, J. J. (2006). *Fundamentals of fire phenomena* (First edit). London: John Wiley & Sons.

Repsol. (2003). DIESEL e +. Retrieved October 11, 2015, from http://www.repsol.com/imagenes/es_es/fds_diesel_e__58083_tcm7-43027.pdf

Rew, P. J., Hulbert, W. G., & Deaves, D. M. (1997). Modelling of Thermal Radiation From External Hydrocarbon Pool Fires. *Process Safety and Environmental Protection*, *75*(2), 81–89. http://doi.org/10.1205/095758297528841

Rubini. (2008). *Lecture: Credible CFD – Verification and Validation*. Lund: Lund University.

Tarragó Clivillé, D. (2010). *Estudi de la capacitat predictiva del simulador WFDS per a l'avaluació d'incendis forestals a escala de laboratori*.

Thomas, P. H. (1963). *The size of flames from natural fires* (No. 1). *En Symposium (International) on Combustion*.

Tieszen, S. R., O'Hern, T. J., Weckman, E. J., & Schefer, R. W. (2004). Experimental study of the effect of fuel mass flux on a 1-m-diameter methane fire and comparison with a hydrogen fire. *Combustion and Flame*, *139*(1–2), 126–141. http://doi.org/10.1016/j.combustflame.2004.08.006

Trouvé, A. (2008). The Second International Energy 2030 Conference CFD Modeling of Large-Scale Pool Fires The Second International Energy 2030 Conference, 413–422.

Weckman, E. J., & Sobiesiak, A. (1988). The effects of digital compensation on temperature measurements in an intermittent combusting flow. In *Collected papers in heat transfer* (pp. 65–72).

Wen, J. X., Kang, K., Donchev, T., & Karwatzki, J. M. (2007). Validation of FDS for the prediction of medium-scale pool fires. *Fire Safety Journal*, *42*(2), 127–138. http://doi.org/10.1016/j.firesaf.2006.08.007

Xin, Y. (2005). Baroclinic effects on fire flow field. In *Fourth Joint Meeting of the US Sections of the Combustion Institute*. Pittsburgh, Pennsylvania.

Yao, W., Yin, J., Hu, X., Wang, J., & Zhang, H. (2013). Numerical Modeling of Liquid n-heptane Pool Fires based on Heat Feedback Equilibrium. *Procedia Engineering*, *62*, 377–388. http://doi.org/10.1016/j.proeng.2013.08.079

Zukoski, Cetegen, & Kubota. (1985). *Visible structure of buoyant diffusion flames*. *Twentieth Symp. (Int.) on Combustion*. Pittsburgh.

A.1 Evolution of FDS through different versions

The software, which has been under development over 25 years, was first released in February of year 2000. Since then, it has been constantly improved with changes that brought more realistic results of simulations; for example, first version of FDS used Lagrange particle models for soot formation and ray-tracing models for thermal radiation transport, that were replaced in version 2 for mixture fraction combustion and finite volume radiation models respectively, providing several improvements in the quality of the obtained results, as figure 3.2 (Floyd et al., 2003) shows for a same burner modelled by FDS v.1 (left) and v.2 (right).

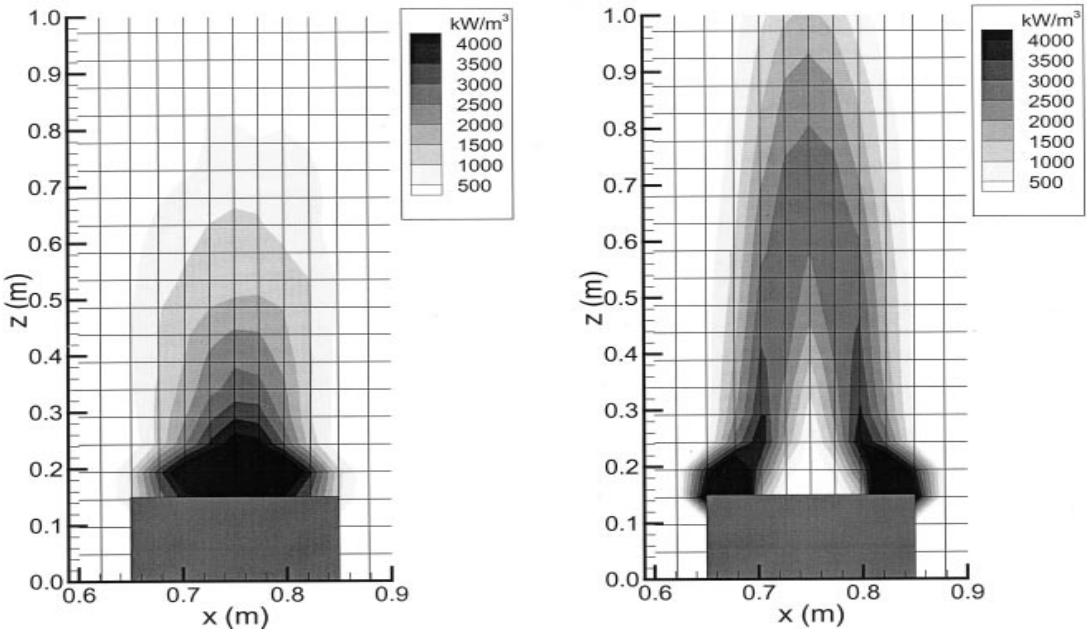

Figure A1.1 Comparison of HRR contours for FDS v1 (Left) and FDS v2 (Right) for a 0.2m square burner of 60 kW

FDS version 3 introduced an improvement to mixture fraction model used by FDS v.2, which implied a better accuracy in heat release rate calculation and also improved the accuracy of radiative heat flux and made the model less grid-dependent. Improvements in radiation modelling were also carried out, letting water droplets to absorb radiation.

One of the most important new features of FDS 3 was the ability to transfer heat through solid obstructions by convection. In previous versions, energy was lost when arrived to an obstacle, but from this version forth, FDS allows heat fluxes to reach, for example, a space near the simulated fire, but that is isolated by solid walls.

This version brought more visual characteristics, such as the possibility to create obstacles that did not occupy a full cell. However, "thin" obstacles that did not occupy a whole cell could not transfer heat by conduction, as this release allowed to obstructions that occupied whole cells. It was also added the option to paint the surfaces with different colours or textures.

Version 3 also introduced the possibility to divide the computational domain into different meshes, which was not allowed in previous versions. This was a very important advance for modelling geometries that required regions which different grid sizes, as a realistic fuel layer thickness, and would mean a significant decrease of computational time, as a multi-core computer can solve at the mean time different meshes, one per core. This function was

reinforced in version 4, which also allowed running a single FDS simulation through different computers via Message Passing Interface (MPI).

FDS version 4 brought many new features that meant more realistic simulations, like the introduction of a model that allows the simulation of fuels that suffer charring (the user has to specify physical properties of the charred and the virgin fuel, which are separated) or the possibility to vary the material properties as function of temperature. This version also allowed creating holes in obstructions, which made much easier the creation of doors and windows.

FDS 5 introduced a new multi-step combustion feature, which allowed multi-step reaction schemes to describe local extinction and CO production among many more phenomena. This new model reflects a more accurate heat release rate calculation and a better treatment of a local flame extinction. This version also allowed setting material properties to solid layers, and therefore, a same solid boundary can be modelled with different layers of materials and made possible environmental parameters setting as atmosphere stratification. The possibility of declaring single pressure zones (different to environmental pressure) was also added, bringing the possibility, for example, to model fuel leakage of pressured recipients.

Last FDS version, v.6, is probably the release that has introduced more mathematical models improvements, referred to the previous version. New version features are summarized below:

- **Hydrodynamics and turbulence:** A new model for scalar transport has been implemented, which prevents over-shoots and under-shoots of species concentration and temperature. New modified version of Deardorff turbulence model is now used by default for turbulent viscosity, which provides more dynamic range for flow field in coarse resolutions and a correct solution convergence in fine resolution, which replaces former Smagorinsky turbulence model: Errors due to numerical mixing have been removed in energy transport equation, among other significant changes.

- **Combustion:** Now is it possible to define lumped species that allow among other possibilities, the simulation of mixture fuels as gasoline or diesel. Chemical reactions mechanisms can be modified by users and may include reversible reactions, although their kinetics is considered infinitely fast by default unless the user specifies an Arrhenius rate law. Species like CO or soot can from this new version forth be produced, transported and consumed.

- Now, the surfaces can shrink or swell according to the materials density.

These described improvements and many others introduced in FDS v.6, makes this new release more computationally expensive than previous versions. That is why is very important to define the most proper computational domain and grid size that ensures at the mean time accuracy and not much computational expense.

In order to achieve mathematical models that are able to provide more realistic results, several validations have been carried out to verify how simulation results explain the reality, compared to experimental data of fires provoked in the same conditions that simulations are set.

A.2 Study of domain using a single mesh

In order to confirm results of first study of domain (see section 6.2), a second study of domain was performed. However, in this case, as FDS technical reference guide (McGrattan et al., 2014) affirmed that information exchange between different meshes is not as good as between cells that are inside a same mesh, simulations consisted in a single mesh.

These simulations represented an open-air scenario with a pool fire at the centre of the domain during 50 seconds. Due to lack of time, coarser cells were chosen (δx=12.5 cm) and only domains with a height over 6 m were studied (4×4×8, 3×3×8 and 2×2×8 m^3). As (Wen et al., 2007) affirmed that too narrow domains may bring to inaccurate results, data of a 8×8×8 will be also plotted in order to estimate the error that could be committed by choosing too narrow domains. Time evolution of temperatures at different thermocouple z-positions are compared below[9].

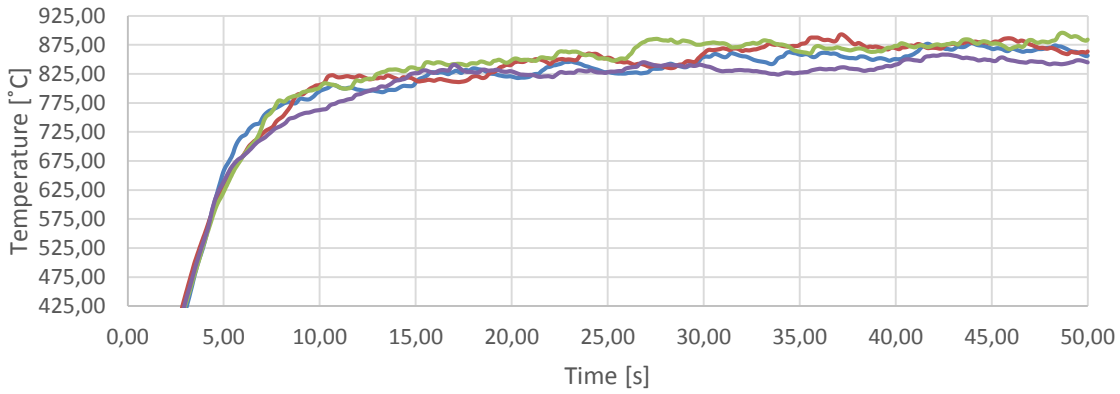

Figure A2.2 Temperature evolution of different domains caught by thermocouple at z=0.50 m

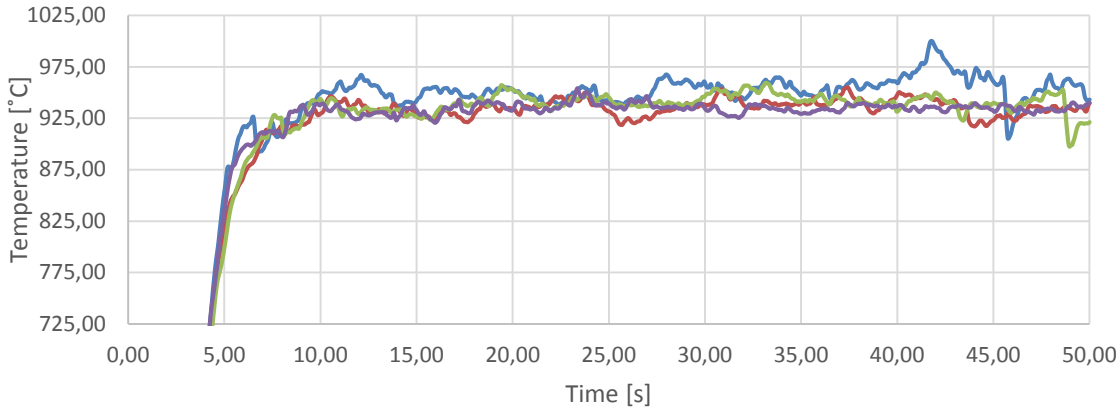

Figure A2.3 Temperature evolution of different domains caught by thermocouple at z=1.50 m

[9] Time evolution of temperature for domains of 8×8×8 is denoted with purple, for domains 4×4×8 with blue, for 3×3×8 with red and for 2×2×8 with green. Notice that minimum value of ordinate axis varies between different figures.

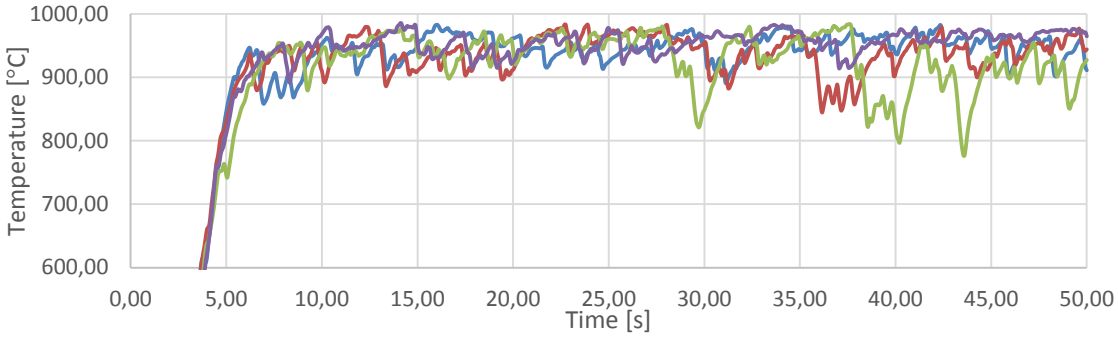

Figure A2.4 Temperature evolution of different domains caught by thermocouple at z=2.84 m

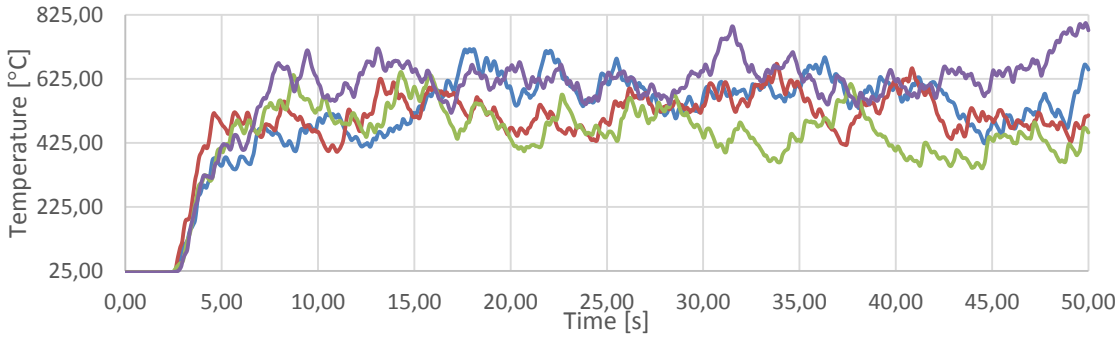

Figure A2.5 Temperature evolution of different domains caught by thermocouple at z=5.53 m

The thermocouple placed at z=0.50 m height registers temperatures around 860 ˚C for 2×2×8 domain, 850 ˚C for 3×3×8 domain and 840 ˚C for 4×4×8 m^3 domain. There are no significantly different standard deviations between different domains, although mean temperature difference is significant.

In the case of the temperatures caught by the thermocouple set at z=1.50 m position, there is not a significant difference between mean temperatures, although 4×4×8 domain presents a significantly higher standard deviation regarding the smaller domains, which have a similar deviation to the value that experimental data collected by Chatris presents.

Temperatures registered by thermocouple set at z=5.53 are very oscillating. 8×8×8 domain has the highest mean temperature, while mean and maximum decrease when the number of cells does.

Choosing a wide domain of 8×8×8 m^3 does not seem to be worthy, as results do not seem significantly different in areas inside the flame (despite large differences in high z thermocouple positions), and computational time is significantly increased. In addition to the computational time expense increase, temperatures registered in z=0.5 m in the domain of 8×8×8 show the lowest values, which means a displacement from Muñoz and Ferrero experimental data.

The chosen domain is 3×3×8, as gives the most stable time evolution of temperature (this domain presents the smallest standard deviation). This domain also shows the higher temperature for the thermocouple set at 0.5 m height; this means this set is the most nearby to values caught in the downfire region by Muñoz and Ferrero. Moreover, registered mean temperature in the case of z=1.5 m height (935.76 ˚C) is near the maximum registered temperature in Chatris experimental data (930.66 ˚C). This confirms that 3×3×8 will be the domain chosen for the following studies.

A.3 Study of heat release rate behaviour according to pool fire shape

As Trouvé (see section 3.2.3) reported that radiative fraction decreases with the pool size when used FDS capabilities in large-scale pool fires, different fire shapes could imply different behaviour in terms of radiation emission. This is the reason why HRR and radiation heat are results are compared for experiments 1, 2 and 3 of chapter 7.

Results obtained show that heat release rate, radiation heat losses and convection heat loses increase with the number of elements that constitute the fire, as expected. It is logical, as mass loss rate per unit area and heat of combustion were the variables specified to FDS, which calculates from these the heat release rate per unit area. As HRRPUA are the same for the different simulations (MLRPUA and heat of combustion have not been changed), the total HRR is higher for higher areas, as it is given by the product between HRRPUA and the total surface area. Means and standard deviations (multiplied by a constant factor in order to reach the same rank of magnitude that means) of all three simulations have been plotted versus the number of elements of the pool. Results show that while mean heat release rates increase lineally with the number of cells forming the burner surface, standard deviations grow showing a second power polynomial pattern (Figure A3.6). Heat transferred by convection shows the same pattern as total heat release rate; however, heat transferred by convection shows a correlation between standard deviation and the number of cells that constitute the fire surface, which is almost lineal (Figure A3.7).

Fraction of total heat release that is exchanged as radiation does not seem to vary between the different simulations and stays constant with a value of 0.335, which is very nearby to radiative fraction value set by FDS by default (0.35).

In addition, standard deviations need to be multiplied for a constant value, in order to reach a similar magnitude than means. The chosen values are 7 for HRR, 7.5 for $\dot{Q}_r$ and 8.25 for $\dot{Q}_c$, which denotes that heat release rate shows the higher deviations of all the analysed data sets, as gathers deviations coming from both convection and radiation, whose deviation is significantly higher than values presented by convection.

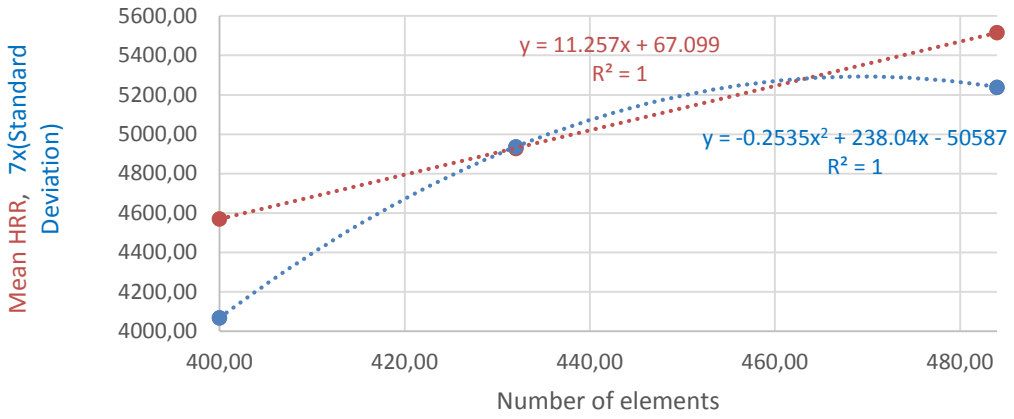

Figure A3.6 Means of HRR from experiments 1, 2 and 3 & standard deviations multiplied by a factor of 7

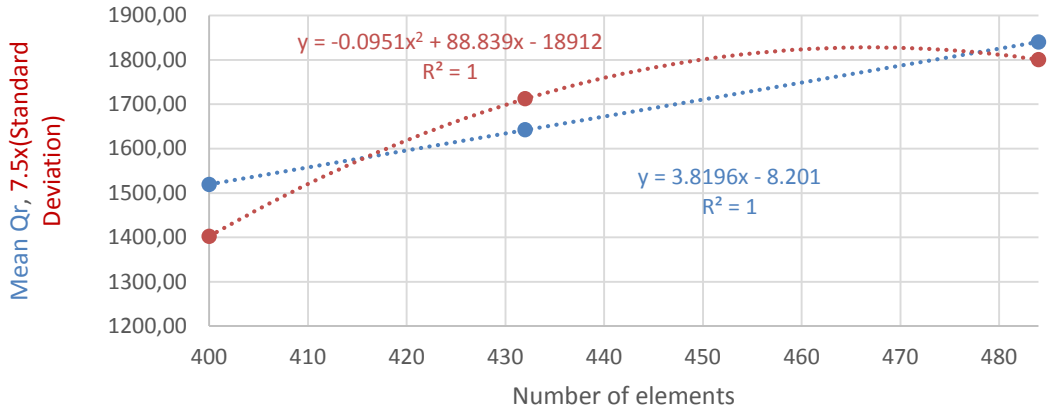

Figure A3.7 Means of HRR from experiments 1, 2 and 3 & standard deviations multiplied by a factor

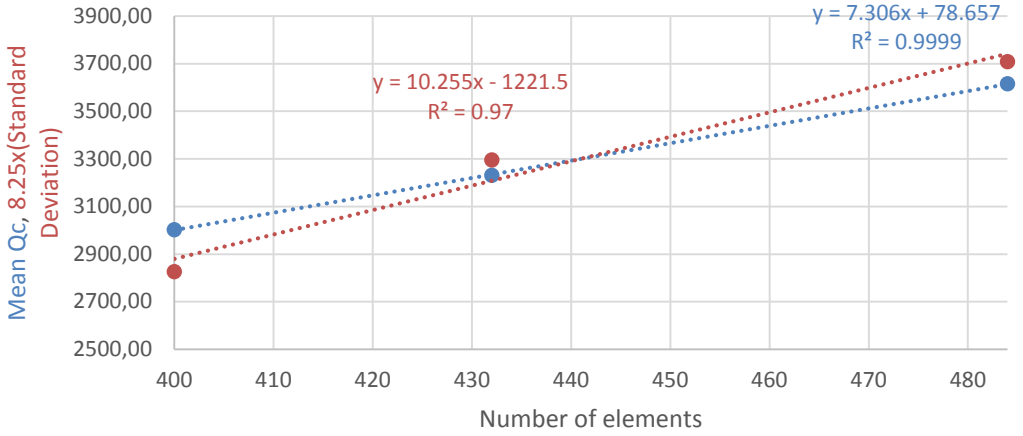

Figure A3.8 Means of HRR from experiments 1, 2 and 3 & standard deviations multiplied by a factor

A.4 Matlab® program for calculation of flame lengths

```
srcFiles =dir('C:\Users\jcbueno\Desktop\Estudi Bassa Quadrada\Gasolina\3×3×8qcorrecte\*.png');  %
the folder in which ur images exists
baseimg=strcat('C:\Users\jcbueno\Desktop\Estudi Bassa
Quadrada\Gasolina\3×3×8qcorrecte\',srcFiles(1).name);
i=240;
t=0;
k=0;
Z=zeros(length(srcFiles),4);

while i<length(srcFiles);
   filename = strcat('C:\Users\jcbueno\Desktop\Estudi Bassa
Quadrada\Gasolina\3×3×8qcorrecte\',srcFiles(i).name);
   hAxes = axes();
   I = imread(filename);
   J=imrotate(I,180);
   imageHandle = imshow(J);
   objectHandle=imageHandle;
   figure, imshow(J);
   ScrSize = get(0,'ScreenSize');
   %set(imageHandle,'ButtonDownFcn');
      axesHandle  = get(objectHandle,'Parent');
      coordinates = get(axesHandle,'CurrentPoint');
      coordinates = coordinates(1,1:2);
      %message     = sprintf('x: %.1f , y: %.1f',coordinates (1) ,coordinates (2));
      %helpdlg(message);
      pause(3);
      Z(i,1)=k;  %num. fotograma
      Z(i,2)=t;
      Z(i,3)=Z(i,2)+coordinates(2);  %alçada flama, restarli 79
      Z(i,4)=coordinates(1); %posició y a la que es produeix l'alçada
      i=i+1;
      k=k+1;
      t=t+0.005; %temps
   end
```

A.5 FDS scripts used in sensitivity analysis

Gasoline pool fire – FOC_03_21.fds

```
&HEAD CHID='gasolina_15 ', TITLE='SIMULACIO EXPERIMENT CAN PADRO - BASSAL GASOLINA: 1,5M' /

&MESH IJK=48,48,32, XB=0,3,0,3,0,2 /

&MESH IJK=48,48,32, XB=0,3,0,3,2,4 /

&MESH IJK=48,48,32, XB=0,3,0,3,4,6 /

&MESH IJK=48,48,32, XB=0,3,0,3,6,8 /

&TIME T_END= 50.0 /

&MISC U0=0.4

   TMPA=20.8

        HUMIDITY=91./

&REAC ID = 'GASOLINE'

        HEAT_OF_COMBUSTION=43676.28571

        SOOT_YIELD = 0.01

        C=7.

        H=14.

        IDEAL = .TRUE. /

&MATL ID='GASOLINE'

        DENSITY=709.0

        BOILING_TEMPERATURE=94.0

        SPECIFIC_HEAT=2.22

        CONDUCTIVITY=0.116

        EMISSIVITY=0.9167

        HEAT_OF_REACTION=349.0 /

&MATL ID='CONCRETE'

        CONDUCTIVITY=1.4

        SPECIFIC_HEAT=0.658

        DENSITY=2307. /

&MATL ID='LIQUIDWATER'

        CONDUCTIVITY=0.6063

        SPECIFIC_HEAT=1.8639
```

```
      DENSITY=994.7
      BOILING_TEMPERATURE=100.0
      HEAT_OF_REACTION=2435.1 /
&SURF ID='BURNER' MLRPUA=0.067, MATL_ID='GASOLINE', COLOR='BLACK', THICKNESS=0.02 /
&SURF ID='PARET', RGB=200,200,200, MATL_ID='CONCRETE', THICKNESS=0.12 /
&SURF ID='FONS', RGB=10,10,250, MATL_ID='LIQUIDWATER', THICKNESS=0.1875 /
&OBST XB=0.8750, 2.1250, 0.8750, 2.1250, 0.06250, 0.1875, SURF_ID='FONS'/
&OBST XB=0.8750, 2.1250, 0.8750, 2.1250, 0.1875, 0.25000, SURF_ID='BURNER'/
&OBST XB=0.7500, 0.8750, 0.8750, 2.1250, 0.06250, 0.2500, SURF_ID='PARET'/
&OBST XB=2.1250, 2.2500, 0.8750, 2.1250, 0.06250, 0.2500, SURF_ID='PARET'/
&OBST XB=0.7500, 2.2500, 0.7500, 0.8750, 0.06250, 0.2500, SURF_ID='PARET'/
&OBST XB=0.7500, 2.2500, 2.1250, 2.2500, 0.06250, 0.2500, SURF_ID='PARET'/
&OBST XB=0.0, 3.0, 0.0, 3.0, 0.0, 0.06250, SURF_ID='PARET' / Terra
&VENT XB=0.00, 3.00, 0.00, 0.00, 0.00, 8.00, SURF_ID='OPEN' / Vent
&VENT XB=0.00, 3.00, 3.00, 3.00, 0.00, 8.00, SURF_ID='OPEN' / Vent
&VENT XB=0.00, 0.00, 0.00, 3.00, 0.00, 8.00, SURF_ID='OPEN' / Vent
&VENT XB=3.00, 3.00, 0.00, 3.00, 0.00, 8.00, SURF_ID='OPEN' / Vent
&VENT XB=0.00, 3.00, 0.00, 3.00, 8.00, 8.00, SURF_ID='OPEN' / Vent
;;;;;;;;;;;;;;;;;;TERMOPARELLS;;;;;;;;;;;;;;;;;;;;;;
;;;;;;;;;;;;;;;;;;;;MIDA TERMOPARELLS;;;;;;;;;;;;;;;;
&PROP ID='DOBLE', BEAD_DIAMETER=0.0015/
&PROP ID='TRIPLE', BEAD_DIAMETER=0.0030/
;;;;;;;;;;;;;;;;;;ZONA FLAMA CONTÍNUA;;;;;;;;;;;;;;;;
&DEVC XYZ=1.5, 1.5, 0.30, QUANTITY='THERMOCOUPLE', PROP_ID='DOBLE', ID='TAC1'/
&DEVC XYZ=1.5, 1.2, 0.30, QUANTITY='THERMOCOUPLE', PROP_ID='DOBLE', ID='TAM1'/
&DEVC XYZ=1.5, 0.9, 0.30, QUANTITY='THERMOCOUPLE', ID='TAE1'/
&DEVC XYZ=1.5, 1.5, 0.40, QUANTITY='THERMOCOUPLE', PROP_ID='DOBLE', ID='TAC2'/
&DEVC XYZ=1.5, 1.2, 0.40, QUANTITY='THERMOCOUPLE', PROP_ID='DOBLE', ID='TAM2'/
&DEVC XYZ=1.5, 0.9, 0.40, QUANTITY='THERMOCOUPLE', ID='TAE2'/
&DEVC XYZ=1.5, 1.5, 0.50, QUANTITY='THERMOCOUPLE', PROP_ID='DOBLE', ID='TAC3'/
&DEVC XYZ=1.5, 1.2, 0.50, QUANTITY='THERMOCOUPLE', PROP_ID='DOBLE', ID='TAM3'/
&DEVC XYZ=1.5, 0.9, 0.50, QUANTITY='THERMOCOUPLE', ID='TAE3'/
```

```
&DEVC XYZ=1.5, 1.5, 0.60, QUANTITY='THERMOCOUPLE', PROP_ID='DOBLE', ID='TAC4'/
&DEVC XYZ=1.5, 1.2, 0.60, QUANTITY='THERMOCOUPLE', ID='TAM4'/
&DEVC XYZ=1.5, 0.9, 0.60, QUANTITY='THERMOCOUPLE', ID='TAE4'/
&DEVC XYZ=1.5, 1.5, 0.70, QUANTITY='THERMOCOUPLE', PROP_ID='DOBLE', ID='TAC5'/
&DEVC XYZ=1.5, 1.2, 0.70, QUANTITY='THERMOCOUPLE', ID='TAM5'/
&DEVC XYZ=1.5, 0.9, 0.70, QUANTITY='THERMOCOUPLE', ID='TAE5'/
&DEVC XYZ=1.5, 1.5, 0.80, QUANTITY='THERMOCOUPLE', PROP_ID='DOBLE', ID='TAC6'/
&DEVC XYZ=1.5, 1.2, 0.80, QUANTITY='THERMOCOUPLE', ID='TAM6'/
&DEVC XYZ=1.5, 0.9, 0.80, QUANTITY='THERMOCOUPLE', ID='TAE6'/
;;;;;;;;;;;;;;;;;ZONA NO EXPERIMENTADA;;;;;;;;;;;;;;;;;
&DEVC XYZ=1.5, 1.5, 1.00, QUANTITY='THERMOCOUPLE', ID='TXX1'/
&DEVC XYZ=1.5, 1.5, 1.25, QUANTITY='THERMOCOUPLE', ID='TXX2'/
&DEVC XYZ=1.5, 1.5, 1.50, QUANTITY='THERMOCOUPLE', ID='TXX3'/
&DEVC XYZ=1.5, 1.5, 1.80, QUANTITY='THERMOCOUPLE', ID='TXX4'/
&DEVC XYZ=1.5, 1.5, 2.00, QUANTITY='THERMOCOUPLE', ID='TXX5'/
&DEVC XYZ=1.5, 1.5, 2.25, QUANTITY='THERMOCOUPLE', ID='TXX6'/
&DEVC XYZ=1.5, 1.5, 2.50, QUANTITY='THERMOCOUPLE', ID='TXX7'/
&DEVC XYZ=1.5, 1.5, 2.84, QUANTITY='THERMOCOUPLE', ID='TXX8'/
;;;;;;;;;;;;;;;;;ZONA NO INTERMITENT;;;;;;;;;;;;;;;;;
&DEVC XYZ=1.5, 1.5, 3.96, QUANTITY='THERMOCOUPLE', ID='TB1'/
&DEVC XYZ=1.5, 1.5, 5.53, QUANTITY='THERMOCOUPLE', ID='TB2'/
&DEVC XYZ=1.5, 1.5, 6.96, QUANTITY='THERMOCOUPLE', ID='TB3'/
&SLCF PBX=1.5, QUANTITY='TEMPERATURE'/
&SLCF PBY=1.5, QUANTITY='TEMPERATURE'/
&ISOF QUANTITY='TEMPERATURE', VALUE=800./
&BNDF QUANTITY='NET HEAT FLUX'/
&TAIL /
```

Diesel pool fire – FOC_03_22.fds

```
&HEAD CHID='diesel_15', TITLE='SIMULACIO EXPERIMENT CAN PADRO - BASSAL GASOIL: 1,5M' /

&MESH IJK=48,48,32, XB=0,3,0,3,0,2 /

&MESH IJK=48,48,32, XB=0,3,0,3,2,4 /

&MESH IJK=48,48,32, XB=0,3,0,3,4,6 /

&MESH IJK=48,48,32, XB=0,3,0,3,6,8 /

&TIME T_END= 50.0 /

&MISC U0=0.82
   TMPA=22.0
        HUMIDITY=91./
&REAC ID = 'GASOIL'
        HEAT_OF_COMBUSTION=41165.09
        SOOT_YIELD = 0.01
        C=16.
        H=28.
        IDEAL = .TRUE. /
&MATL ID='GASOIL'
        DENSITY=833.0
        BOILING_TEMPERATURE=305.0
        SPECIFIC_HEAT=3.05
        CONDUCTIVITY=0.116
        EMISSIVITY=0.9167
        HEAT_OF_REACTION=250.8 /
&MATL ID='CONCRETE'
        CONDUCTIVITY=1.4
        SPECIFIC_HEAT=0.658
        DENSITY=2307. /
&MATL ID='LIQUIDWATER'
        CONDUCTIVITY=0.6063
        SPECIFIC_HEAT=1.8639
        DENSITY=994.7
        BOILING_TEMPERATURE=100.0
```

```
        HEAT_OF_REACTION=2435.1 /
&SURF ID='BURNER' MLRPUA=0.054, MATL_ID='GASOIL', COLOR='BLACK', THICKNESS=0.02 /
&SURF ID='PARET', RGB=200,200,200, MATL_ID='CONCRETE', THICKNESS=0.12 /
&SURF ID='FONS', RGB=10,10,250, MATL_ID='LIQUIDWATER', THICKNESS=0.1875 /
&OBST XB=0.8750, 2.1250, 0.8750, 2.1250, 0.06250, 0.1875, SURF_ID='FONS'/
&OBST XB=0.8750, 2.1250, 0.8750, 2.1250, 0.1875, 0.25000, SURF_ID='BURNER'/
&OBST XB=0.7500, 0.8750, 0.8750, 2.1250, 0.06250, 0.2500, SURF_ID='PARET'/
&OBST XB=2.1250, 2.2500, 0.8750, 2.1250, 0.06250, 0.2500, SURF_ID='PARET'/
&OBST XB=0.7500, 2.2500, 0.7500, 0.8750, 0.06250, 0.2500, SURF_ID='PARET'/
&OBST XB=0.7500, 2.2500, 2.1250, 2.2500, 0.06250, 0.2500, SURF_ID='PARET'/
&OBST XB=0.0, 3.0, 0.0, 3.0, 0.0, 0.06250, SURF_ID='PARET' / Terra
&VENT XB=0.00, 3.00, 0.00, 0.00, 0.00, 8.00, SURF_ID='OPEN' / Vent
&VENT XB=0.00, 3.00, 3.00, 3.00, 0.00, 8.00, SURF_ID='OPEN' / Vent
&VENT XB=0.00, 0.00, 0.00, 3.00, 0.00, 8.00, SURF_ID='OPEN' / Vent
&VENT XB=3.00, 3.00, 0.00, 3.00, 0.00, 8.00, SURF_ID='OPEN' / Vent
&VENT XB=0.00, 3.00, 0.00, 3.00, 8.00, 8.00, SURF_ID='OPEN' / Vent
;;;;;;;;;;;;;;;;;;;TERMOPARELLS;;;;;;;;;;;;;;;;;;;;;;;
;;;;;;;;;;;;;;;;;;;;MIDA TERMOPARELLS;;;;;;;;;;;;;;;;;
&PROP ID='DOBLE', BEAD_DIAMETER=0.0015/
&PROP ID='TRIPLE', BEAD_DIAMETER=0.0030/
;;;;;;;;;;;;;;;;;;;ZONA FLAMA CONTÍNUA;;;;;;;;;;;;;;;;
&DEVC XYZ=1.5, 1.5, 0.30, QUANTITY='THERMOCOUPLE', PROP_ID='DOBLE', ID='TAC1'/
&DEVC XYZ=1.5, 1.2, 0.30, QUANTITY='THERMOCOUPLE', PROP_ID='DOBLE', ID='TAM1'/
&DEVC XYZ=1.5, 0.9, 0.30, QUANTITY='THERMOCOUPLE', ID='TAE1'/
&DEVC XYZ=1.5, 1.5, 0.40, QUANTITY='THERMOCOUPLE', PROP_ID='DOBLE', ID='TAC2'/
&DEVC XYZ=1.5, 1.2, 0.40, QUANTITY='THERMOCOUPLE', PROP_ID='DOBLE', ID='TAM2'/
&DEVC XYZ=1.5, 0.9, 0.40, QUANTITY='THERMOCOUPLE', ID='TAE2'/
&DEVC XYZ=1.5, 1.5, 0.50, QUANTITY='THERMOCOUPLE', PROP_ID='DOBLE', ID='TAC3'/
&DEVC XYZ=1.5, 1.2, 0.50, QUANTITY='THERMOCOUPLE', PROP_ID='DOBLE', ID='TAM3'/
&DEVC XYZ=1.5, 0.9, 0.50, QUANTITY='THERMOCOUPLE', ID='TAE3'/
&DEVC XYZ=1.5, 1.5, 0.60, QUANTITY='THERMOCOUPLE', PROP_ID='DOBLE', ID='TAC4'/
&DEVC XYZ=1.5, 1.2, 0.60, QUANTITY='THERMOCOUPLE', ID='TAM4'/
```

```
&DEVC XYZ=1.5, 0.9, 0.60, QUANTITY='THERMOCOUPLE', ID='TAE4'/
&DEVC XYZ=1.5, 1.5, 0.70, QUANTITY='THERMOCOUPLE', PROP_ID='DOBLE', ID='TAC5'/
&DEVC XYZ=1.5, 1.2, 0.70, QUANTITY='THERMOCOUPLE', ID='TAM5'/
&DEVC XYZ=1.5, 0.9, 0.70, QUANTITY='THERMOCOUPLE', ID='TAE5'/
&DEVC XYZ=1.5, 1.5, 0.80, QUANTITY='THERMOCOUPLE', PROP_ID='DOBLE', ID='TAC6'/
&DEVC XYZ=1.5, 1.2, 0.80, QUANTITY='THERMOCOUPLE', ID='TAM6'/
&DEVC XYZ=1.5, 0.9, 0.80, QUANTITY='THERMOCOUPLE', ID='TAE6'/
&DEVC XYZ=1.5, 1.5, 1.00, QUANTITY='THERMOCOUPLE', ID='TXX1'/
&DEVC XYZ=1.5, 1.2, 1.00, QUANTITY='THERMOCOUPLE', ID='TXM1'/
&DEVC XYZ=1.5, 0.9, 1.00, QUANTITY='THERMOCOUPLE', ID='TXE1'/
&DEVC XYZ=1.5, 1.5, 1.25, QUANTITY='THERMOCOUPLE', ID='TXX2'/
&DEVC XYZ=1.5, 1.2, 1.25, QUANTITY='THERMOCOUPLE', ID='TXM2'/
&DEVC XYZ=1.5, 0.9, 1.25, QUANTITY='THERMOCOUPLE', ID='TXE2'/
&DEVC XYZ=1.5, 1.5, 1.50, QUANTITY='THERMOCOUPLE', ID='TXX3'/
&DEVC XYZ=1.5, 1.2, 1.50, QUANTITY='THERMOCOUPLE', ID='TXM3'/
&DEVC XYZ=1.5, 0.9, 1.50, QUANTITY='THERMOCOUPLE', ID='TXE3'/
&DEVC XYZ=1.5, 1.5, 1.80, QUANTITY='THERMOCOUPLE', ID='TXX4'/
&DEVC XYZ=1.5, 1.5, 2.00, QUANTITY='THERMOCOUPLE', ID='TXX5'/
&DEVC XYZ=1.5, 1.5, 2.25, QUANTITY='THERMOCOUPLE', ID='TXX6'/
&DEVC XYZ=1.5, 1.5, 2.50, QUANTITY='THERMOCOUPLE', ID='TXX7'/
&DEVC XYZ=1.5, 1.5, 2.84, QUANTITY='THERMOCOUPLE', ID='TXX8'/
;;;;;;;;;;;;;;;;;ZONA NO INTERMITENT;;;;;;;;;;;;;;;;;
&DEVC XYZ=1.5, 1.5, 3.96, QUANTITY='THERMOCOUPLE', ID='TB1'/
&DEVC XYZ=1.5, 1.5, 5.53, QUANTITY='THERMOCOUPLE', ID='TB2'/
&DEVC XYZ=1.5, 1.5, 6.96, QUANTITY='THERMOCOUPLE', ID='TB3'/
&SLCF PBX=1.5, QUANTITY='TEMPERATURE'/
&SLCF PBY=1.5, QUANTITY='TEMPERATURE'/
&ISOF QUANTITY='TEMPERATURE', VALUE=800./
&BNDF QUANTITY='NET HEAT FLUX'/
&TAIL /
```

A.6 FDS simulations summary

As mentioned at project finality section, this project intends to be a solid tool for these users who are beginning with FDS modelling, and specially, FDS modelling of pool fires. During the stance at CERTEC, several simulations have been performed, and among them, there are many parameters that vary from a simulation to another one. This appendix summarizes in a single table all simulations carried out for this project, their filenames and the parameters featuring in each simulation.

All files are found in the directory called TFG_JCB, where there are different folders, one per study performed:

- **Study of domain**, which includes 6 subfolders (one per experiment performed for this study).

- **Symmetry study**, which contains three folders. 3×3×8a corresponds to the case in which pool is not split into two meshes, 3×3×8b to the case in which pool is split by the X direction and finally, gasoline_15_3×3×8, which contains the simulation selected as optimal in the previous study.

- **Mesh study**, which contains four folders (gasoline_15_efi, gasoline_15_fi, gasoline_15_large and gasoline_15_med). The simulation file called gasoline_15_efi was an attempt to use extra-fine cells of 1.56 cm width, but computational restrictions of CERTEC computers did not permit to perform the simulation.

- **Shape study**, which contains two folders (gasoline and gasoil). Each one of these folders include three cases (null wind speed, wind speed of 2 m/s and wind speed of 4 m/s).

- **Sensitivity study**, which also contains two folders (gasoline and gasoil). These folders are each one divided into four folders (one for each studied parameter), and each one of these four contain two additional folders (one for the simulation for which that parameter is increased in 10% and the other one for the case in which the parameter is decreased in 10%).

- **Basis cases**, which contains the basis cases used in sensitivity study for gasoline (FOC_03_21) and for gasoil (FOC_03_22).

All folders containing simulation data include the .devc and .hrr output files, the Smokeview animation and the source code (.fds file).Summary table is given on the following page.

Table A6.1 Summary of all simulations performed for this project.

Study	Simulation filename	Domain [m³]	Δ_{Pool} [cm]	Δ [cm]	Shape	Area [m²]	Fuel	ε	ρ_F [kg/m³]	ΔH_c [kJ/kg]	$\dot{m}'''$ [kg/(m²·s)]	χ	u_w [m/s]
Study of domain	gasolina_15_4×4×8.fds	4×4×8	3.13	12.50	Circular	1.69	Gasoline	0.75	709.00	46816.00	0.07	0.35	0.00
	gasolina_15_3×3×8.fds	3×3×8	3.13	12.50	Circular	1.69	Gasoline	0.75	709.00	46816.00	0.07	0.35	0.00
	gasolina_15_2×2×8.fds	2×2×8	3.13	12.50	Circular	1.69	Gasoline	0.75	709.00	46816.00	0.07	0.35	0.00
	gasolina_15_3×3×6.fds	3×3×6	3.13	12.50	Circular	1.69	Gasoline	0.75	709.00	46816.00	0.07	0.35	0.00
	gasolina_15_2×2×6.fds	2×2×6	3.13	12.50	Circular	1.69	Gasoline	0.75	709.00	46816.00	0.07	0.35	0.00
	gasolina_15_2×2×4.fds	2×2×4	3.13	12.50	Circular	1.69	Gasoline	0.75	709.00	46816.00	0.07	0.35	0.00
Symmetry study	3×3×8a.fds (not split)	3×3×8	3.13	12.50	Circular	1.69	Gasoline	0.75	709.00	46816.00	0.07	0.35	0.00
	3×3×8b.fds	3×3×8	3.13	12.50	Circular	1.69	Gasoline	0.75	709.00	46816.00	0.07	0.35	0.00
	gasolina_15_2×2×8.fds	3×3×8	3.13	12.50	Circular	1.69	Gasoline	0.75	709.00	46816.00	0.07	0.35	0.00
Mesh study	gasolina_15_large.fds	3×3×8	12.50	12.50	Circular	1.69	Gasoline	0.75	709.00	46816.00	0.07	0.35	0.00
	gasolina_15_med.fds	3×3×8	6.25	6.25	Circular	1.69	Gasoline	0.75	709.00	46816.00	0.07	0.35	0.00
	gasolina_15_fi.fds	3×3×8	3.13	3.13	Circular	1.69	Gasoline	0.75	709.00	46816.00	0.07	0.35	0.00
Pool shape study	3×3×8ccorrecte.fds	3×3×8	6.25	6.25	Circular	1.69	Gasoline	0.92	709.00	43676.29	0.07	0.35	0.00
	3×3×8qcorrecte.fds	3×3×8	6.25	6.25	Square	1.89	Gasoline	0.92	709.00	43676.29	0.07	0.35	0.00
	3×3×8q2.fds	3×3×8	6.25	6.25	Square	1.56	Gasoline	0.92	709.00	43676.29	0.07	0.35	0.00
	3×3×8cw2.fds	3×3×8	6.25	6.25	Circular	1.69	Gasoline	0.92	709.00	43676.29	0.07	0.35	2.00
	3×3×8qw2.fds	3×3×8	6.25	6.25	Square	1.89	Gasoline	0.92	709.00	43676.29	0.07	0.35	2.00
	3×3×8q2w2.fds	3×3×8	6.25	6.25	Square	1.56	Gasoline	0.92	709.00	43676.29	0.07	0.35	2.00
	3×3×8cw4.fds	3×3×8	6.25	6.25	Circular	1.69	Gasoline	0.92	709.00	43676.29	0.07	0.35	4.00
	3×3×8qw4.fds	3×3×8	6.25	6.25	Square	1.89	Gasoline	0.92	709.00	43676.29	0.07	0.35	4.00
	3×3×8q2w4.fds	3×3×8	6.25	6.25	Square	1.56	Gasoline	0.92	709.00	43676.29	0.07	0.35	4.00
	FOC_03_22.fds	3×3×8	6.25	6.25	Circular	1.69	Diesel	0.92	833.00	41165.09	0.05	0.35	0.00
	FOC_03_QG.fds	3×3×8	6.25	6.25	Square	1.89	Diesel	0.92	833.00	41165.09	0.05	0.35	0.00
	FOC_03_2Q2.fds	3×3×8	6.25	6.25	Square	1.56	Diesel	0.92	833.00	41165.09	0.05	0.35	0.00
	gasoil_15w2.fds	3×3×8	6.25	6.25	Circular	1.69	Diesel	0.92	833.00	41165.09	0.05	0.35	2.00

	gasoil_15qw2.fds	3×3×8	6.25	6.25	Square	1.89	Diesel	0.92	833.00	41165.09	0.05	0.35	2.00
	gasoil_15q2w2.fds	3×3×8	6.25	6.25	Square	1.56	Diesel	0.92	833.00	41165.09	0.05	0.35	2.00
	gasoil_15w4.fds	3×3×8	6.25	6.25	Circular	1.69	Diesel	0.92	833.00	41165.09	0.05	0.35	4.00
	gasoil_15qw4.fds	3×3×8	6.25	6.25	Square	1.89	Diesel	0.92	833.00	41165.09	0.05	0.35	4.00
	gasoil_15q2w4.fds	3×3×8	6.25	6.25	Square	1.56	Diesel	0.92	833.00	41165.09	0.05	0.35	4.00
Sensitivity study	FOC_03_21.fds	3×3×8	6.25	6.25	Square	1.56	Gasoline	0.92	709.00	43676.29	0.07	0.35	0.40
	FOC_03_22.fds	3×3×8	6.25	6.25	Square	1.56	Diesel	0.92	833.00	41165.09	0.05	0.35	0.82
	DENS_01.fds	3×3×8	6.25	6.25	Square	1.56	Gasoline	0.92	638.10	43676.29	0.07	0.35	0.40
	DENS_02.fds	3×3×8	6.25	6.25	Square	1.56	Gasoline	0.92	780.00	43676.29	0.07	0.35	0.40
	DENS_03.fds	3×3×8	6.25	6.25	Square	1.56	Diesel	0.92	749.70	41165.09	0.05	0.35	0.82
	DENS_04.fds	3×3×8	6.25	6.25	Square	1.56	Diesel	0.92	916.30	41165.09	0.05	0.35	0.82
	HC_01.fds	3×3×8	6.25	6.25	Square	1.56	Gasoline	0.92	709.00	39308.66	0.07	0.35	0.40
	HC_02.fds	3×3×8	6.25	6.25	Square	1.56	Gasoline	0.92	709.00	48043.91	0.07	0.35	0.40
	HC_03.fds	3×3×8	6.25	6.25	Square	1.56	Diesel	0.92	833.00	37048.58	0.05	0.35	0.82
	HC_04.fds	3×3×8	6.25	6.25	Square	1.56	Diesel	0.92	833.00	45281.60	0.05	0.35	0.82
	MLRPUA_01.fds	3×3×8	6.25	6.25	Square	1.56	Gasoline	0.92	709.00	43676.29	0.08	0.35	0.40
	MLRPUA_02.fds	3×3×8	6.25	6.25	Square	1.56	Gasoline	0.92	709.00	43676.29	0.06	0.35	0.40
	MLRPUA_03.fds	3×3×8	6.25	6.25	Square	1.56	Diesel	0.92	833.00	41165.09	0.05	0.35	0.82
	MLRPUA_04.fds	3×3×8	6.25	6.25	Square	1.56	Diesel	0.92	833.00	41165.09	0.06	0.35	0.82
	RADIATIF_01.fds	3×3×8	6.25	6.25	Square	1.56	Gasoline	0.92	709.00	43676.29	0.07	0.32	0.40
	RADIATIF_02.fds	3×3×8	6.25	6.25	Square	1.56	Gasoline	0.92	709.00	43676.29	0.07	0.39	0.40
	RADIATIF_04.fds	3×3×8	6.25	6.25	Square	1.56	Diesel	0.92	833.00	41165.09	0.05	0.32	0.82
	RADIATIF_05.fds	3×3×8	6.25	6.25	Square	1.56	Diesel	0.92	833.00	41165.09	0.05	0.39	0.82